DESIGN OF NEURO-FUZZY SYSTEM CONTROLLER FOR DC SERVO MOTOR BASED SATELLITE TRACKING SYSTEM

LINUS ALWAL ALOO

MASTER OF SCIENCE

(Electrical Engineering)

JOMO KENYATTA UNIVERSITY OF AGRICULTURE AND TECHNOLOGY

2017

Design of Neuro-Fuzzy System Controller For

DC Servo Motor Based Satellite Tracking System

Linus Alwal Aloo

A thesis submitted in partial fulfillment for the degree of Master of

Science in Electrical Engineering in the Jomo Kenyatta University of

Agriculture and Technology

2017

DECLARATION

This thesis is my original work and has not been presented for a degree in any other University

Signature.. Date................................... ………………

Linus Alwal Aloo

This thesis has been submitted for examination with our approval as university supervisors

Signature.. Date................................. …………….

Dr. Peter K. Kihato, PhD

JKUAT, Kenya

Signature... Date................................... ……………

Prof. Stanley I. Kamau, PhD

JKUAT, Kenya

DEDICATION

This work is dedicated to my parents who showed me the path to follow in life and also inspired me to appreciate the indispensability of education.

ACKNOWLEDGMENT

First, is to thank Almighty God for the gift of good health and protection throughout the study period.

Second, I am highly indebted to my supervisors Dr. Peter K. Kihato and Prof. Stanley I. Kamau for the exemplary support and supervision accorded. In particular; their patience, kindness, availability, continuous support as well as enormous academic experience, has been invaluable to me throughout the period.

My special gratitude goes to JKUAT for sponsoring me towards the programme, without which the success of this work would have not been possible. In addition, I credit the informal support and encouragement of a number of friends and colleagues including their positive and constructive criticisms.

Last but not least, I would not have contemplated this road if not for the inspiration and moral support received from my family.

TABLE OF CONTENTS

LIST OF TABLES

LIST OF FIGURES

xi

APPENDICES

LIST OF ABBREVIATIONS

AC	Alternating current
ADC	Analogue to Digital Converter
ANFIS	Adaptive Neuro-Fuzzy Inference System
ANN	Artificial Neural Network
BLDC	Brushless Direct Current
BSS	Broadcast Satellite Service
C/N	Carrier to Noise Ratio
DAC	Digital to Analogue Converter
DC	Direct Current
DE	Change in Error
DOF	Degrees of Freedom
DSS	Digital Satellite Service
DTH	Direct-to-Home
E	Error
FLC	Fuzzy Logic Control
FL	Fuzzy Logic
FSS	Fixed Satellite Service
FTC	Fault Tolerant Control
GEO	Geostationary Orbit
GPS	Global Positioning System
GUI	Graphical User Interface

LEO	Low Earth Orbit
LoS	Line of Sight
LQG	Linear Quadratic Gaussian
LQR	Linear Quadratic Regulator
MEO	Medium Earth Orbit
MPC	Model Predictive Control
MSS	Mobile Satellite Service
NB	Negative Big
NFSC	Neuro Fuzzy System Controller
NM	Negative Medium
NNC	Neural Network Control
NN	Neural Network
NS	Negative Small
PB	Positive Big
PI	Proportional Integral
PID	Proportional Integral Derivative
PM	Positive Medium
PS	Positive Small
PWM	Pulse Width Modulation
RADAR	RAdio Detection And Ranging
RSL	Received Signal Level
USB	Universal Serial Bus

VSAT	Very Small Aperture Terminal
Z-N	Ziegler Nichols
ZR	Zero

LIST OF NOMENCLATURES

A_v Average value

B_m Viscous friction coefficient (Nms/rad)

E_b Back electromotive force (V)

H_∞ H-Infinity

I_a Armature Current (A)

I_f Field Current (A)

J_m Rotor Inertia (kgm^2)

K_P Proportional gain

K_I Integral gain

K_D Derivative gain

K_B Back electromotive force constant ((Vs)/rad)

K_T Torque constant (Nm/A)

L_a Armature Inductance (H)

M_P Maximum Overshoot ($\%$)

R_a Armature resistance (Ω)

T_m Motor torque (Nm)

t_r Rise Time (sec)

t_s Settling Time (sec)

V_a Armature voltage (V)

θ Rotor shaft angular position (rad)

ω	Shaft angular velocity (rad/s)
X	Reactance (Vars)
e_{ss}	Steady-state error

ABSTRACT

There are increasing needs to develop control systems that can be used to automatically point Direct Current (DC) servo motor driven parabolic antennas to moving targets, notably in satellite tracking. This is in order to maintain the desired Line of Sight (LoS) and Received Signal Level (RSL) to guarantee quality communication. The problem is to design a reliable closed-loop control system with suitable algorithms to achieve accurate dish positioning and the establishment of a strong communication link between an earth station and a target over 400km in space. Conventional methods such as the three term Proportional Integral Derivative (PID) controller have been applied to this problem, mostly due to its simplicity and low cost. However, such techniques have failed to work for nonlinearities associated with servo motor such as saturation, backlash, friction, inertia, mechanical parameter variation and un-modeled dynamics which lead to lack of precise mathematical model. The aim of this research is to design a Neuro-Fuzzy System Controller (NFSC) which can be applied to a DC servomotor-based parabolic dish antenna positioning system.

To achieve this, first, a Fuzzy Logic Controller (FLC) was designed using expert knowledge. Next, NFSC was designed based on the FLC algorithms by employing Neural Network (NN) learning to tune the Fuzzy Logic (FL) rule base through hybrid training technique. The architecture of the antenna control system utilized Adaptive Neuro-Fuzzy Inference System (ANFIS) design environment of MATLAB/SIMULINK. The advantage of using NFSC method is that it has a high degree of nonlinearity tolerance, learning ability and solves problems that are difficult to address with the

conventional techniques such as PID. For convenience, experiments were conducted offline based on the DC servo motor other than with a live antenna load. The results obtained were compared with those of a conventional PID controller as part of analysis. It was observed that the NFSC method was able to work for the nonlinear parameters and dynamic factors involved in the original DC servo motor system. Consequently, as seen from the results obtained, it achieved the desired output DC servomotor position with reduced rise time, settling time and overshoot in comparison with the PID controller. In an online system an antenna is treated as the load which is directly coupled to the DC servomotor shaft. Therefore, the ability of the developed NFSC to accurately control the antenna azimuth and elevation positions based on the location of satellite under interest with respect to the earth station antenna site was tested.

CHAPTER ONE

INTRODUCTION

1.1. Background Information

Parabolic antennas mounted at earth stations which are commonly used in satellite tracking applications, are prone to suffer from environmental disturbances [1]. For many years DC servo motor based controllers have been applied in closed loop control systems to position the satellite dishes [2]. However, servo motor systems are known to have nonlinear parameters and dynamic factors, such as saturation, backlash and friction that make it difficult to control the systems using conventional control methods such as Proportional-Integral (PI) and Proportional Integral Derivative (PID) controllers [3], [4]. Several controller models have been developed over time to solve the problem of antenna pointing in satellite and movable targets tracking using servomechanism [5], [6] and [7]. Recently, new intelligent control techniques such as Neural Networks, Genetic Algorithms and Fuzzy Logic methods are under research consideration as a viable solution to the problem [8], [9] and [10]. Although Fuzzy Logic Controller (FLC) has proven effective for complex, nonlinear and imprecisely defined systems still there are difficulties of derivation of correct fuzzy logic rules and difficulties in tuning parameters of the controller. Artificial Neural Networks (ANN) on the other hand, though it reduces development time and cost, it does not explain the way decisions have been reached.

1.2. Problem Statement

The ability to maintain communication over long distances beyond 550km in space for moving targets and satellites has always been a challenge. For instance, in mobile platform satellite communication, receiver systems are mounted on the movable device

such as ship, train, car or airplane. For a seamless reception of signals, the antenna system must be steered in both azimuth and elevation angles to track a specified satellite or target [1], [2], [3] and [4]. The most common problem when aligning a dish is aiming at the correct satellite or target for the broadcasts required. The problem can be addressed by developing a dedicated control algorithm that uses the received signals from the satellite to control a DC servo motor system which will in turn point the antenna to the desired position. On the other hand, a DC servo motor control system suffers from disturbances and errors caused by nonlinear variations in load conditions, motor saturation, backlash, friction and wind pressures and gusts.

For a long time, classical controllers such as PID control have been utilized mostly due to low cost and simplicity. However, the PID controller is poor at dealing with nonlinearities and disturbances and also requires an accurate mathematical model of the system which may not be practically realizable. Such weaknesses of the PID controller have made the Fuzzy Logic Controllers (FLC) a viable alternative [10] and [11]. The FLC can handle problems with nonlinearities, imprecise and incomplete data, uncertainties and vague description of the system because it uses expert knowledge based on fuzzy rules with linguistic labels. However, the main drawback of FLC is that it usually takes a lot of time to design and tune the membership functions which quantitatively define the linguistic labels. Neural Network learning techniques can automate this process and substantially reduce development time and cost while improving performance but it will not explain how decisions have been made. These limitations formed a central driving force behind the Neuro-Fuzzy System Controller under study in this research. Consequently, the NFSC has been used to merge

advantages of FLC with those of Artificial Neural Networks (ANN) and its performance investigated in comparison with the PID controller for bench-marking purposes.

1.3. Justification

In a motorized parabolic dish satellite tracking application, the most common conventional method is the PID controller owing to its low cost and ease of implementation but it can only be designed for linear conditions using precise mathematical models. However, in the case servo motor system internal nonlinearities such as saturation, backlash and friction as well as external disturbances like wind pressures cause error in achieving desired output motor position. The NFSC method adopted in this research offers the following benefits over existing strategies:

1) It takes care of the operational knowledge of the dynamical servo system as it is a knowledge-based approach.

2) There is no need of precise system mathematical model.

3) It can work for the stated nonlinearities and external disturbances.

4) The approach combines the mapping and learning ability of ANN with the linguistic and fuzzy inference advantages of FL.

5) It is more accurate in achieving target position with not only reduced overshoots and settling times but also faster rise times as compared to the PID controller.

1.4. Objectives of the Research

1.4.1. Main Objective

To design Neuro-Fuzzy System Controller for controlling the position of DC servo motor to achieve desired antenna elevation and azimuth orientation in a satellite tracking system.

1.4.2. Specific Objectives

1. To design a DC servo motor Fuzzy Logic Controller using expert knowledge and simulate in MATLAB/SIMULINK.

2. To design a DC servo motor Neuro-Fuzzy System Controller and simulate in MATLAB/SIMULINK.

3. To implement the designed controller and compare performance with conventional PID controller.

1.5. Scope of the Study

This work has covered how mathematical modeling of a practical DC servomotor based parabolic antenna positioning and tracking system can be carried out. This enabled the said system to be represented in terms of a transfer function. Focus was made on the control system design which included PID, FLC and NFSC control strategies, each algorithm developed and applied in turn to the system in MATLAB/SIMULINK simulation environment and the obtained results were analyzed. A prototype was developed using Arduino Mega 2560 microcontroller and other components. This was then used to test the NFSC performance off-line with Spring SM-S4309M DC servomotor from which experimental results were obtained. Since the dish was

considered off-line the aspect of real time telecommunication signal tracking has not been covered as it is beyond the scope of this study.

1.6. Organization of Thesis

The thesis is organized into five chapters including the chapter of introduction which forms Chapter 1. Chapter 2 deals with Literature Review. Here, an overview of related work, DC servomotor, Fuzzy Logic, Neuro-Fuzzy Systems and satellite dish tracking basics are covered as well as the research gaps are presented. Chapter 3 handles methodology. First, it describes modeling and analysis of satellite tracking antenna control system and design of a PID Controller for the same system. Secondly, Fuzzy Logic Controller and NFSC are designed and separately applied to the system. Finally, the MATLAB/SIMULINK models created and the overall experimental setup developed on a simplified prototype deploying an Arduino hardware model for off-line investigations of NFSC are presented. Chapter 4 presents the results obtained from the simulation models as well as those obtained from the experimental prototype developed. The performance of FLC and NFSC is compared with that of conventional PID controller. The comparison is done in a MATLAB/SIMULINK environment and the results are verified. Chapter 5 concludes the work performed in the study based on results obtained and also highlights the possible limitations. Moreover, further research work that can be carried out to improve the present scenario is mentioned. This section is followed by the reference materials that have been used in the development of the thesis. Finally, appendices are given which outline the supplementary experiments and

results obtained with the selected DC servomotor, Ziegler-Nichols PID Tuning Method as well as the NFSC training, testing and checking data.

1.7. Motivation

Apart from the need to automatically point parabolic antennas utilized in satellite communication, radio telescopes as well as tracking of satellites or moving targets, the same have to be aligned at line of sight for their successful operation in the presence of uncertainties and nonlinearities [8]. This calls for a suitable control system to perform the positioning task. However, technology has kept evolving, therefore classical control strategies have to be replaced by new intelligent controllers to counteract these challenges. This forms the basis of the problem addressed by this research.

1.8. Contribution of the Thesis

The key contribution made through this research work is the development of a NFSC with better dynamic performance and response to the nonlinearities of a DC servo motorized parabolic antenna pointing in terms of reduced rise time, settling time and percentage overshoot as compared to the most common classical PID controller. Also, the dependency of the DC servo motor Fuzzy Logic Controller performance on the knowledge level of the control human expert has been greatly reduced by fusing ideas of FLC and ANN to form NFSC.

CHAPTER TWO

LITERATURE REVIEW

This chapter presents existing control techniques for motorized parabolic antenna systems, related satellite and dish pointing concepts and Arduino Library in MATLAB.

2.1. Review of Existing Strategies for Parabolic Antenna Control

This section gives a brief overview of the various methods used by the researchers in the field of control systems to solve for antenna positioning and tracking problems [8]. In order to make understanding easier, the main techniques used are categorized into the following four groups: Linear Control, Adaptive Control, Artificial Neural Networks and Fuzzy Logic Control Approach.

2.1.1. Linear Control Approach

This approach uses the linear control theorems and approaches for control system analysis and design [3], [5], [6], [7], [12] and [13]. Different control methods have been used for the positioning/tracking control of the parabolic dish antenna system to improve the precision and system response to both internal and external disturbances.

M. N. Soltani, et al [3] considers the case of overseas satellite telecommunication where the control system directs on-board motorized antenna towards a selected satellite in the presence of disturbances from the high sea waves. Fault Tolerant Control (FTC) system is designed to maintain the tracking functionality. The effectiveness of this method is tested using the ship simulator facility. However, the fault estimation has proved to be an extremely challenging task. Consequently, the team proposed use of fault estimation in an adaptive reconfiguration system as future research.

The problem presented to Liu Xuan, et al [5] was to analyze and implement a controller on an off the-shelf antenna azimuth position control system. They analyzed the open-loop and closed-loop characteristics of the system and determined the most stable and implementable controller. The suggested solution was to implement a PID controller between the power amplifier and the preamplifier as shown in Figure 2.1. This allowed for better stability and response times as was observed from the MATLAB simulations.
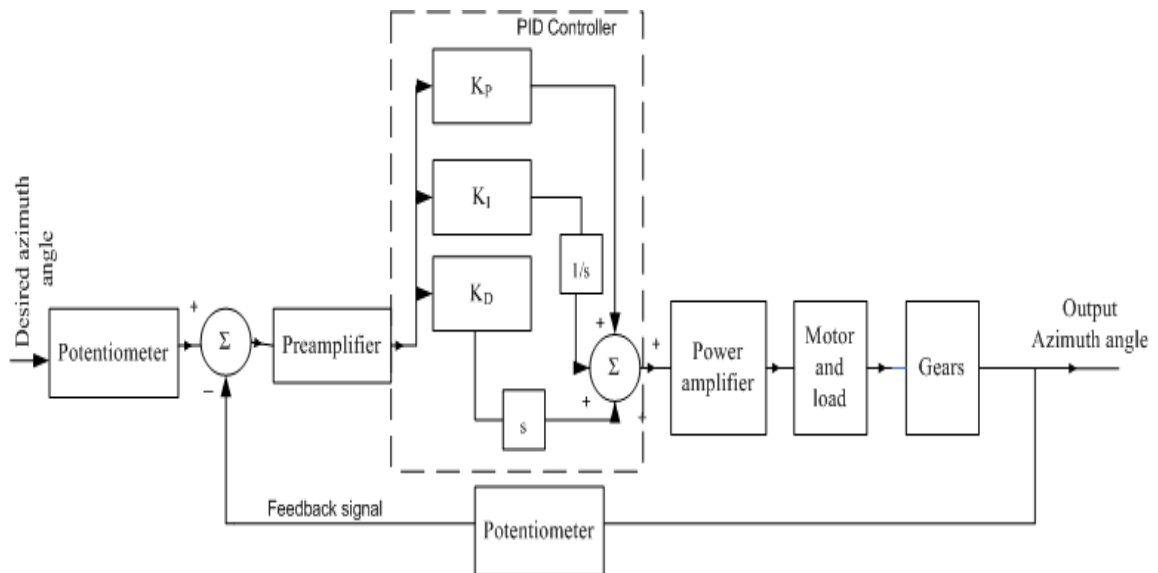
Figure 2.1: Antenna Azimuth Position Control System Block Diagram

S. S. Sheth and S. K Gonsai [6] provided an overview of different antenna pointing mechanisms modeled and implemented for varied space applications. Traditionally, servo systems with DC motors or hydraulic actuators are used for antenna driving and different control algorithms: PI, PID, Linear Quadratic Gaussian (LQG), is used to improve performance of the pointing systems. PI controllers are easy to implement but take much time to reach set point and have degraded performance under system

8

nonlinearities. LQG controllers are not only optimal but also have the ability to estimate non-measurable states by using observers to reconstruct them and provide better performance in case of wind gusts noise. As future work, they proposed the use of stepper motors which provide good torque, to replace DC motor and servos which adds backlash and friction.

C.H. Chang, et al [7] designed discrete-time controller for tracking of a target communication satellite using the sampled-data H-Infinity (H_∞) control theory along with the reference signal generated by an improved conventional step tracking algorithm. This controller demonstrated superior robustness for the longer sampling period when compared with a simple PID controller. However, the performance of the antenna tracking system largely depends on step sizes, with smaller step sizes creating computational delay. Further work is needed to design attitude correction systems so that surface vehicles such as ships may receive satisfactory satellite broadcasts.

An H-infinity controller was proposed by W. Gawronski, [13] for tracking operation of the DSS-13 antenna with the aim of reducing disturbances due to wind. The H-infinity controller shows superior performance in terms of wind disturbance rejection and stability, followed by the linear-quadratic-Gaussian (LQG) controller and then the proportional-integral (PI) controller.

2.1.2. Adaptive Control Approach

The adaptive control strategy [14], [15], [16], [17] is an online control parameter estimation method based on certain system measured parameters and originated seven decades ago. The control method has been applied to systems with constant or varying

uncertain parameters such as ship and aircraft steering, robots and processes control. An adaptive controller may be designed using either model reference method or the self tuning method [14]. It is used by H.S.Ahn, et al. [15] for tracking control of a dish antenna system in order to establish reliable communication with a low orbit satellite. Simulation results have shown that the control system was stable and did well in eliminating disturbances.

Jia, et al. [16] developed satellite antenna position controller using adaptive variable structure with the aim of getting rid of the problem of model uncertainties which was achieved using the feed-forward compensation technique. Tests were conducted using the satellite antenna pointing compound full-physical simulation system and results showed that the controller had improved the pointing accuracy of the system.

2.1.3. Artificial Neural Networks Approach

Artificial Neural Network (ANN) mimics how the central nervous system of the human body functions. It was applied in control systems as far back as 1964 [22].

Artificial Neural Network (ANN) is a very powerful tool to solve complex problems and therefore complex control systems. Main advantages of ANN include:

1. Very high speed of operation: Ability to accept large data and process it at one time owing to parallel structure.

2. Is capable to generalize, which makes it act as a smart controller. This means that the controller is able to deal with new type of input data and decides how to deal with any change in the non-linear parameters to reduce their effect.

3. In case failure occurs the effects are not sudden and will not lead to complete failure.

The basic structure of an ANN, shown in Figure 2.3, is composed of three layers, namely: input layer, hidden layer and output layer. The input layer has to accept the input data; which are the training set of data, or the set of data that will be used to simulate the network. The hidden layers (there may be several layers), are used to modify the inputs and define the interconnections of the neurons; and the final layer is the output layer that produces the single output of the ANN [23].

INPUTS   HIDDEN LAYER   OUTPUTS
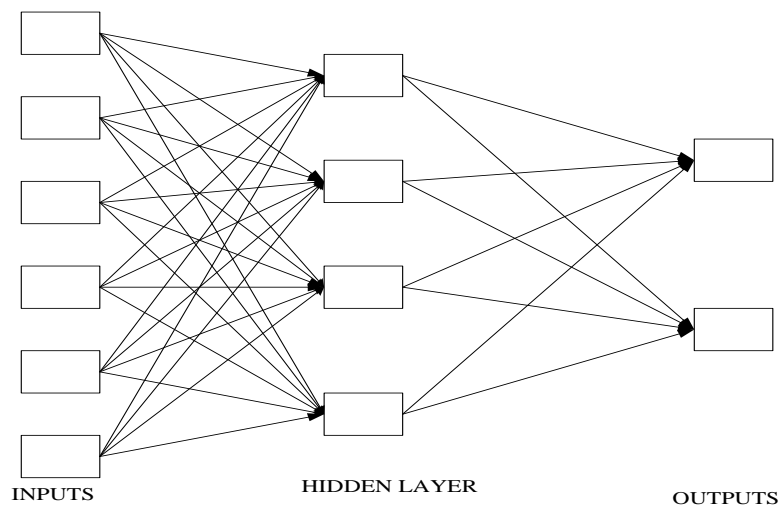
Figure 2.2: Basic Artificial Neural Network (ANN) Structure

The ANN was used by M. Palamar [24] in his paper. An antenna tracking controller was implemented for remote sensing of the earth using the low earth orbit satellites. Simulation results portrayed that aims of the study were achieved.

T. B. Reddy, et al [21] presented a Brushless DC (BLDC) motor drive performance with ANFIS controller under varying operating conditions. The dynamic characteristics of the BLDC motor such as speed, torque, current and voltages of the inverter components are observed and analyzed. It is observed that the performance of the drive is improved with ANFIS controller when compared to PID controller.

The main shortcoming of ANN in control of DC servomotors is that it usually treats the servo system like a black box. This means that it hides some vital information from the user such as on how it arrives at a conclusion thus making it extremely difficult for the designer to comprehend how it manages to handle the error in the system.

2.1.4. Fuzzy Logic Control Approach

Lotfi A. Zadeh was first researcher to develop the Fuzzy logic in 1965 which he presented as a research paper and later gave further explanations in another paper presented in 1973. It was first applied in the manufacturing industry in 1975 when it was used in a cement kiln in Denmark. A Fuzzy Logic Controller is a controller that is intended to manage some vaguely known or vaguely described process. It has numerous advantages which make it suitable for many engineering applications, some of which are it allows for high level of automation since it can handle imprecise and incomplete data, achieving robust nonlinear control and it is easier to adjust the control algorithms in the program [22]. Figure 2.2 is a block diagram of a FLC system showing its various elements [11]. The controller can be used with the process in two modes:

- Feedback mode when the Fuzzy Controller determination acts as a control device.
- Feed forward mode where the controller can be used as a prediction device.

The Fuzzy Controller has four main components [11]:

1. Fuzzification Interface: The fuzzification interface performs a conversion from a crisp point into a fuzzy set. The shapes of the membership functions of the linguistic sets are determined according to the expert experience.
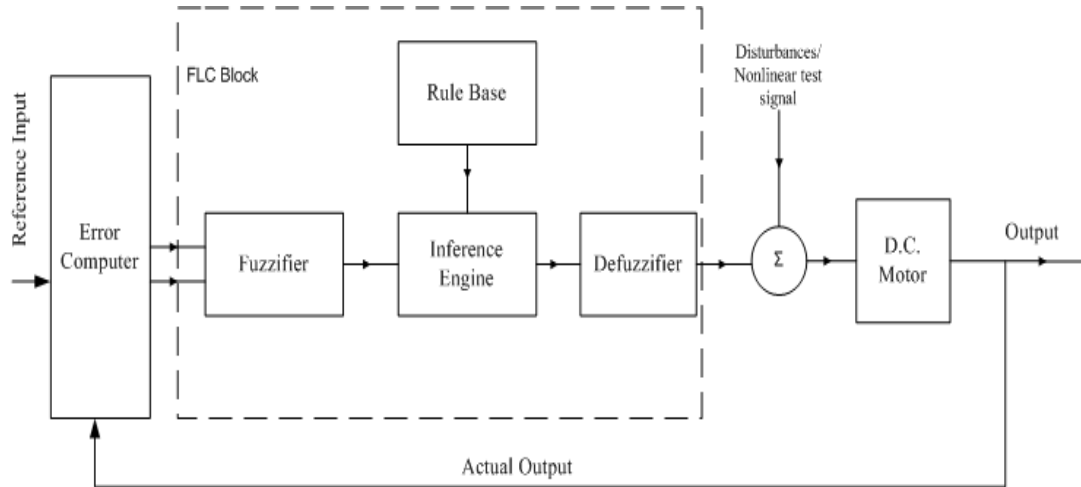
Figure 2.3: Block Diagram of a Fuzzy Logic Control System

2. Knowledge Base: The knowledge base commonly consists of two sections: a database and a rule-base. The database contains the membership functions of the fuzzy sets used in the fuzzy rules and the rule-base contains a number of fuzzy IF-THEN rules.

3. Inference Engine: Inference Mechanism or Engine is the processing program in a Fuzzy Control system. It derives a conclusion from the facts and rules contained in the knowledge base using various human expert techniques.

4. Defuzzification Interface: Defuzzification is a process that maps a fuzzy set to a crisp set. Four most common defuzzification methods:

    a) Max membership method

    b) Center of gravity method

    c) Weight average method

    d) Mean-max membership method

13

J.K Kim, et al [1] designed Fuzzy-PID controller using step tracking algorithm for a 2-axes data link antenna system mounted on movable targets such as ships and spacecrafts. For these cases, the problem arises from the instability owing to the vehicle's roll, pitch and yaw motion. The computer simulated results showed superior performance compared to the conventional PID controller. However, the fuzzy rule base chosen limited performance of the antenna tracking system in the presence of increased disturbances.

T.V. Hoi, et al [4] discussed the results of study, design and manufacture of a satellite searching and tracking system used for mobile receiver. This system applies both the traditional PID control and the Fuzzy PID control methods. First, the PID controller was designed by Ziegler Nichols (Z-N) tuning method to obtain control parameters.

Then, a Fuzzy Controller was applied to tuning online parameters of the PID controller. Simulated and experimental results indicate that the system performances obtained from applying the fuzzy PID controller were better than traditional PID controller.

In [9], a study on position control problem for DC servo motor is presented where three different motion controllers: PI, FLC and Adaptive Neuro Fuzzy Inference System (ANFIS) controllers were designed and simulated in MATLAB under variable conditions. Results showed that at 3Nm load the PI controller position response is stabilized at 0.4 second but with overshoot. At the same working conditions, no overshoot is observed for FLC and ANFIS controllers.

A.K. Pandey [10] presents efficient method for speed control of a separately excited DC motor using FLC. The simulation results show significant improvement in maintaining system performance. However, the controllers based on Fuzzy Logic theory are used only in simple configurations and their analytic knowledge is still poor.

M.C. Rafael et al [23], developed an automated system for maneuvering of a parabolic reflector antenna of a satellite communication in Brazil. The approach adopted a Fuzzy Logic Controller possessing 63 rules that were generated on the basis of the rules of thumb applicable to the manual process of maneuvering a satellite dish. The solution resulted in better placement of the antenna and hence achieving a Carrier to Noise (C/N) ratio which was above the set minimum of $\geq 8dB$ for good reception. An experiment was also conducted and the results showed a perfect match between the automated process which took only about 3 minutes compared to the manual dish positioning process that took about 50 minutes.

A. H. Vardhan, et al [24] designed and implemented Fuzzy PID controller to track the changes occurred in position of DC motor. MATLAB/SIMULINK simulation results proved that the Fuzzy PID control method is more effective way to enhance stability of time domain performance of the DC motor. As future work, they propose that the position of DC motor can be controlled by using adaptive controllers like Neuro-Fuzzy, Model Predictive Control (MPC) and self-tuning regulator.

Fuzzy Logic approach was also used by [25] in their work of antenna azimuth position control. The FLC outperformed the PID controller based on reduced settling time and maximum overshoots.

The main setbacks of FLC in control of DC servomotors are that it is difficult to generate accurate rule base and tune the controller parameters to ensure accurate and smooth position and velocity control of the motor and its load.

2.2. Preference of Servo motors to Stepper motors

In this study, the DC servo motors were preferred to the stepper motors because of the following reasons:

1. Servo motors consume power only to rotate to the commanded position but consume no power in rest position. Stepper motors run warm and draw more current (power) to lock in and hold the commanded position.

2. Stepper motors are often used in open-loop position control, with the number of steps of movement already specified. This then requires the controller to be able to tell the position of the stepper motor on power up. A servo motor will immediately turn to whatever angle the controller instructs it to, regardless of the initial position at power up.

3. A stepper motor lacks feedback which limits its performance to driving a load that is well within its capacity; otherwise missed steps under accelerating load may occur leading to positioning errors. The encoder and controller of a servo

motor though additional cost, relatively optimize the performance of the overall

system.

4. Stepper motors suffer from vibration and resonance problems at certain speeds

or load dynamics causing skipped steps, stalling, excessive vibration and noise.

2.3. DC Servo Motor Description

Electric motors can be classified by their functions as servomotors, gear motors, and so

forth, and by their electrical configurations as Direct Current (DC) and Alternating

Current (AC) motors [9]. A further classification can be made as single phase and poly-

phase with synchronous and induction motors in terms of their operating principles for

AC motors, and Permanent Magnet and shunt DC motors for DC motors. Servomotor is

an automatic device used for position or speed control in closed loop control systems as

shown in Figure 2.4.
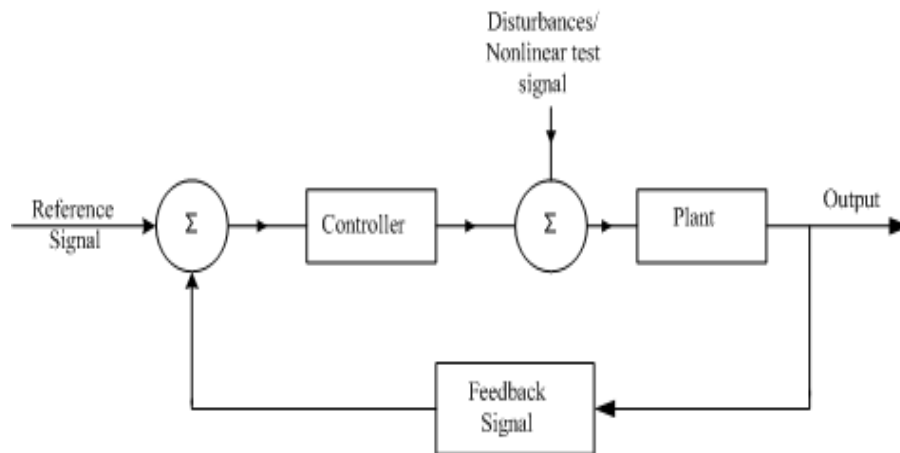
Figure 2.4: Servo Mechanism Basic Structure

The requirement from a servomotor is to turn over a wide range of speeds and also to

perform position and speed instructions given. Usually, servos operate on the principle

of negative feedback, where the control input is compared to the actual position of the

mechanical system as measured by some sort of transducer at the output. Any difference between the actual and wanted values (error signal) is amplified and used to drive the system in the direction necessary to reduce or eliminate the error. Today, DC servo motors have been used in disc drives of computers, numeric control machines, industrial equipment, satellite tracking antennas, weapon industry, speed control of alternators, control mechanism of full automatic regulators as the first starter and starters [10]. In the field of control of mechanical linkages and robots, research works are mostly found on DC motors. Figure 2.5 shows a typical model of a servomotor system [25], [26] and [27]. Servomotor has two main components: the first is the electrical component, which consists of armature resistance R_a (Ω), armature inductance L_a (H), armature voltage V_a (V) and the back electromotive force E_b (V). The second component of the servomotor is the mechanical part, from which we get the useful mechanical rotational movement at the shaft. The mechanical parts are the motor's shaft, inertia of the motor and load inertia J_m (kgm^2) and viscous friction coefficient B_m (Nms/rad). θ (rad) refers to the angular position of the output shaft which can be used to find the angular speed of the shaft ω(rad/s).
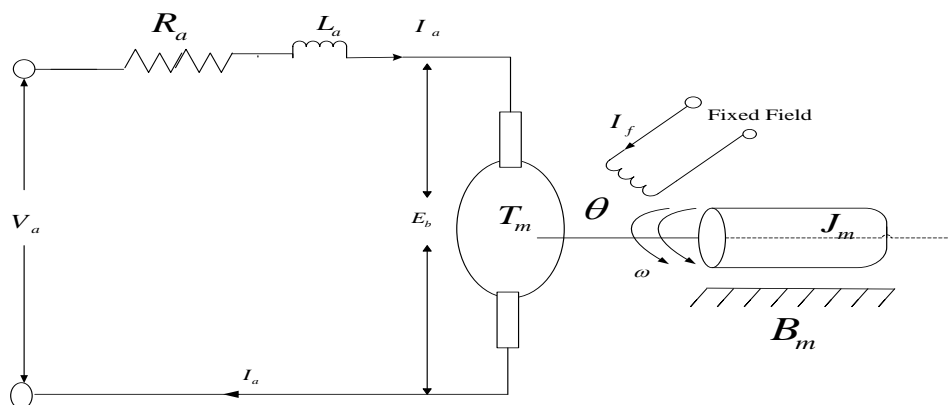
Figure 2.5: DC (servo) motor Circuit Diagram

18

2.4. DC Servo Motor System Equations

For an armature controlled separately excited DC motor, the voltage applied to the armature of the motor is varied without changing the voltage applied to the field. Using Kirchhoff's Voltage Law, the output voltage and motor torque is related to equation (2.1). The motor torque T_m, is related to the armature current I_a by a constant factor K_T given in equation (2.2).

$$V_a(t) = R_a I_a(t) + L_a \frac{dI_a(t)}{dt} + E_b(t) \tag{2.1}$$

$$T_m(t) = K_T I_a(t) \tag{2.2}$$

Also, the back electromotive force (e.m.f) E_b is related to the angular velocity by equation (2.3). On the basis of Newton's Law combined with the Kirchhoff's Law equations (2.4) and (2.5) are obtained.

$$E_b = K_B \omega = K_B \frac{d\theta}{dt} \tag{2.3}$$

$$J_m \frac{d^2\theta}{dt^2} + B_m \frac{d\theta}{dt} = K_T I_a(t) \tag{2.4}$$

$$L_a \frac{dI_a(t)}{dt} + R_a I_a = V_a - K_B \frac{d\theta}{dt} \tag{2.5}$$

To obtain transfer functions, Laplace transform is applied to equations (2.4) and (2.5) to get:

$$J_m s^2 \theta(s) + B_m s\theta(s) = K_T I_a(s) \tag{2.6}$$

$$L_a s I_a(s) + R_a I_a(s) = V_a(s) - K_B s\theta(s) \tag{2.7}$$

where s denotes the Laplace operator. Making current the subject in equation (2.7):

$$I_a(s) = \frac{V_a(s) - K_B s\theta(s)}{R_a + L_a s} \tag{2.8}$$

19

Substituting equation (2.8) in equation (2.6) generates equation (2.9):

$$J_m s^2 \theta(s) + B_m s \theta(s) = K_T \frac{V_a(s) - K_B s \theta(s)}{R_a + L_a s} \qquad (2.9)$$

Figure 2.6 is a block diagram of a DC (servo) motor system showing elements of the transfer function.
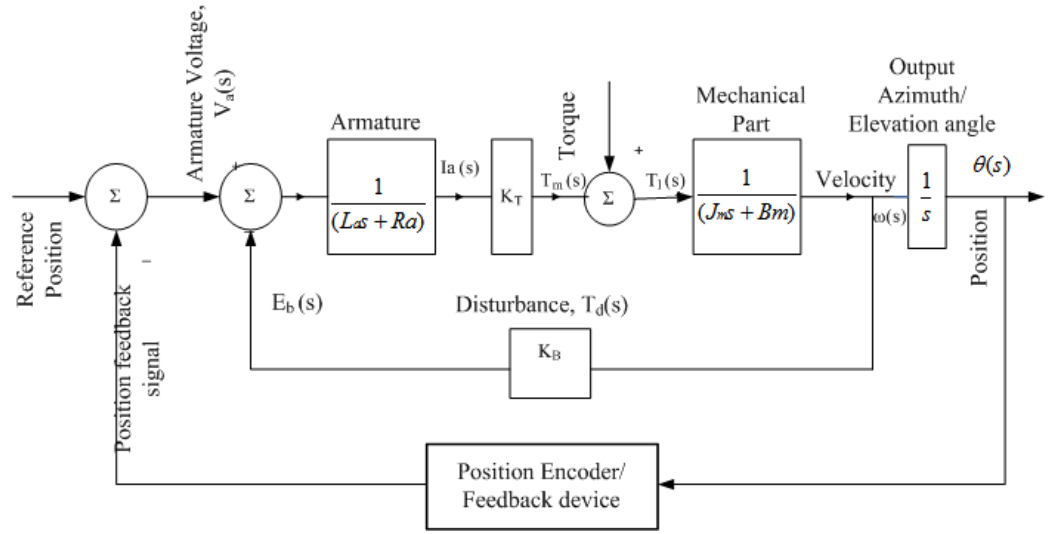
Figure 2.6: Block Diagram of DC (servo) motor Transfer Function System

From equation (2.9), the transfer function from the input voltage, $V_a(s)$, to the output angle θ directly follows equation (2.10):

$$G_a(s) = \frac{\theta(s)}{V_a(s)} = \frac{K_T}{s[(R_a + L_a s)(\ J_m s + B_m) + K_T\ K_B]} \qquad (2.10)$$

In addition, by multiplying the output angle equation by s, the transfer function from the input voltage, $V_a(s)$, to the angular velocity, ω is obtained as in equation (2.11).

$$G_v(s) = \frac{\omega(s)}{V_a(s)} = \frac{K_T}{[(R_a + L_a s)(\ J_m s + B_m) + K_T\ K_B]} \qquad (2.11)$$

20

2.5. Combining Neural Networks and Fuzzy Systems

Neural networks automatically acquire knowledge courtesy of the training algorithm utilized. However, the learning process is relatively slow and analysis of the trained network is difficult. Fuzzy systems on the other hand are more favorable in that their behavior and action can be explained based on linguistic variables termed fuzzy rules and thus their performance can be adjusted by tuning the rules. In Neuro-Fuzzy Systems, Neural Networks are incorporated into fuzzy systems which can acquire knowledge automatically by learning algorithms of neural networks [28]. Generally, all the combinations of techniques based on neural networks and fuzzy logic are referred to as Neuro-Fuzzy Systems. The different combinations of these techniques can be divided into the following classes. Neural Fuzzy Systems, Fuzzy-Neural Networks and Fuzzy-Neural Hybrid Systems [29].

2.5.1.   Neural Fuzzy Systems

Neural Fuzzy Systems, whose block diagram is shown in Figure 2.7, are characterized by the use of Neural Networks (NN) to furnish fuzzy systems with a kind of automatic tuning strategy, but without varying their functionality. The Neural Network simulates the processing of a fuzzy system in which the neurons of the first layer are responsible for the fuzzification process [29]. The neurons of the second layer represent the fuzzy words used in the fuzzy rules. Finally, the neurons of the last layer are responsible for the defuzzification process. This kind of combination is mostly used in control applications. For instance in [30], it is used to control speed of a DC motor.
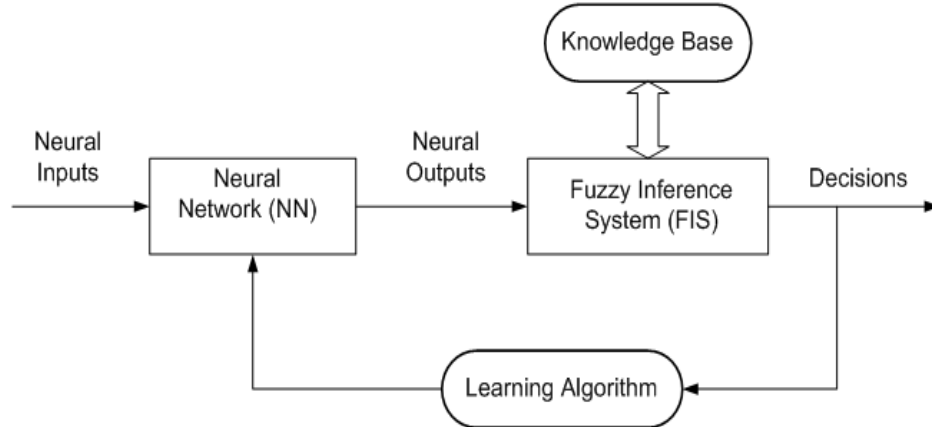
Figure 2.7: Block diagram of a Neural Fuzzy System

2.5.2. Fuzzy-Neural Networks

The main goal of this approach is to `fuzzify' some of the elements of NN, using fuzzy logic. In this case, a crisp neuron can become fuzzy. Figure 2.8 shows the block diagram of this scheme.
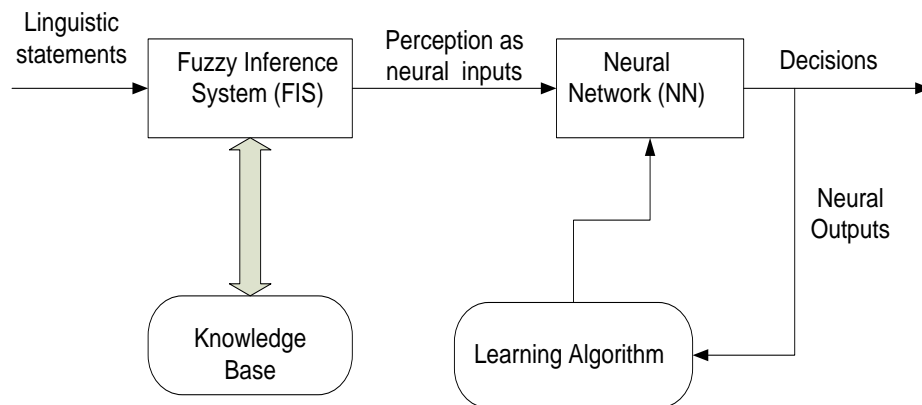
Figure 2.8: Block diagram of a Fuzzy Neural Network

Since Fuzzy Neural Networks are inherently Neural Networks, they are mostly used in Pattern Recognition Applications. In these fuzzy neurons, the inputs are non-fuzzy, but the weighting operations are replaced by membership functions. The result of each weighting operation is the membership value of the corresponding input in the fuzzy set [28] and [29].

2.5.3. Fuzzy-Neural Hybrid Systems

In this approach, a hybrid system is formed in which both fuzzy and neural networks techniques retain their designated features. Each one performs its own task in accomplishing various functions in the system, incorporating and complementing each other in order to achieve a common goal. The idea of a hybrid model lies in the interpretation of the fuzzy rule base in terms of a neural network. In this way the fuzzy sets can be interpreted as weights, and the rules, input variables, and output variables can be represented as neurons [29]. The learning algorithm results, like in neural networks, in a change of the architecture, i.e. in an adaption of the weights, and/or in creating or deleting connections. These changes can be interpreted both in terms of a neural net and in terms of a fuzzy controller. This last aspect is very important as the black box behavior of neural nets is avoided. Hybrid neuro-fuzzy controllers are realized by approaches like Fuzzy Adaptive Learning Control Network (FALCON), Generalized Approximate Reasoning based Intelligence Control (GARIC) and Adaptive Neuro-Fuzzy Inference System (ANFIS) models [29]. The majority of the researchers use the neuro-fuzzy term to refer only to hybrid Neuro-Fuzzy System.

2.6. Arduino Library in MATLAB

MATLAB 2012a and higher versions provide for direct communication with Arduino Uno and Arduino Mega 2560 in SIMULINK. The SIMULINK Support Package for Arduino Hardware allows for creation of algorithms that can communicate with Arduino sensors and actuators through the USB-serial port cable by using inbuilt blocks. Digital and analog data can be easily sent from Arduino to MATLAB and vice versa through

these pins. Other provisions include blocks for servo motor control, pulse width modulated (PWM) signals and serial transmission of data between MATLAB and Arduino. Figure 2.9 depicts the blocks as they appear in MATLAB SIMULINK environment [31].
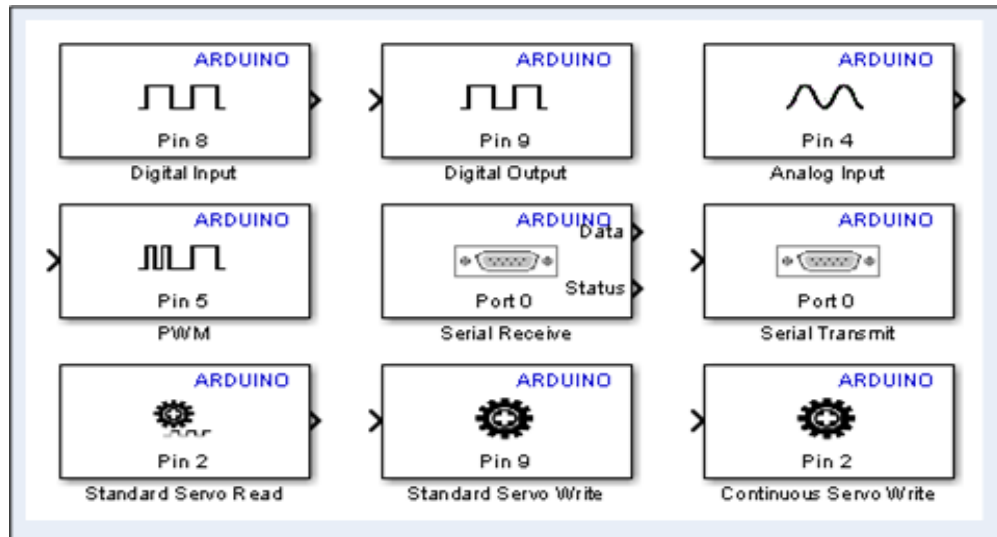
Figure 2.9: Inbuilt blocks for use with Arduino in SIMULINK

2.7. Satellite Communication Basics

A communications satellite is an artificial satellite launched in space for the purposes of telecommunications. It allows communication between various source transmitters and target receivers located at widely separated points on the Earth by amplifying and then relaying the signals. These satellites have several uses, notably serving communication needs in television, telephone, radio, internet and military applications. At the moment, there are more than 2,000 communications satellites in Earth's orbit, utilized by both private and government organizations [32]. Figure 2.10 shows block diagram of how satellite communication system works.
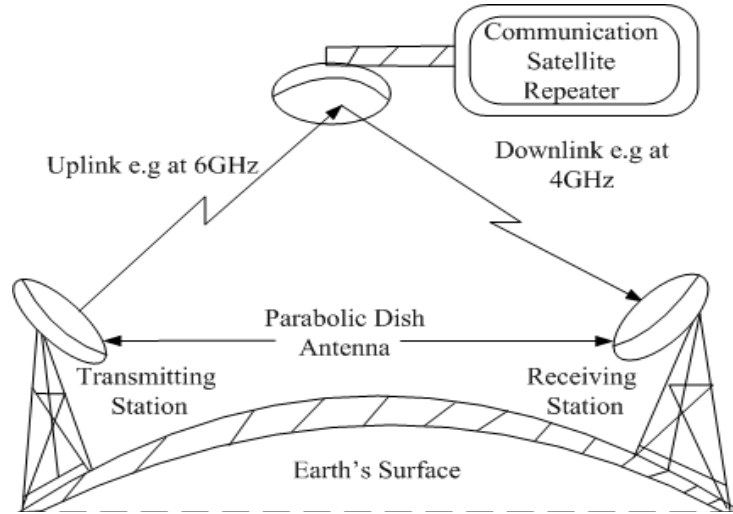
Figure 2.10: Satellite Communication System

A satellite is made up of the following major components: communications system (which consists of the antennas and transponders that receive and retransmit signals), the power system (which includes the solar panels that supply power) and the propulsion system (which includes the rockets that propel the satellite). The original signal being transmitted from the earth station to the satellite is called the uplink and is usually at a higher frequency e.g. 6GHz. The retransmitted signal from the satellite to the receiving stations is called the downlink and is at a lower frequency e.g. 4GHz. The transmitter-receiver set in the satellite is known as a transponder.

There are three altitude classifications for satellite orbits, [33], [34], [35] and [36] as follows:

1. **Low Earth Orbit (LEO)**

   LEO satellites are positioned at an altitude between 160 km and 1,600 km (100 and 1,000 miles) above Earth and take approximately 1.5 hrs for a full orbit. From LEO, a constellation of 20 or more satellites are required to cover the entire earth's surface

[33]. Due to the proximity to Earth, LEO satellites have a lower latency and require less amplification for transmission but need tracking antenna systems [34].

2. **Medium Earth Orbit (MEO)**

MEO satellites operate from 10,000 to 20,000 km (6,300 to 12,500 miles) from Earth. These satellites are traditionally used for Global Positioning Systems (GPS) navigation systems and are sometimes used by satellite operators for voice and data communications. MEO satellites require a constellation of 10 or more satellites to provide continuous coverage and can be used to provide mobile and voice services. Tracking antennas are needed to maintain the link as satellites move in and out of the antenna range [35].

3. **Geostationary Orbit (GEO)**

GEO satellites are positioned at 35,786 km (22,236 miles) above the equator and orbit the earth in the same direction and speed as the earth rotates on its axis taking 24 hours to complete one revolution [35]. This makes it appear to be fixed at the same spot in the sky. At least 3 GEO satellites are required to cover the whole surface of the Earth. Such satellites are mostly used for broadcasting and data applications because of the larger area on the ground that they can cover. However, due to the distance from the earth, there is a longer latency (0.22 seconds). It is important to note that satellites do not operate between LEO and MEO because of the inhospitable environment for electronic components in that area, which is attributed to the Van Allen radiation belt [33].

2.8. Frequency Bands

Communication and military satellites operate at very high radio frequency ranges or bands falling within (1-50GHz). The bands are identified by letters from low to high frequencies as: L-, S-, C-, X-, Ku-, Ka-, and V-bands. Table 2.1 shows Frequency bands available for satellite communication.

Table 2.1: Satellite Communication Frequency Band Designations

S/No.	Band	Frequency Range	Total Bandwidth	General Application
1.	L	1 to 2GHz	1GHz	Mobile satellite service (MSS)
2.	S	2 to 4GHz	2GHz	MSS, NASA, deep space research
3.	C	4 to 8GHz	4GHz	Fixed satellite service (FSS)
4.	X	8 to 12.5GHz	4.5GHz	FSS military, terrestrial earth exploration, meteorological satellites
5.	K_u	12.5 to 18GHz	5.5GHz	FSS, broadcast satellite service (BSS)
6.	K	18 to 26.5GHz	8.5GHz	BSS,FSS
7.	K_a	26.5 to 40GHz	13.5GHz	FSS

Signals in the lower range (L-, S-, and C-bands) of the satellite frequency spectrum are transmitted with low power, and thus larger antennas are needed to receive such signals, e.g. 1.8m for C-band. However, owing to lower frequencies they are less susceptible to adverse weather condition and hence will not suffer from signal fading even in the presence of rainfall. On the other hand, signals in the higher end (X-, Ku-, Ka-, and V-bands) of the spectrum contain more power; therefore, parabolic dishes as small as 0.45m in diameter can receive them. As a result, the Ku-band (dish sizes 0.6m-1.2m) and Ka-band (0.9m-1.2m) spectrum become ideal for direct-to-home (DTH) broadcasting, broadband data communications, and mobile telephony and data

applications. However, they are more susceptible to adverse weather conditions such as rainfall which causes signal fading [33], [34] and [35].

2.9.Antenna Positioning Basics

A ground station, or earth station, is the terrestrial base of satellite communication system. The ground station communicates with the satellite to carry out the designated mission. The earth station consists of five major subsystems: The antenna subsystem, the receive subsystem, the transmit subsystem, the ground control equipment subsystem and power subsystem. Essentially, two angles are necessary to locate a given satellite from a known point on the surface of the earth and hence establish a direct signal path (Line of Sight) between the satellite and earth station antenna. Usually, in order to refer to these look angles; it is customary to use the elevation and azimuth angles [35].

2.9.1. Azimuth

Azimuth is the angle relating to the horizontal positioning of the antenna or dish. The angle is expressed in terms of degrees, with North = 0 degrees, South = 180 degrees (Refer to Figure 2.11). The azimuth would be 180 degrees (relative to true north) if the satellite is at the same longitude that one is on. If the satellite is east, or west, of the said longitude the azimuth will be less than, or greater than 180 degrees respectively [36].

2.9.2. Elevation

This is the angle by which the antenna or dish must be \tilted Up or Down" in relation to the theoretical horizon, in order to position it precisely for the desired satellite. The actual elevation pointing angle to the satellite is determined by user's latitude & longitude and the longitude of the satellite. In general terms the elevation angle will be

low when one is located at high latitudes and will increase as you get closer to the equator [36], (Refer to Figure 2.11). Additionally, from any given latitude, the elevation will be highest when the satellite is at the same longitude that one is situated.
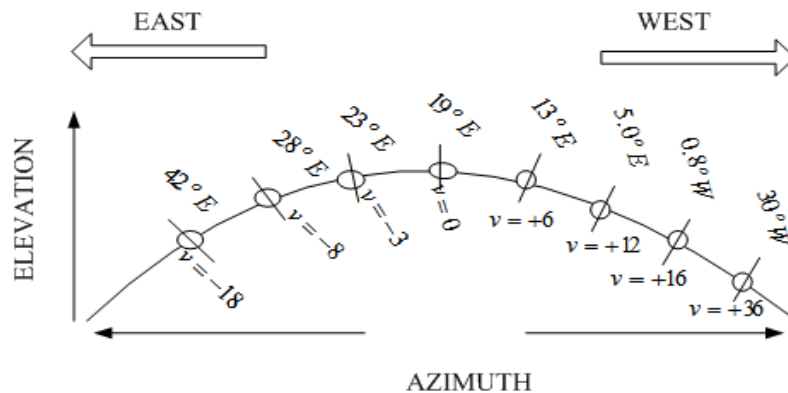
Figure 2.11: Satellite antenna orientation properties

2.9.3. Calculation for the reference position of earth station antenna

With the geographic coordinates of satellite and the ground station, the azimuth angle is given as in equation (2.12) [23], [34] and [35]:

$$\widehat{A} = \arctan\left(\frac{\tan|\theta_s + \Phi_T|}{\sin \theta_T}\right). \tag{2.12}$$

where

θ_T = Latitude of the earth station,

Φ_T = Longitude of the earth station,

θ_s = Longitude of the satellite

For the southern hemisphere with the earth station west of the satellite:

$$A = \widehat{A}. \tag{2.13}$$

For the southern hemisphere with the station east of the satellite:

$$A = 360^0 - \widehat{A}. \tag{2.14}$$

For the northern hemisphere with the earth station west of the satellite:

$$A = 180^0 - \widehat{A}. \tag{2.15}$$

For the northern hemisphere with the earth station east of the satellite:

$$A = 180^0 + \widehat{A}. \tag{2.16}$$

According to [23], [34] and [35] the value of the elevation angle (E) can be obtained from equation:

$$E = \left(\frac{r - R_e.\cos\Phi_T.\cos|\theta_s - \Phi_T|}{R_e\sin\left[\arccos\left(\cos\Phi_T.\cos|\theta_s - \Phi_T|\right)\right]} \right) - \arccos(\cos\Phi_T.\cos|\theta_s - \Phi_T|) \tag{2.17}$$

where:

r = Radius of the geostationary orbit [42,164 km],

R_e = Radius of the Earth [6,378km].

2.9.4. Antenna polarization

The polarization of an antenna refers to the orientation of the electric field (E-plane) of the radio wave with respect to the Earth's surface and is determined by the physical structure of the antenna and by its orientation. Thus, a vertical antenna receives and emits best vertically polarized waves, and a horizontal antenna receives or emits horizontally polarized waves. In the case of parabolic dish antenna a Linear LNB is installed to receive linear polarized satellite signals whereas a circular LNB is used to receive circularly polarized satellite signals [34] and [35].

2.10. Tracking Antenna Systems

An earth station's tracking system, whose pedestal unit is as presented in Figure 2.12, is required to perform some of the functions such as Satellite acquisition, Automatic tracking, Manual tracking and Program tracking.
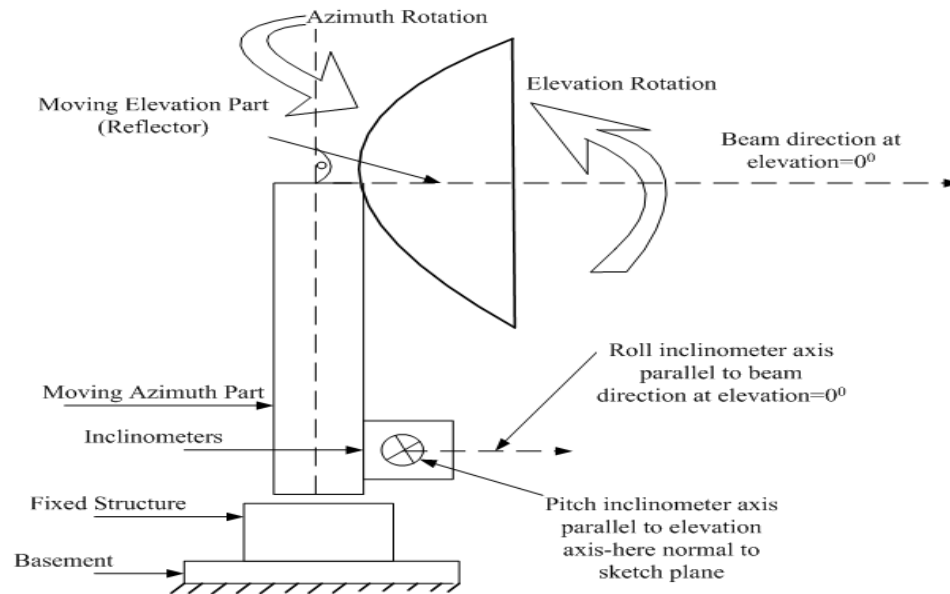
Figure 2.12: Two axis satellite earth station tracking antenna mount

The look angles for the ground station antenna are required so that it points directly at the satellite. These angles change in order to track the satellite. For geostationary orbit, the angle values do not change as the satellites are fixed with respect to earth. Thus large earth stations are used for commercial communications. Communicating with satellites in LEO and MEO requires tracking antennas on the ground to ensure seamless connection between satellites [33]. For home antennas, antenna beam width is quite broad and hence no tracking is essential. This leads to a fixed position for these antennas [34].

2.11. Summary of Research Gaps

The previous research studies related to satellite tracking earth station dish systems have been presented. From these, it is noted that different approaches have been used to control the position of the parabolic dish in order to achieve desired signal line of sight so as to guarantee quality communication. However, a close examination of these strategies from the classical PID to intelligent FLC has revealed that each has its own shortcoming when used on its own. For example, with PID control strategy, the system has to be linear with known mathematical models yet it still suffers from high overshoots in the presence of nonlinearities. On the other hand, FLC though does not require knowledge about the antenna system model suffers from the difficulties in establishing the correct rule base and parameter tuning. ANN approach offers an alternative to FLC with its learning ability but it usually treats the system like a black box hence making it extremely difficult for the designer or operator to understand how it manages to handle the error in the system. Therefore, the current work seeks to fill this gap by developing a NFSC control system that would improve automatic satellite dish positioning. This is made possible by combining the descriptive nature of FLC with the learning ability of the ANN so as to optimize the parabolic dish positioning process without the need for an accurate system model. The controller will minimize DC servomotor positioning errors (hence load) by first learning the process and then using this information to compare desired position with actual position for both the elevation and azimuth motors and hence sending the appropriate control signal to the respective motor drivers within the desired time frames defined in section 3.1.

CHAPTER THREE

METHODOLOGY

This chapter presents the approach adopted in developing a control system with the proposed algorithms to solve the problem of parabolic antenna positioning in a satellite tracking system. The design task began with problem formulation and system modeling followed by the development of control algorithms which include: Proportional Integral Derivative (PID) on one hand, and Fuzzy Logic (FL) and Adaptive Neuro-Fuzzy Inference System (ANFIS) on the other. The algorithms are tested on a DC servomotor-based antenna positioning or tracking system models, both industrial and prototype.

3.1. Antenna Control System Problem Formulation and Set up

Figure 3.1 is the control block diagram of the DC servo motor parabolic antenna pointing system. The basic components are summers, controller, motor driver, nonlinear disturbance, target motors and sensors. The control is triggered by the need to adjust the dish antenna look angles from the earth station i.e. angles of elevation (0^0 to 70^0) and azimuth (0^0 to 180^0) of the antenna (load) in accordance with the changing positions of the target satellite (refer to Table 4.4 for selected satellite locations) to maintain desired line of sight. This is the interpretation of satellite tracking adopted in this study. Moreover, it is important to note that the antenna movements are only applicable to cases of LEO or MEO satellites and are usually performed at low speeds and within the stated range, yet critical precision is required to maintain correct signal levels. If this is not the case, e.g. for GEO satellites, then the control algorithms can be used for a one time automatic dish antenna positioning instead of carrying out the process manually.

The first input to the summer is set position r(t), the desired position at which the azimuth or elevation motor is expected to run to and stop at.
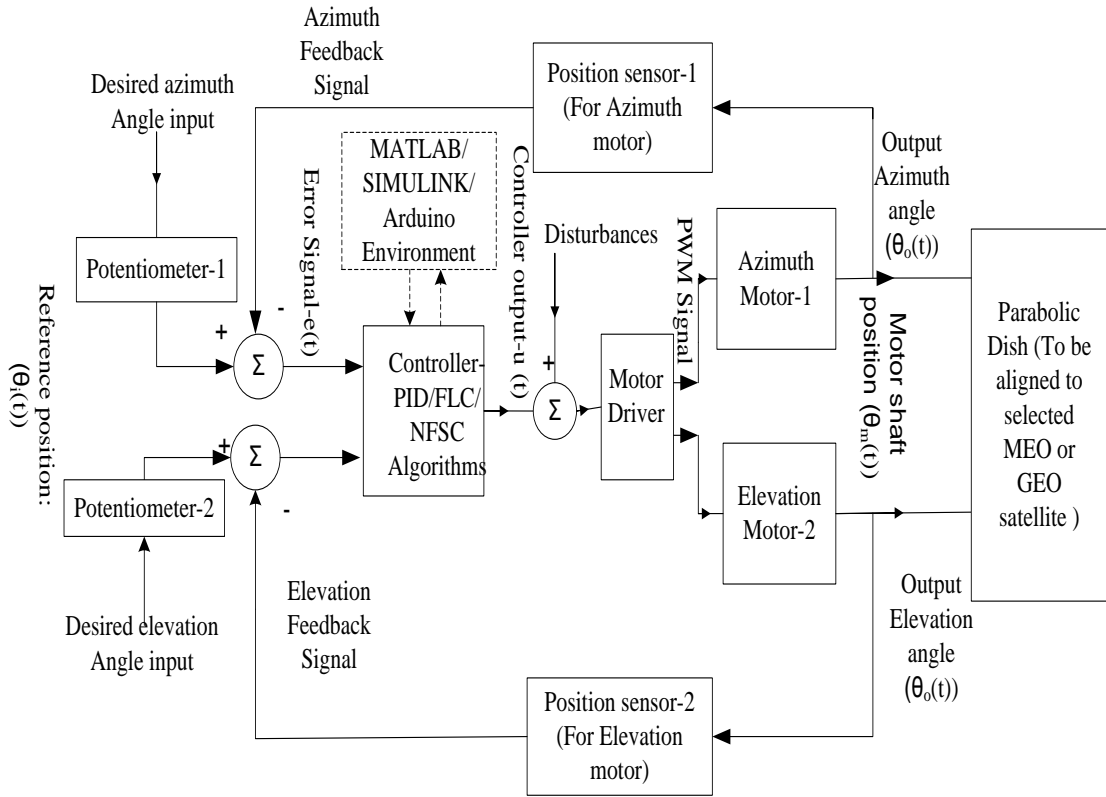
Figure 3.1: Block diagram of antenna control system

The second input to the summer is the feedback signal, the current position of the azimuth or elevation motor, captured by feedback sensor, the potentiometer and subsequently transformed to a summer readable format. The difference between these two inputs is called position error signal e(t) and is given to the controller. The controller reads the error signal and produces respective output signal, called controller output u(t). The controller output then reaches the motor driver, which produces a proportional output to rotate the respective motor in either direction according to the sign of the error signal (positive or negative). As the desired position is approached, the

error signal reduces to zero and the motor stops. The armature controlled DC servomotor takes in a voltage signal whose magnitude is proportional to the desired degrees of rotation, and has an almost flat speed-torque characteristic curve. Consequently, the step input signals of varying amplitudes were selected to represent reference or desired positions which could be directly applied through pre-calibrated potentiometers. The potentiometers enabled the conversion of continuous angular changes to corresponding continuous voltage changes.

The flowchart shown in Figure 3.2 summarizes the sequential events involved in a practical parabolic dish pointing system.
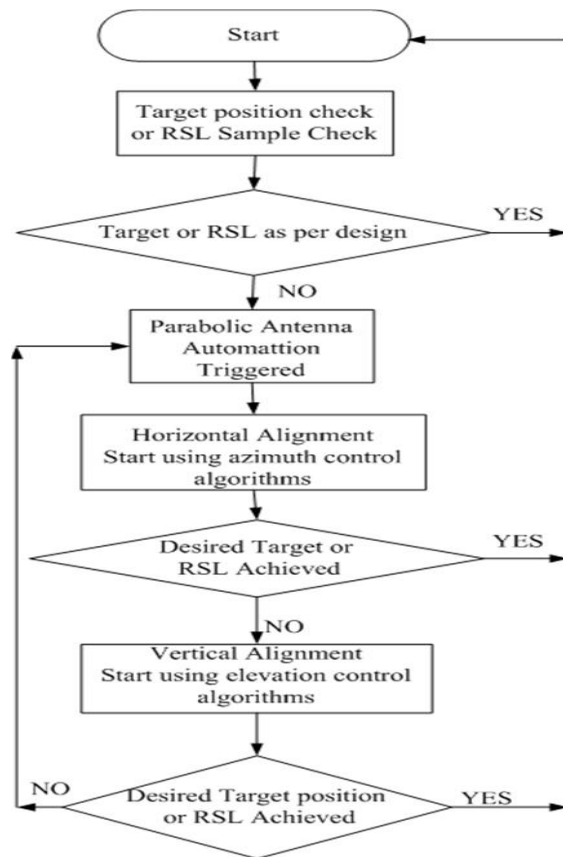
Figure 3.2: Flow chart of proposed system antenna pointing automation

The problem is to develop a suitable control system to position the antenna to the desired azimuth and/or elevation position and best satisfy the following tracking performance criteria:

1. Rise time $(t_r) \leq 4s$

2. Settling time $(t_s) \leq 5s$

3. Maximum Overshoot $(M_p) \leq 10\%$

4. In addition, the parabolic dish pointing accuracy should be within tolerance of $(\pm 2^0)$ or $\pm 5\%$ of the target azimuth and elevation angular information to maintain the LoS.

The steady state error (e_{ss}) was negligible and hence has not been captured in the results presented (see Appendix 5).

These values have been selected based on practical industrial standards which are typical requirements for a satellite dish positioning and tracking system [26]. The specifications are applicable to satellite dish sizes of 0.2m and 1.2m in diameter and weighing 5Kg and 10Kg respectively deployed at a frequency of 6GHz. The motor ratings are 5V for the prototype DC servomotor and 10V for the industrial DC motor with a torque of 7.5Kgcm and 15Kgcm respectively. The two motors have been used to capture both the industrial and the prototype scenarios. This is because the former is characterized with a bigger (1.2m) and heavier (10Kg) dish antenna load which requires DC motor with greater torque (15Kgcm) as well as external feedback and power amplifiers. The latter case presents a smaller (0.2m) and lighter (5Kg) dish which could easily be driven with a small DC servomotor-SM-4309M usable with the microcontroller (Arduino Mega

2560). The dish antenna look angles from the earth station required to follow the satellite is specified as 0^0 to 70^0 for angles of elevation and 0^0 to 180^0 for azimuth so as to maintain desired line of sight. In order to achieve the control system design objectives and satisfy the stated performance criteria, a PID controller was first developed, followed by FLC and lastly the NFSC. The response of each controller was analyzed and the performance noted in terms of the above criteria with varying step input signal.

3.2. Mathematical Modeling of Antenna Positioning System

In order to model the system, several parameters and variables which represent the DC servomotor, significant inputs, outputs and signals were defined in table format. Table 3.1 shows Parameters of Model with DC servo motors for both a practical system and the one developed as a prototype. The system for controlling the azimuth (or elevation) position of an industrial satellite tracking antenna comprises of two potentiometers, one is utilized at the input and the other at output as transducer, a power amplifier, a preamplifier, a load and motor. The comprehensive block diagram of the system for controlling antenna position was shown in Figure 2.1 [5] and [26]. To model and analyze this system, the following assumptions were made [5] and [26]:

- The system is well described by the provided project data. This means that the values for modeling the motor, gears, load, Preamplifier, Power Amplifier, potentiometers and voltage references are accurate.

- The transfer functions given for the power amplifier and preamplifier are accurate and that saturation is never reached.

- There are no disturbances or interference in the signals sent between parts of the controller system. This means that the dynamics of the potentiometers and the two amplifiers are neglected.

Table 3.1: Parameters of Industrial and Prototype Model with DC servo motors

S/No.	Parameter	Definition	Industrial	Prototype
1	a	Power Amplifier Pole	100	10
2	a_m	Motor and Load Pole	1.71	5.9
3	B_a	Motor Dampening Constant [Nms/rad]	0.01	0.015
4	B_L	Load Dampening Constant [Nms/rad]	1	0.0057
5	B_m	Equivalent viscous friction coefficient [Nms/rad]	0.02	0.015
6	J_a	Motor Inertial Constant [kgm^2]	0.02	0.032
7	J_L	Load Inertial Constant [kgm^2]	1	0.0057
8	J_m	Equivalent Moment of Inertia [kgm^2]	0.03	0.03
9	K	Preamplifier Gain	–	–
10	K_1	Power Amplifier Gain	100	10
11	K_B	Back e.m.f Constant Vs/rad	0.5	0.72
12	K_g	Gear Ratio	2.083	7.5
13	K_m	Motor and Load Gain	0.0057	0.0057
14	K_{pot}	Potentiometer Gain	0.318	0.159
15	K_T	Motor Torque Constant [Nm/A]	0.5	0.72
16	L_a	Motor Armature Inductance [H]	0.045	0.00392
17	N	Turns on Potentiometer	10	10
18	N_1, N_2, N_3	Gear Teeth (Respectively)	25,250,250	1,270,270
19	R_a	Motor Armature Resistance (Ω)	8	3.2
20	V_p	Voltage across Potentiometer [V]	10	5

Source of Industrial Parameters: [26].

First, ignoring the PID compensator, there are five subsystems of the entire system, each with its associated transfer function.

1. **Input and Output Potentiometer**: The input and feedback potentiometer each has an associated transfer function, in the form of a gain, K_{pot}, which is the same since the potentiometers are configured in the same way. The potentiometer converts the input angle, $\theta_i(s)$ to a voltage, $V_i(s)$. In the center position, the output voltage is zero while 5 turns towards either the $\pm 10V$ yields a voltage change of 10volts. Thus to obtain the potentiometer gain, the voltage change is divided by the angular displacement as in equation (3.1):

$$\frac{V_i(s)}{\theta_i(s)} = K_{pot} = \frac{10}{10\pi} = \frac{1}{\pi} = 0.318 \tag{3.1}$$

2. **Preamplifier and Power Amplifier:** The Preamplifier (error detector amplifier) amplifies the input error signal voltage by some gain K to give a voltage that is usable by the Power Amplifier which in turn converts it to a voltage that the motor can use. The parameters for transfer functions of both amplifiers are given in Table 3.1. The transfer functions for the Preamplifier and Power Amplifier are determined as the ratio of the Laplace transforms of the output voltage divided by the input voltage and are given in equations (3.2) and (3.3) respectively.

$$\frac{V_p(s)}{V_e(s)} = K \tag{3.2}$$

$$\frac{E_a(s)}{V_p(s)} = \frac{K_1}{s+a} = \frac{100}{s+100} \tag{3.3}$$

The value of the Preamplifier gain "K" can be determined for a stable system by utilizing the Routh-Hurwitz criterion [37] and [38]. According to this criterion, it was found that the system gave stable response if the value of "K" was chosen in the range $0 < K <$

2623. Here, the value of the gain taken is 100 since it falls within the above mentioned range [37].

3. **Motor and Load**: After the Power Amplifier, is the motor attached to the gears and the load (the antenna). All of these items must be considered when computing the transfer function of the resulting mechanical system. It is assumed that the motor is armature controlled DC servomotor and therefore has a fixed field. The equation relating the input voltage to the motor to the output position of the armature had been obtained earlier in section 2.4. Hence, from equation (2.10) it can be written in equation (3.4) that:

$$E_a(s) = \left[\frac{(J_m s^2 + B_m s)(R_a + L_a s) + K_T K_B}{K_T}\right] \theta_m(s) \tag{3.4}$$

The equivalent inertia J_m, is obtained from motor inertia J_a and load inertia J_L as in equation (3.5) while the equivalent viscous damping B_m is calculated from motor friction and load friction as in equation (3.6):

$$J_m = J_a + J_L (\frac{N_1}{N_2})^2 = 0.02 + 1(\frac{25}{250})^2 = 0.03 \tag{3.5}$$

$$B_m = B_a + B_L (\frac{N_1}{N_2})^2 = 0.01 + 1(\frac{25}{250})^2 = 0.02 \tag{3.6}$$

In the above equations, N_1 and N_2 represent the gear teeth and their ratio gives the Gear ratio K_g. In a fixed field motor, at steady state, it is assumed that $K_B = K_T$. Assuming that $R_a \gg L_a$, equation (3.4) is further simplified to equation (3.7). The assumption that the armature inductance L_a, is small compared to the armature resistance R_a, is usual for a DC (servo) motor [26]. Motor and load block's pole and zero is represented by

equations (3.8) and (3.9) with the transfer function as in equation (3.10). The transfer function relating load displacement to armature voltage, equation (3.11), is obtained by multiplying by K_g.

$$\frac{\theta_m(s)}{E_a(s)} = \frac{\frac{K_T}{JR_a}}{s(s + \frac{B_m R_a + K_T K_B}{JR_a})} = \frac{K_m}{s(s + a_m)} \tag{3.7}$$

$$a_m = \frac{B_m R_a + K_T K_B}{JR_a} = \frac{(0.02)(8) + (0.5)(0.5)}{(0.03)(8)} = 1.71 \tag{3.8}$$

$$K_m = \frac{K_T}{JR_a} = \frac{0.5}{(0.03)(8)} = 2.083 \tag{3.9}$$

$$\frac{\theta_m(s)}{E_a(s)} = \frac{K_m}{s(s + a_m)} = \frac{2.083}{s(s + 1.71)} \tag{3.10}$$

$$\frac{\theta_o(s)}{E_a(s)} = 0.1 \frac{\theta_m(s)}{E_a(s)} = \frac{0.2083}{s(s + 1.71)} \tag{3.11}$$

The open loop transfer function of antenna control system is obtained by omitting the feedback such that only the power amplifier and motor with load are considered. The transfer function relating the input voltage $Vp(s)$ to output angle of the motor and load $\theta_o(s)$ is given in equation (3.12) and to the output angular velocity, $\omega_o(s)$ is obtained by differentiating the angular position (multiplication by s), in equation (3.13) as given in [37]:

$$G(s) = \frac{\theta_o(s)}{V_p(s)} = \frac{20.83}{s[s^2 + 101.71s + 1.71]} \tag{3.12}$$

$$G(s) = \frac{\omega_o(s)}{V_p(s)} = \frac{20.83}{s^2 + 101.71s + 1.71} \tag{3.13}$$

The closed loop transfer function without the PID compensator can be found using two methods. The first method uses the block diagram reduction whose steps are summarized in Figure 3.3.
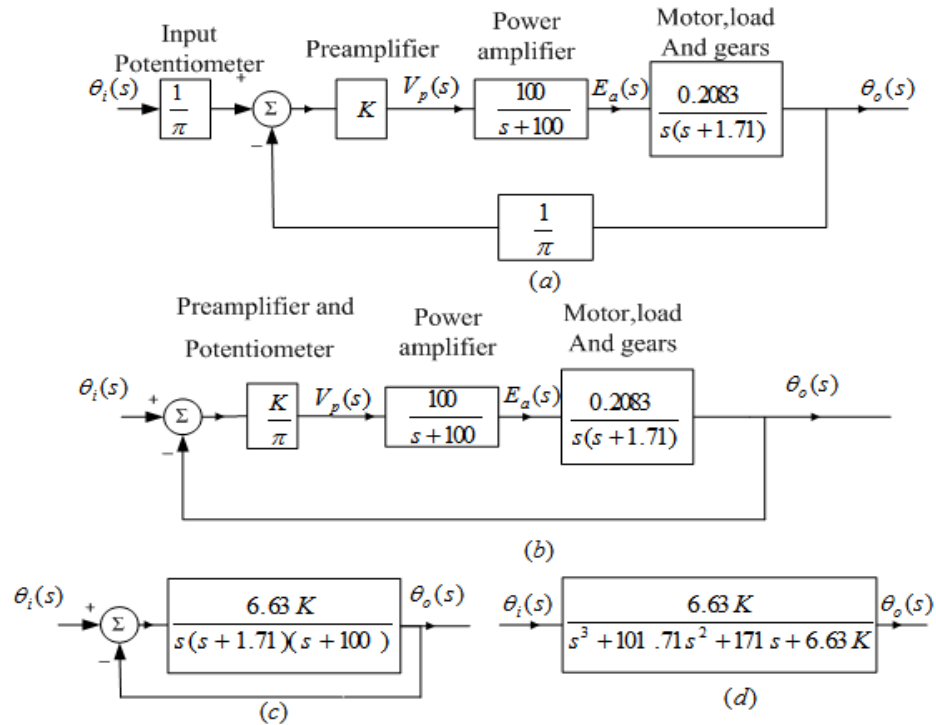
Figure 3.3: Block diagram reduction for antenna azimuth position control system

Here, part (a) shows the original block diagram model, part (b) shows pushing of the input potentiometer to the right past the summing junction, part (c) shows equivalent forward transfer function and lastly, part (d) presents the final closed loop transfer function assuming unity feedback.

The other method uses the general transfer function of a closed-loop system defined by equation (3.14):

$$\frac{\theta_o(s)}{\theta_i(s)} = \frac{\left(G(s)\right) \times C(s)}{1 + \left(G(s)\right) \times C(s)} \tag{3.14}$$

where $C(s)$ is the compensator assumed to be unity and $G(s)$ is the open-loop transfer function given by equation (3.15):

$$G(s) = K_g x \frac{K_m}{s(s + a_m)} x \frac{K_1}{(s + a)} x K x K_{pot} \tag{3.15}$$

The output angle is given by equation (3.16).

$$\theta_0(s) = K_g x \frac{K_m}{s(s + a_m)} x \frac{K_1}{(s + a)} x K x C(s) x V_e(s) \tag{3.16}$$

where $V_e(s)$ is given by equation (3.17):

$$V_e(s) = V_i(s) - V_0(s) = \theta_i(s) x K_{pot} - \theta_0(s) K_{pot} \tag{3.17}$$

By making the necessary substitutions in equation (3.14) the closed loop transfer function of system for controlling the position of antenna azimuth [14] is provided as in equation (3.18):

$$\frac{\theta_o(s)}{\theta_i(s)} = \frac{6.63K}{s^3 + 101.71s^2 + 171s + 6.63K} \tag{3.18}$$

Similarly, the prototype transfer function with DC servomotor (SM-S4309M) and experimentally determined parameters including an offline load of diameter 0.20m and weight of 5N were obtained as follows. The potentiometer gain is given in equation (3.19) while the equivalent inertia J_m and the equivalent viscous damping B_m as in equations (3.20) and (3.21) respectively:

$$\frac{V_i(s)}{\theta_i(s)} = K_{pot} = \frac{5}{10\pi} = \frac{1}{2\pi} = 0.159 \tag{3.19}$$

$$J_m = J_a + J_L(\frac{N_1}{N_2})^2 = 0.03 + 0.0057(\frac{1}{270})^2 = 0.03 \tag{3.20}$$

$$B_m = B_a + B_L(\frac{N_1}{N_2})^2 = 0.015 + 0.0057(\frac{1}{270})^2 = 0.015 \tag{3.21}$$

Prototype Motor and load block transfer function is given by equation (3.22) and this can be multiplied by the gear reduction ratio of 0.004.

$$\frac{\theta_m(s)}{E_a(s)} = \frac{\frac{K_T}{JR_a}}{s(s + \frac{B_m R_a + K_T K_B}{JR_a})} = \frac{K_m}{s(s + a_m)} = \frac{7.5}{s(s + 5.9)} \tag{3.22}$$

The open loop transfer function relating the input voltage to output angle is given in equation (3.23) and to the output angular velocity, in equation (3.24).

$$G(s) = \frac{\theta_o(s)}{V_p(s)} = \frac{612.24}{s[s^2 + 81.68s + 481.63]} \tag{3.23}$$

$$G(s) = \frac{\omega_o(s)}{V_p(s)} = \frac{612.24}{s^2 + 81.68s + 481.63} \tag{3.24}$$

In order to realize a stable system, the closed loop poles ought to be in the left half of the s-plane. As the loop gain is changed, the locations of the poles are also changed, creating the possibility that the poles could move into the right half of the s-plane, which may yield instability. That is why a proper gain setting is essential for the stability of the system and this must be taken care of in the formulation of the closed loop system. The range of the Preamplifier gain K required to keep the closed loop system stable was determined by Routh-Hurwitz criterion. Using the denominator of equation (3.18), the Routh table shown as Table 3.2 was created.

Table 3.2: Routh Table for antenna azimuth control stability

Column One	Column Two	Column Three
s^3	1	171
s^2	101.71	6.63K
s^1	$(17392.41 - 6.63K)/101.71$	0
s^0	6.63K	—

The third row of the table showed that a row of zeros occurred if $K = 2623$. This value of K makes the system marginally stable. Therefore, there will be no sign changes in the first column if $0 < K < 2623$ and this serves as the condition for stability. If the value of gain K as found by using Routh-Hurwitz criterion is used [37] and [38] i.e. $K = 100$, then, equation (3.18) becomes equation (3.25):

$$\frac{\theta_o(s)}{\theta_i(s)} = \frac{663}{s^3 + 101.71s^2 + 171s + 663} \tag{3.25}$$

The value is chosen as 100 so as to be equal to that of the power amplifier for design convenience and to reduce energy consumption. The closed-loop transfer function for the prototype is similarly obtained as in equation (3.26):

$$\frac{\theta_o(s)}{\theta_i(s)} = \frac{(G(s))xK_{pot}}{1 + (G(s))xK_{pot}} = \frac{97.43}{s^3 + 81.68s^2 + 481.63s + 97.43} \tag{3.26}$$

Where $K_{pot} = \frac{1}{2\pi} = 0.159$.

3.3. PID Controller Design for Antenna Control System

A PID (Proportional-Integral-Derivative) controller is implemented in almost all industrial processes because it is simple and robust. This controller is extremely popular because it can usually provide good closed loop response characteristics, can be tuned using relatively simple rules and easy to construct using either analogue or digital components. The structure of PID controller had been shown in Figure 2.1. Control signal is the sum of three components: proportional, integral and derivative and is defined in the parallel form as follows in equation (3.27):

$$u(t) = K_p e(t) + K_I \int e(t)\, dt + K_D \frac{d}{dt} e(t) \tag{3.27}$$

45

where K_p, K_I and K_D are proportional, integral and derivative gains and error, $e(t)$ is:

$$e(t) = \text{error} = (\text{set point} - \text{output}).\qquad(3.28)$$

By using the Laplace transform, the transfer function of PID controller in frequency domain can be represented as in equation (3.29).

$$\frac{U(s)}{E(s)} = K_p + \frac{K_I}{s} + K_D s = K_p\left(1 + \frac{1}{T_I s} + T_D s\right)\qquad(3.29)$$

where the reset time T_I and the derivative time T_D are defined as:

$$T_I = \frac{K_p}{K_I},\qquad(3.30)$$

$$T_D = \frac{K_D}{K_p},\qquad(3.31)$$

and

$$K_I = \frac{K_p}{T_I},\qquad(3.32)$$

The transfer function of PID controller in its most familiar form is given by equation (3.33):

$$\frac{U(s)}{E(s)} = \frac{K_p T_D}{s}\left[s^2 + \frac{1}{T_D}s + \frac{1}{T_D T_I}\right]\qquad(3.33)$$

The equations of the PID controller for industrial and prototype motors are presented in (3.34) and (3.35) respectively:

$$C_{PID-Industrial}(s) = 14\left(1 + \frac{1}{3.2s} + 0.125s\right) = 2(s^2 + 8s + 2.5)\qquad(3.34)$$

$$C_{PID-Prototype}(s) = 14\left(1 + \frac{1}{4.667s} + 0.143s\right) = 2(s^2 + 7s + 1.5)\qquad(3.35)$$

By using PID, the closed-loop transfer function of position control system of antenna azimuth is expressed as equations (3.36) and (3.37) for industrial and prototype motors respectively:

$$\frac{\theta_o(s)}{\theta_i(s)} = \frac{663K_D s^2 + 663K_P s + 663K_I}{s^4 + 101.71s^3 + (171 + 663K_D)s^2 + 663K_P s + 663K_I} \quad (3.36)$$

$$\frac{\theta_o(s)}{\theta_i(s)} = \frac{97.43K_D s^2 + 97.43K_P s + 97.43K_I}{s^4 + 81.68s^3 + (481.63 + 97.43K_D)s^2 + 97.43K_P s + 97.43K_I} \quad (3.37)$$

The values of K_P, K_I and K_D are obtained using Ziegler Nichols (Z-N) tuning algorithm given in Table Appendix 3.1 in Appendix 3. This method gives automatic oscillation of the process to compute the three gain constants. Ziegler-Nichols presented two methods: Step response method and Frequency response method [30]. In this thesis frequency response method was used. This is because since the PID controller and the plant are already in frequency domain, it was simpler to put the controller in the proportional mode and increase the gain until an oscillation took place. The critical gain (K_u) and periodic oscillations (P_u) were then easily obtained and these, together with Z-N in Table Appendix 3.1 in Appendix 3, assisted in computing the preliminary gain values of the PID controller as follows: $K_P = 15$, $K_I = 0.625$ and $K_D = 90$. However, since these initial gain constants depicted high overshoots, the final PID controller gain parameters which gave the most appropriate response and thus meeting the design constraints were obtained as: $K_P = 16$, $K_I = 5$ and $K_D = 2$ for the industrial motor. Similarly, the PID parameters were obtained as $K_P = 14$, $K_I = 3$ and $K_D = 2$ for the prototype motor. Using these values, the final equations with PID control for industrial motor and prototype motor are as given in equation (3.38) and (3.39).

$$\frac{\theta_o(s)}{\theta_i(s)} = \frac{1326s^2 + 10608s + 3315}{s^4 + 101.71s^3 + 1497s^2 + 10608s + 3315} \tag{3.38}$$

$$\frac{\theta_o(s)}{\theta_i(s)} = \frac{194.86s^2 + 1364.02s + 292.29}{s^4 + 81.68s^3 + 676.47s^2 + 1364.02s + 292.29} \tag{3.39}$$

3.4 Fuzzy Logic Control (FLC) Design

3.4.1 Fuzzy Logic Control (FLC) Method

The Fuzzy Logic Control method involves two steps: formulation of initial rules block and optimizing the rules by hit and trial method using MATLAB. The specific components characteristic of the Fuzzy Controller to support the design procedure are Fuzzifier, Defuzzifier, Knowledge Base and Decision Making unit [10], [22] and [39] . The FLC created had 2 inputs: position error $(e(t))$ designated simply as E and change in position error $(\frac{d}{dt}e(t))$ represented by DE and a single output given as control input to the DC servo motor drivers denoted as CI. Using 7x7 linguistic variables to represent changes in the two inputs, a total number of 49 Mamdani type rules were created and stored in the rule base memory. This choice is made in order to improve on accuracy of the control system. For simplicity, triangular fuzzy sets have been selected for both input (fuzzification) and output (defuzzification). The defuzzification method used is the center of gravity method, also called centroid method as it is the most popular method. For given set of inputs to the FLC, appropriate rule(s) are fired in the rule base and defuzzified to give the control input signal.

3.4.2 FLC Model and Membership Functions Used

The FLC designed in MATLAB used triangular membership functions since they are easily calculated (possess lesser number of parameters) and easier to modify too. Additionally, they are economical since they are specified by only three parameters. The Mamdani FLC model is shown in Figure 3.4 whereas the ranges and parameters with the chosen 7 triangular membership functions defined for E and DE are shown in Figure 3.5. The output MF representing the Control signal (CI) and the 3-D Surface View of the algorithm are shown in Figure 3.6.
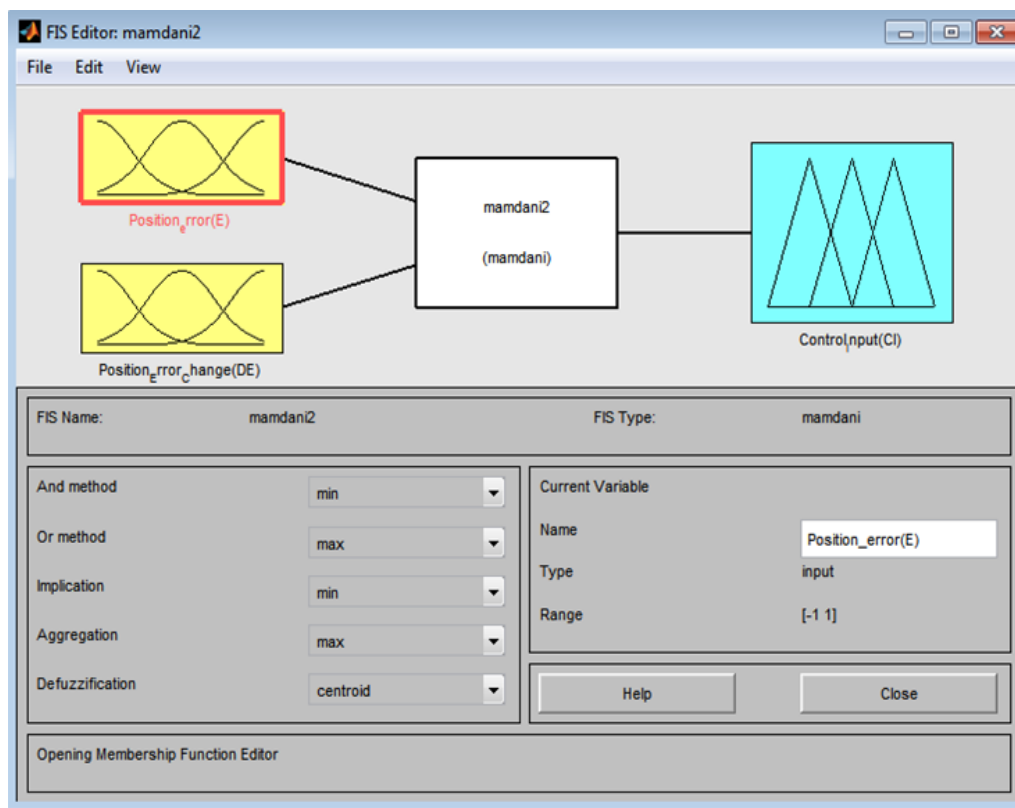
Figure 3.4: Mamdani FLC Model
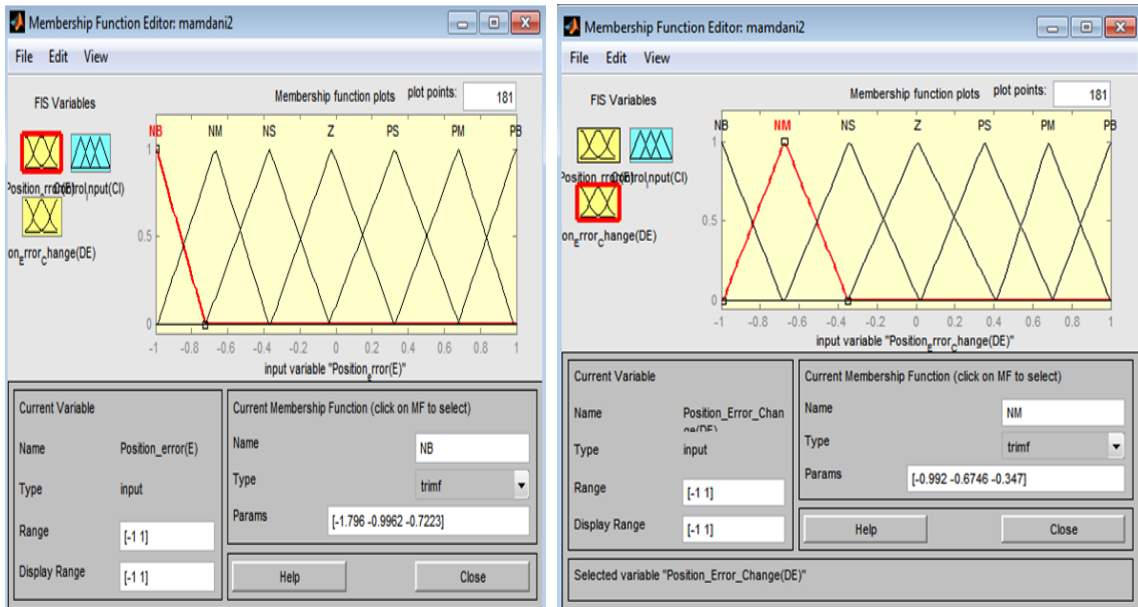
(a) Position Error FIS Input MF (b) Position Error Change FIS Input MF

Figure 3.5: Mamdani FLC Controller Input MFs for the FIS
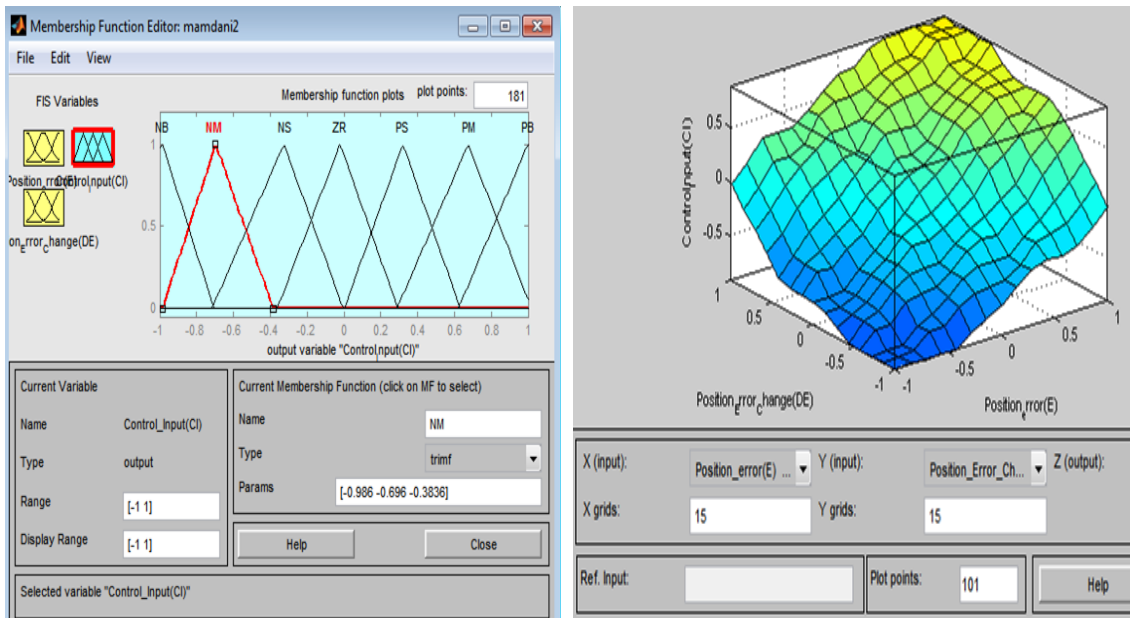
(a) Output MF Used in the FIS File (b) 3D Control Surface Viewer

Figure 3.6: Mamdani FLC output MF and the Surface Viewer

3.4.3 Formulation of FLC Rule Base

It has been stated that the FLC under consideration takes 2 inputs: Position Error and Change in Position Error and gives out one output which is fed to the DC servo motor driver. It controls the direction of rotation and speed of the servo motor based on equations (3.40) and (3.41).

$$E = V_{p1} - V_{p2} \qquad\qquad (3.40)$$

$$DE = (E - PE) \qquad\qquad (3.41)$$

where,

E = Position Error

V_{p1} = Input Potentiometer (Desired) voltage

V_{p2} = Output Potentiometer (Actual) voltage

DE = Change in Position Error

PE = Previous Error

This means that if the error is positive and the change in error is negative then the response is following the right direction and the servomotor should move forward in this direction but if the error becomes negative and the change in error is negative, this implies that the response is following the wrong direction and it should start moving in the opposite direction until the antenna faces the target. To fine tune the transition in the FLC controller parameters the following linguistic variables were defined: NB, NM, NS, ZR, PS, PM, PB, where NB means negative big, NM means negative medium, NS means negative small, ZR means zero, PS means positive small, PM means positive medium and PB means positive big. The span of position error is [-6 6], rate of change

of position error is [-2 2] and that of control is [-7 7]. These inputs are fuzzified to represent their linguistic variables, for which 7 triangular membership functions are used. To formulate the Fuzzy Logic Controller, 49 IF THEN rules with minimum operator are specified using logical reasoning and drawing from the knowledge of an expert i.e. human operator who has previously monitored the behavior of the system. A section of the developed fuzzy rules in the form of $(7 \times 7) = 49$ algorithm included in the Fuzzy Logic Controller are given in Figure 3.7a while a portion of the rule viewer is indicated in Figure 3.7b. Table 3.3 summarizes the control rules for FLC based antenna pointing system which maps the fuzzy inputs to fuzzy output. The fuzzy output is then defuzzified to obtain crisp value of output control.
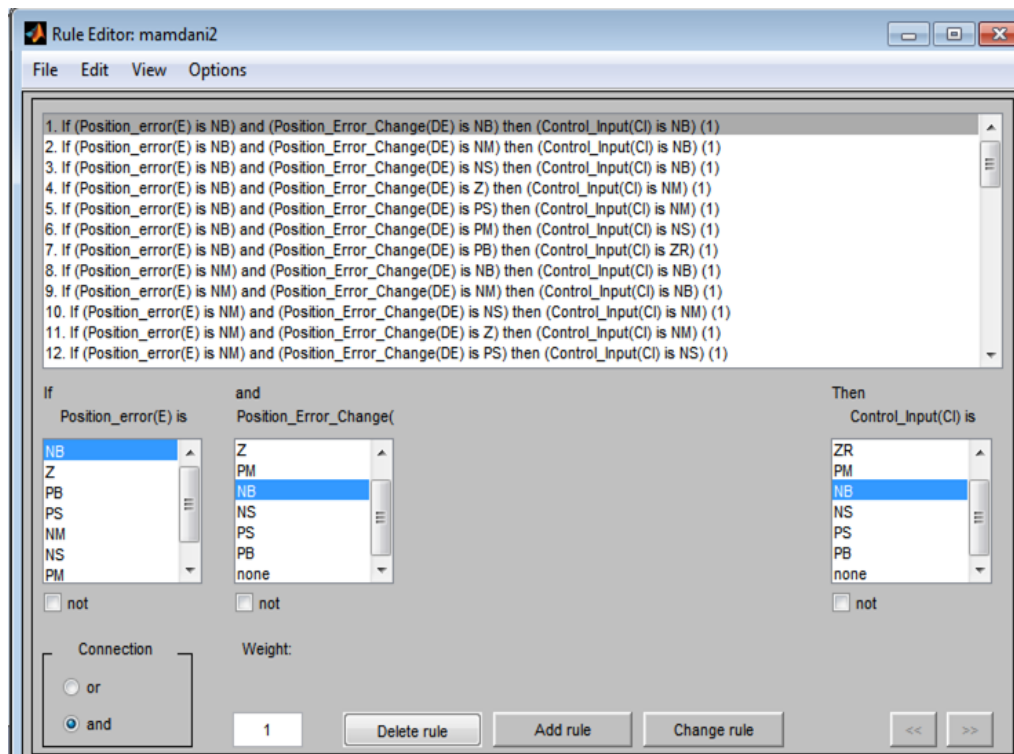
(a) Section of FLC rule base algorithm
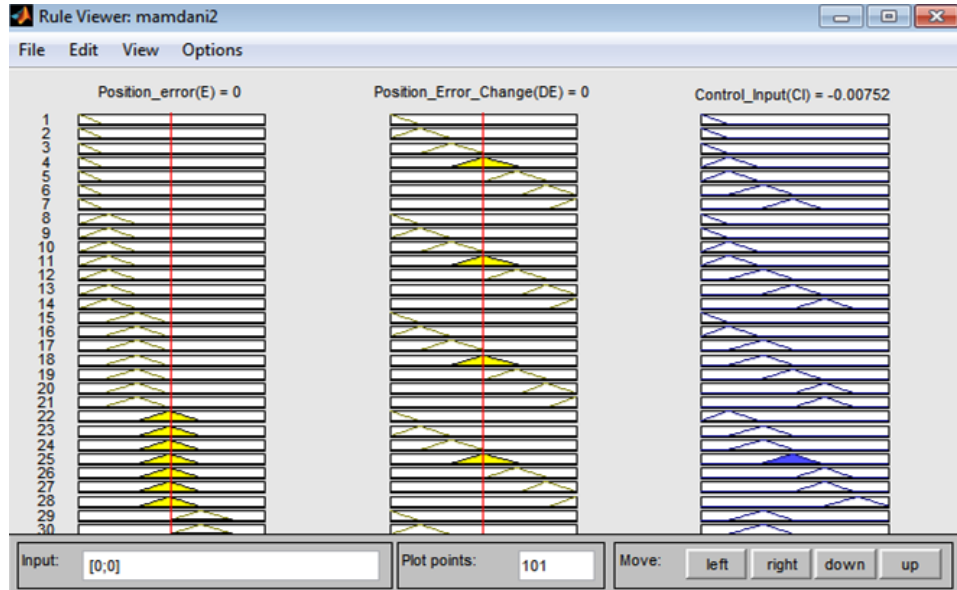
(b) Section of the FLC Rule Viewer

Figure 3.7: Sections of FLC Rule Base and Rule Viewer

Table 3.3: Rule Base Table

DE/E	NB	NM	NS	ZR	PS	PM	PB
NB	NB	NB	NB	NM	NS	NS	ZR
NM	NB	NB	NM	NS	NS	ZR	PS
NS	NB	NM	NS	NS	ZR	PS	PM
ZR	NM	NM	NS	ZR	PS	PM	PM
PS	NM	NS	ZR	PS	PS	PM	PB
PM	NS	ZR	PS	PS	PM	PB	PB
PB	ZR	PS	PS	PM	PB	PB	PB

3.5 Design of Neuro-Fuzzy System Controller

The development of Neuro-Fuzzy System Controller (NFSC) with its associated algorithms for the DC servomotor based satellite antenna positioning and tracking system was created within the Adaptive Neuro-Fuzzy Inference System (ANFIS) framework. This resembles a hybrid Neuro-Fuzzy system in which both fuzzy and neural networks techniques are deployed such that they incorporate and complement

53

each other in order to achieve a common goal. In this study, the two terms, NFSC and ANFIS have been used interchangeably to mean the same thing.

3.5.1 Adaptive Neuro-Fuzzy Inference System (ANFIS)

Adaptive Neuro-Fuzzy Inference System (ANFIS) method is used as a teaching method for Sugeno-type fuzzy systems and was proposed by Jang in 1993 [39]. ANFIS constructs an input-output mapping based both on human knowledge (in the form of fuzzy if then rules) and on generated input-output data pairs by using either back propagation algorithm or a hybrid algorithm that is the combination of the least-squares and back propagation gradient descent method.

In applying ANFIS, usually the number and type of fuzzy system membership functions (MFs) has to be specified by user. The method is more efficient in the sense that it combines the advantages of FLC and NN approach in order to construct a nonlinear self-tuning controller. In addition, since the rules are in linguistic format, intermediate results can be analyzed and interpreted easily. The design parameters required for any ANFIS controller are number of data pairs, training data sets and checking data sets. For training the number of epochs should be chosen to start the training and learning results verified after mentioning the step size.

ANFIS method is also viewed by many researchers, as a hybrid method, which consists of two parts: gradient method that is applied to calculation of input membership function parameters and least square method which is applied to calculation of output function parameters [40]. A typical architecture of ANFIS control structure is shown in Figure

3.8, in which a circle indicates a fixed node, whereas a square indicates an adaptive node [41].

For simplicity, a two inputs x, y and one output z structure is considered. For a first order Sugeno fuzzy model with two fuzzy if-then rules, a common rule set can be expressed as in equations (3.42) and (3.43).
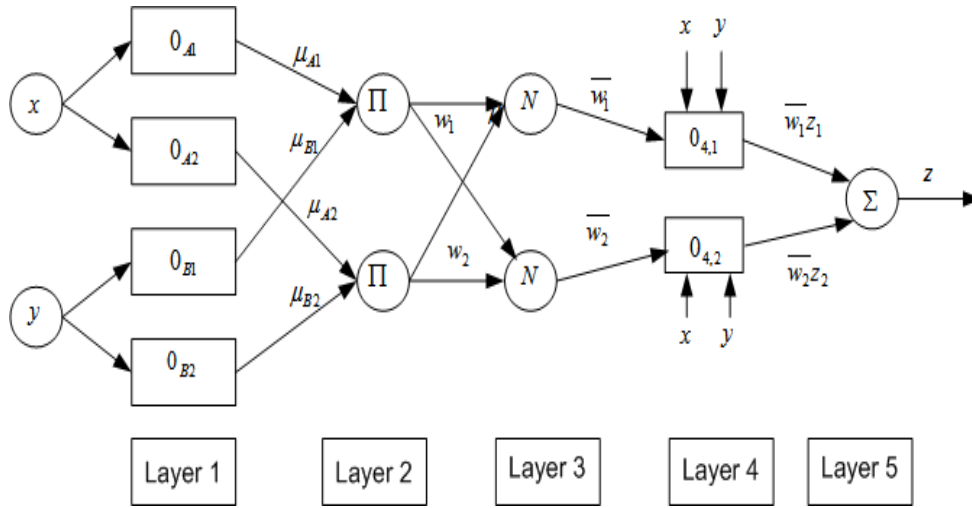
Figure 3.8: A Typical ANFIS architecture

Rule 1: If x is A_1 and y is B_1, then:

$$z_1 = p_1 x + q_1 y + r_1 \qquad (3.42)$$

Rule 2: If x is A_2 and y is B_2, then:

$$z_2 = p_2 x + q_2 y + r_2 \qquad (3.43)$$

where A_i and B_i are the fuzzy sets in the antecedent, and p_i, q_i, and r_i, are the design parameters that are determined during the training process.

The ANFIS network structure, is made up of a set of units (and connections) organized into five connected network layers, 1 to 5 as shown in Figure 3.8. The detailed functions performed by each layer is explained in [39] and [40] and summarized in the next

55

section under ANFIS design. The ANFIS structure can be tuned automatically by the hybrid learning algorithm using a least-square estimation (for output membership functions) and a back propagation algorithm (for output and input membership functions) [41], [42] and [28].

3.5.2 Neuro-Fuzzy System Controller Design

The Adaptive Neuro-Fuzzy Inference System (ANFIS) controller generates change in the reference drive voltage based on position error **E** and derivative in the position error (speed error) **DE** as was defined in equations (3.35) and (3.36). In this study, first order Sugeno-type fuzzy inference is used for ANFIS and the typical fuzzy rule takes the form in equation (3.44). If **E** is A_i and **DE** is B_i then**,**

$$z = f(E, DE) \tag{3.44}$$

where A_i and B_i are fuzzy sets in the antecedent and $z = f(E, DE)$ is a crisp function in the consequent. The significance of each layer and operation of the 2-input-1-output ANFIS structure considered are [39], [40]:

Layer 1: This layer (the fuzzification layer) enables the entry of raw data or crisp inputs from the target system into ANFIS. It is composed of a number of computing nodes whose activation functions are fuzzy logic membership functions, taken as triangular in this thesis. Each adaptive node generates the membership grades called fuzzy spaces for the input vectors A_i; $i = 1, \ldots, n$ and B_i; $i = 1, \ldots, n$, where n is the number of membership functions of the inputs (E and DE) chosen as $n = 7$. The degree to which the inputs lie within the fuzzy space is given a value normalized between 0 and 1 and the output is defined by (3.45).

56

$$0^1{}_{A,i} = \mu_{A,i}(E), \quad 0^1{}_{B,i} = \mu_{B,i}(DE), i = 1, \dots, n \qquad (3.45)$$

Layer 2: Is the rule layer where each node is fixed. Once the locations of inputs in the fuzzy spaces are identified, the product of the degrees to which the inputs satisfy the membership functions is found. This product is called the _ring strength of a rule whose output is given by (3.46). In other words, it selects the minimum (min) value of the inputs. In this layer, the total number of Takagi-Sugeno rules is 49.

$$0^2{}_i = W_i = \min\,(\mu_{Ai}(E).\,\mu_{Bi}(DE), \qquad (3.46)$$

Layer 3: In layer 3, the normalization layer, the ratio of each rule's firing strength is calculated with respect to the sum of the firing strengths of all the rules. Each node in this layer is fixed. The ith node output is the ith input activation level divided by the sum of all the activation levels of other inputs, (3.47).

$$0^3{}_i = \overline{W_i} = \frac{W_i}{\sum_{j=1}^{n} W_j} \qquad (3.47)$$

Layer 4: In layer 4, the defuzzification layer, the output of each node is the weighted consequent value. Adaptive node **i** in this layer calculates the contribution of ith rule towards the overall output, with the following node function (3.48).

$$0^4{}_i = \overline{W_i} Z_i = \overline{W_i}(p_i E + q_i DE + r_i) \qquad (3.48)$$

Layer 5: Layer 5 is the summation layer and its output, which is the sum of all the outputs of layer 4, gives the overall output for the respective inputs within the fuzzy space. The single fixed node in this layer computes the overall output as the sum of each rule's contribution, (3.49).

$$0^5{}_i = \sum_{i=1}^{2} \overline{W_i} Z_i = \frac{W_1 Z_1 + W_2 Z_2}{W_1 + W_2} \qquad (3.49)$$

57

Before the ANFIS system can be used for prediction, the parameters of the rules are determined by first generating an initial FIS where first random values are assigned to the parameters. Next, an optimization scheme is applied to determine the best values of the parameters that would supply rules to idealistically model the target system. After training, the rules remain so that when new input data is presented to the model, the rules provide a corresponding reasonable output [40]. The optimization technique used is a hybrid learning algorithm that minimizes the error between the ANFIS model and the real system using training data from the target system to generate signals that propagate backwards and forwards and update the parameters [41]. The parameters to be trained are A_i and B_i of the premise parameters and p_i, q_i, and r_i, of the consequent parameters.

The ANFIS Editor GUI window in MATLAB includes four distinct areas to support a typical ANFIS design work flow which is shown in Fig. 3.9.

It enables the following tasks to be performed:

  1. Loading, Plotting, and Clearing the Data.

  2. Generating or Loading the Initial FIS Structure.

  3. Training the FIS and last is validating the Trained FIS [42].

There are three constraints of using MATLAB ANFIS method: only Sugeno-type decision method is available, there can be only one output and lastly, defuzzification method is weighted mean value. For generating FIS structure, the triangular MF is used for the two input variables and output type is linear. The number of MFs for the input

58

variables E and DE is 7 and 7; the number of rules is then 7 x 7 = 49. Fig. 3.10 shows

the membership functions for E and DE before training.
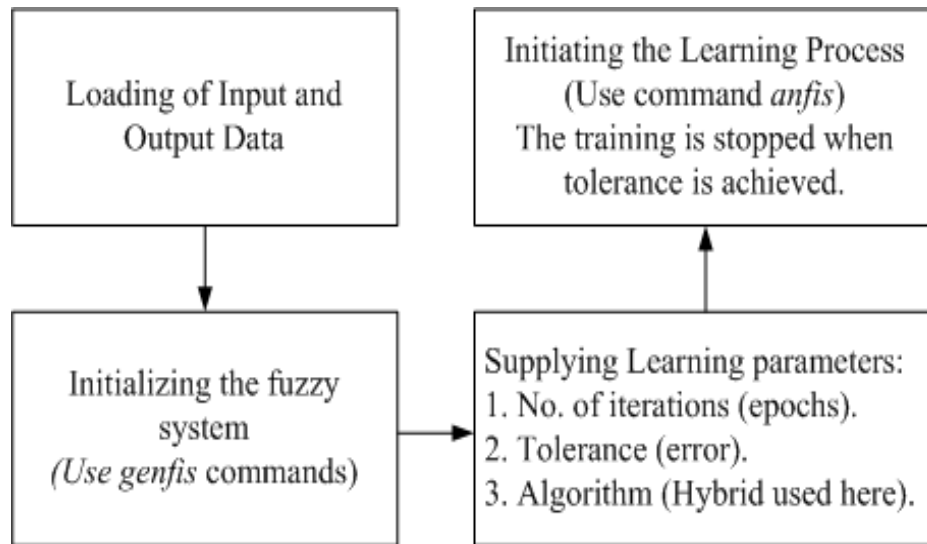
Figure 3.9: Steps for ANFIS controller Design
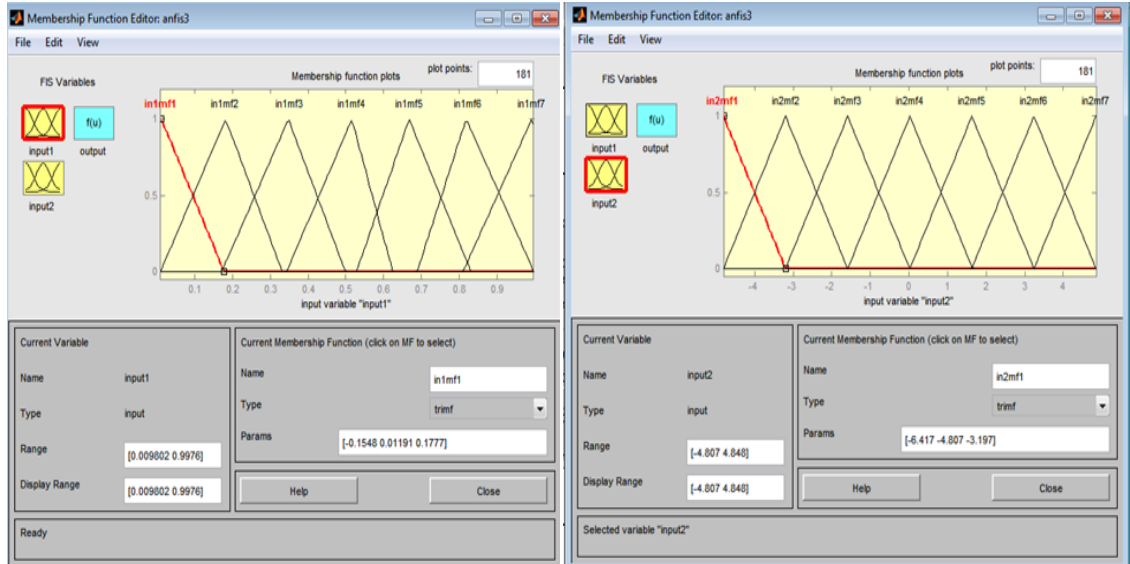
(a) ANFIS Input 1: Position Error (b) ANFIS Input 2: Position Error Change

Figure 3.10: ANFIS MFs for E (Input 1) and DE (Input 2) Before Training

Fig. 3.11 shows the generated ANFIS structure and the rule viewer section used for the

DC servo motor position controller design.
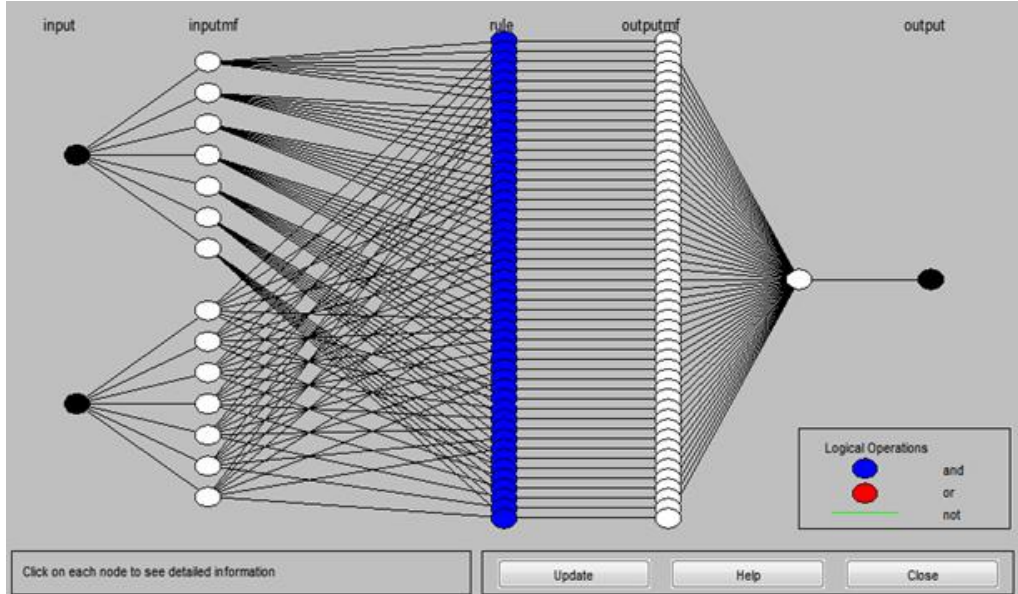
(a) Two input-1-output ANFIS model
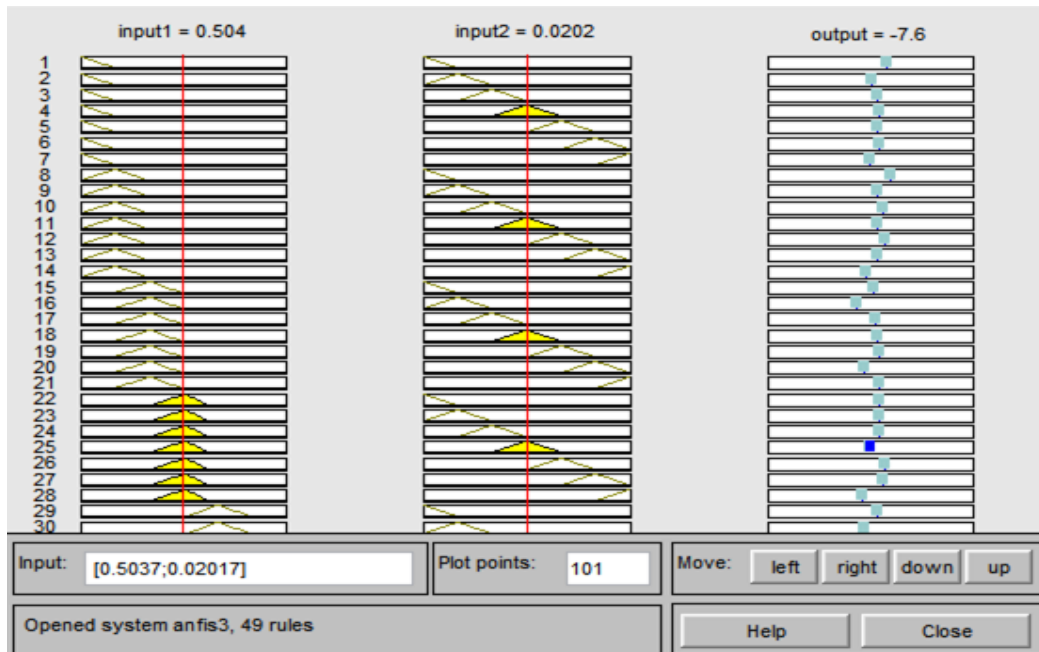
(b) ANFIS Rule Viewer before training

Figure 3.11: ANFIS Model and the Rule Viewer before Training

The training, testing and checking data sets, shown in Table Appendix 4.2 of appendix

4, were generated using code written in MATLAB m-file and experience drawn from the

performance of the PID and FLC controllers in the system. It has been used 80 % of the generated data sets for training the ANFIS system model and 10 % each as testing and checking data. Hybrid learning algorithm was used for training the generated FIS with the number of epochs as 100 and tolerance of 0:01 for best performance. It is already known that the triangular MF is specified by two parameters. Therefore, the ANFIS used here contains a total of 371 fitting parameters, of which 28 (2x7 + 2x7 $=$ 28), are the premise parameters and 343 (7x49 $=$ 343) are the consequent parameters.

Fig.3.12 shows optimized membership function for E and DE as well as the rule viewer after training. Thus an adaptive network that has exactly the same function as a Sugeno fuzzy model has been constructed. In Fig. 3.13, the training error response for trained ANFIS controller is presented.
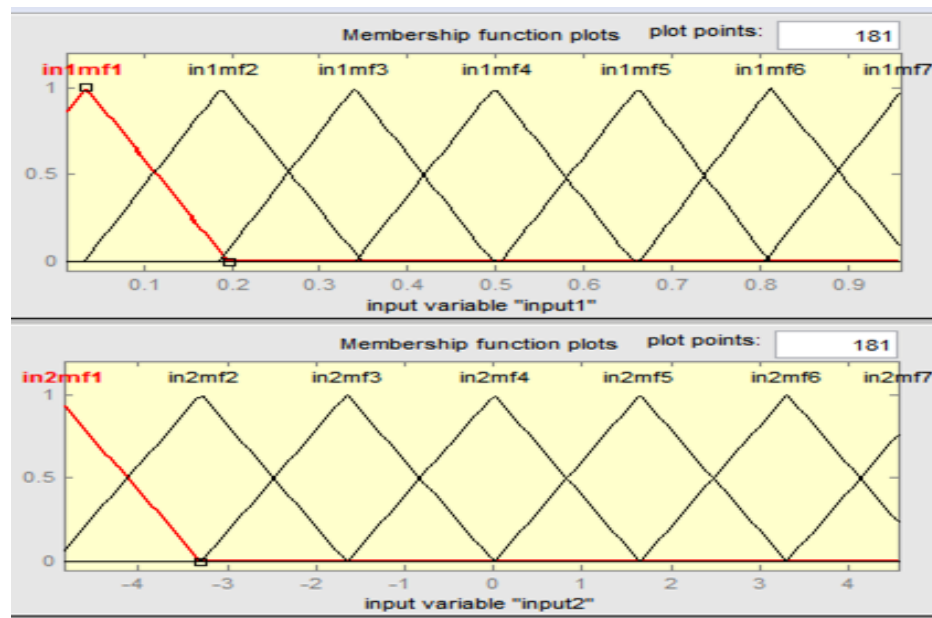
(a) ANFIS MFs: E and DE after training
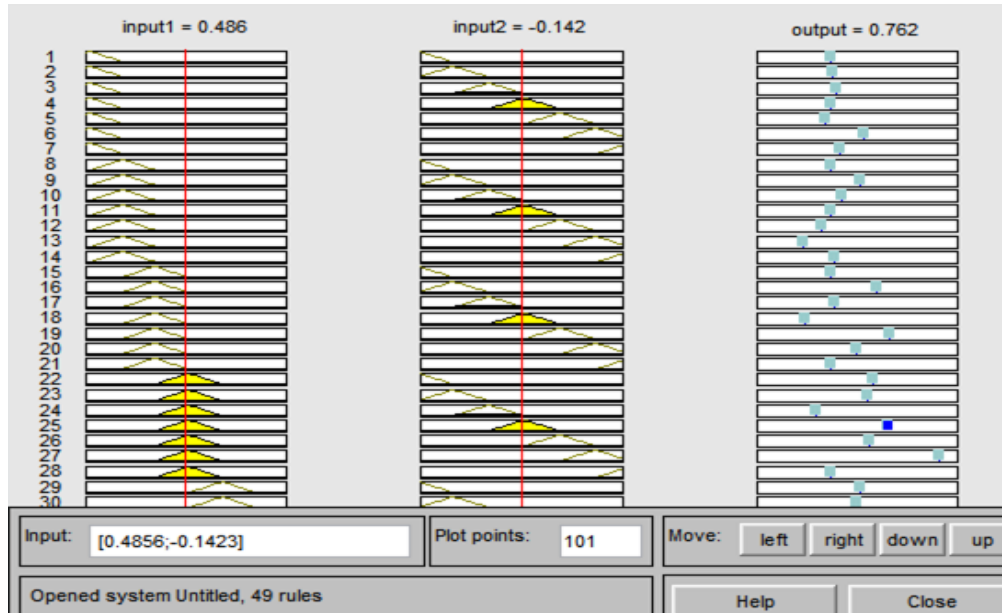
(b) ANFIS Rule Viewer after training

Figure 3.12: Trained ANFIS MFs for E (Input 1) DE (Input 2) and Rule Viewer
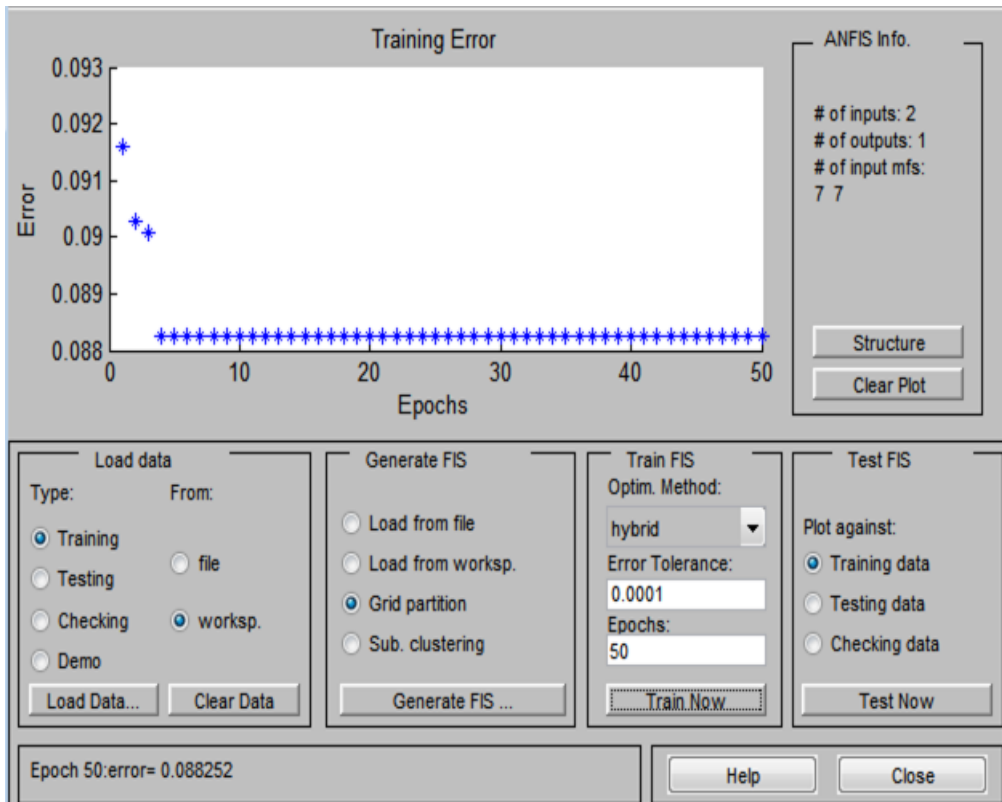
Figure 3.13: Trained ANFIS controller

The testing and checking (validation) plots are shown in Fig. 3.14.
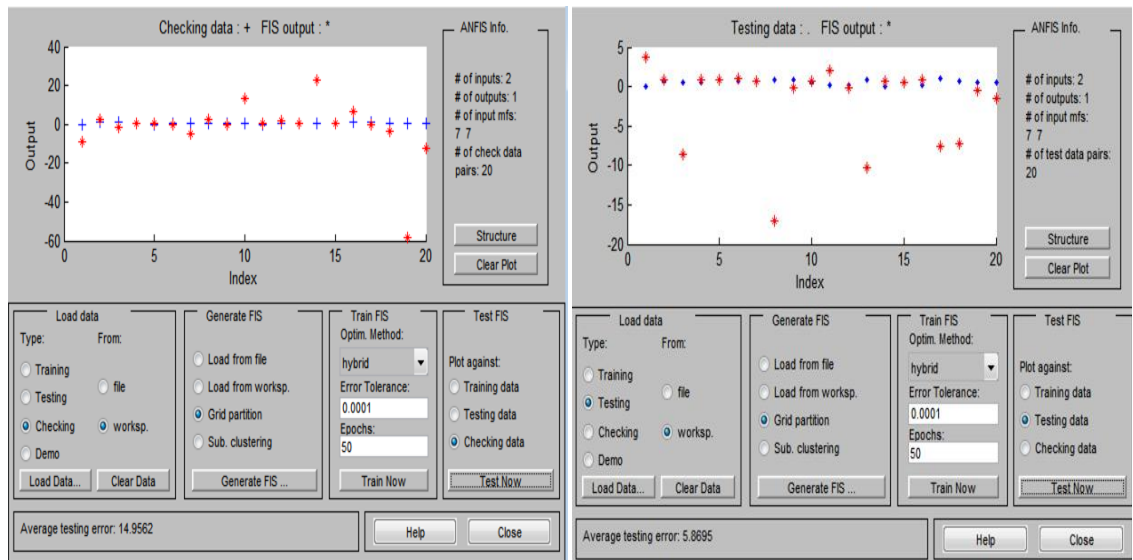
(a) Checking Data Plot for trained ANFIS (b) Testing Data Plot for trained ANFIS

Figure 3.14: Checking and Testing of the Trained ANFIS

Figure 3.15 and Figure 3.16 respectively, gives the surface and contour plots showing

relationship between input and output parameters before training and after training.
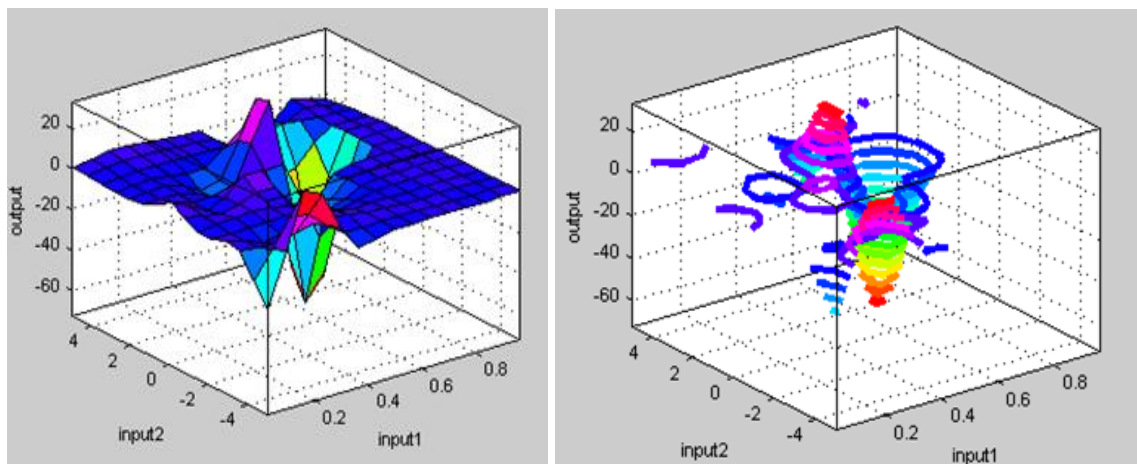
(a) ANFIS Surface Plot Before Training (b) ANFIS Contour Plot Before Training

Figure 3.15: ANFIS Surface and Contour Plots Before Training
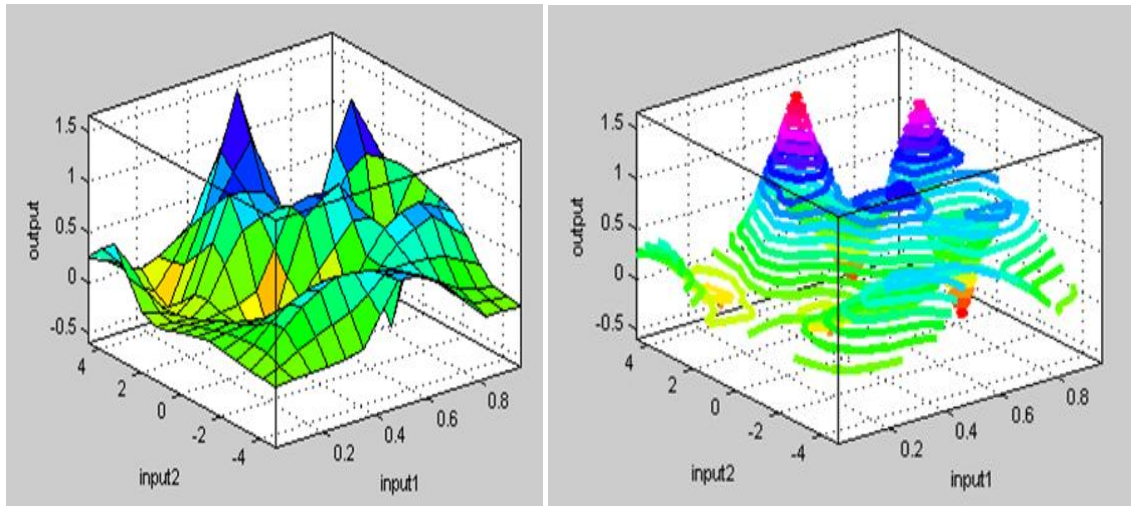
(a) ANFIS Surface Plot After Training (b) ANFIS Contour Plot After Training

Figure 3.16: ANFIS Surface and Contour Plots After Training

In any ANFIS design procedure, it is necessary to have a good set of data to train, check and test the controller model. Model validation is defined as the process by which the input vectors from input/output data sets on which the FIS was not trained, are presented to the trained FIS model, to observe how well the FIS model predicts the corresponding data set output values. In a real system, it is possible the training data set does not include all of the representative features that ought to have been modeled because of presence of noise and other disturbances to the model. That is why, the checking data set-II and testing data set-II were used which resembled the intrigues posed by these noisy conditions. The testing data set enabled checking of the generalization capability of the resulting fuzzy inference system. The rationale behind using a checking data set for model validation is that after a certain point in the training, the model begins over fitting the training data set. Principally, the model error for the checking data set tends to decrease as the training proceeds up to the point that over fitting starts, and then the model error for the checking data suddenly increases. Over fitting may be accounted for

by testing the FIS trained on the training data against the checking data, and selecting the membership function parameters to be those associated with the minimum checking error if these errors indicated model over fitting.

3.5.3 Design Constraints of the Neuro-Fuzzy System Controller

To train the Neuro-Fuzzy System Controller (NFSC), the limiting condition was that either the system could be taken off-line or it would be possible to model or simulate the system accurately. Further, since supervised learning was adopted, the following restrictions applied:

1. Training data was available for the system to be controlled.

2. The system to be controlled could be modeled or simulated.

3. Knowledge base in terms of rules was available to the designer.

The supervised learning was selected because labeled training data was available and the categories or clusters were known as opposed to unsupervised learning which is only used when categories are not known.

3.6 SIMULINK Model Layouts

The combined SIMULINK model for the designed PID, FLC and NFSC controllers created in MATLAB software for conducting the simulations is shown in Fig. 3.17 for industrial motor and in Fig. 3.18 for the prototype. The transfer functions utilized in Fig. 3.17 and Fig. 3.18 are drawn from equations (3.25) (for industrial motor) and (3.26) (for prototype motor) respectively, where the denominators represent the corresponding characteristic polynomials. The FLC controller and MATLAB code were used to generate the required training data. The inputs of the controller were taken as reference

position represented by a step input signal and the actual position obtained from the actual output signal feedback. The output is the driving voltage to the motor driver. It is important to mention that the transfer function approach has been deployed in this section because of the following reasons:

1. It is a mathematical model that gives the gain of the given block/system

2. Once transfer function is known, any output for any given input, can be obtained

3. From the knowledge of the transfer function the poles and zeros of the system (which play a very important role in response of the system) can be computed.

4. From the characteristic equation, system stability can be inferred.

5. The value of the transfer function is dependent on the parameters of the system and independent of the input applied. The value also represents the characteristic and property of the system itself.

3.7 Prototype Development and Experimental Set Up

3.7.1. Prototype Design Assumptions

1. As a position reference, it shall be accepted that the North is 0^0, the East is 90^0, the South is 180^0 and the West is 270^0.

2. The case location for parabolic dish to be steered shall be assumed to be at Juja, Kenya (1.1018^0S; 37.0144^0E, Magnetic declination: 0.5333^0 E).

3. The antenna will be off-line i.e. not receiving any signals transmitted by the satellites selected.
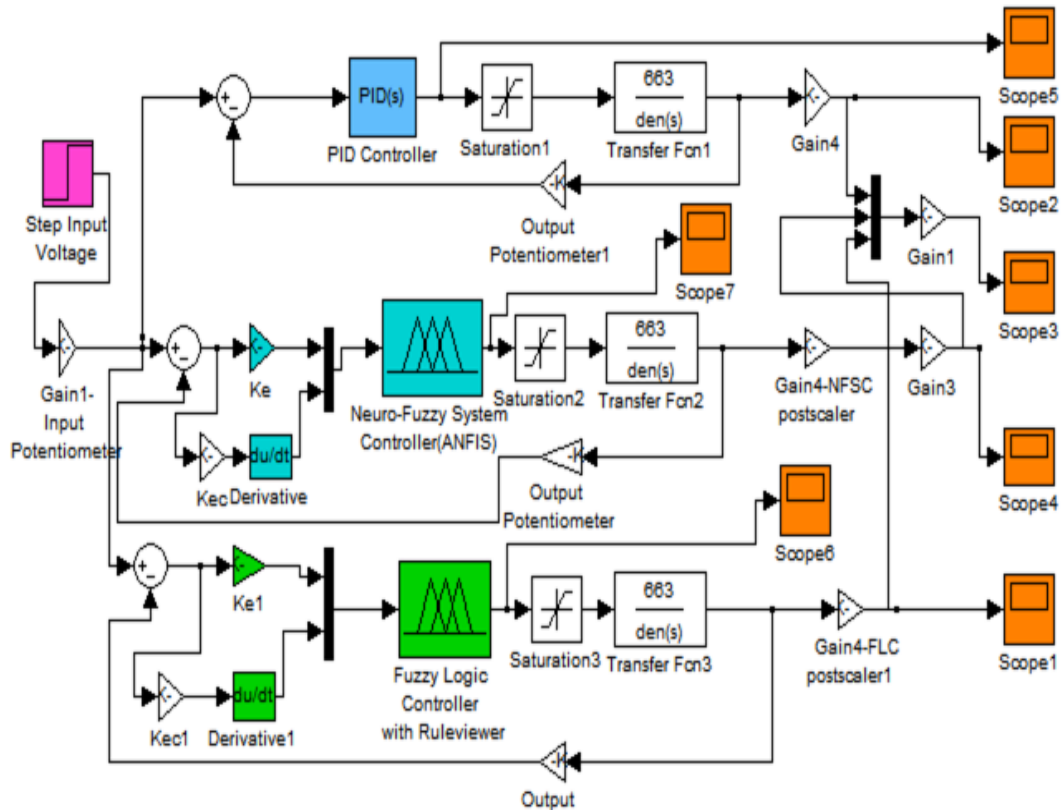
Figure 3.17: PID, FLC and NFSC Industrial SIMULINK Model Layout

3.7.2 Testing Control Algorithm and Software Design Implementation

The control algorithm for positioning the antenna in the satellite tracking system was tested by the established communication link between the Arduino microcontroller and the MATLAB/SIMULINK software models via the USB port.

In the prototype model shown in Fig. 3.19, the system could be driven based on any of the two sets of inputs, that is:

   (a) Desired DC servomotor angular position representing the satellite dish position versus the current measured position.

   (b) Desired received signal level by the satellite dish which is represented in the prototype by a signal generator against actual received signal strength.
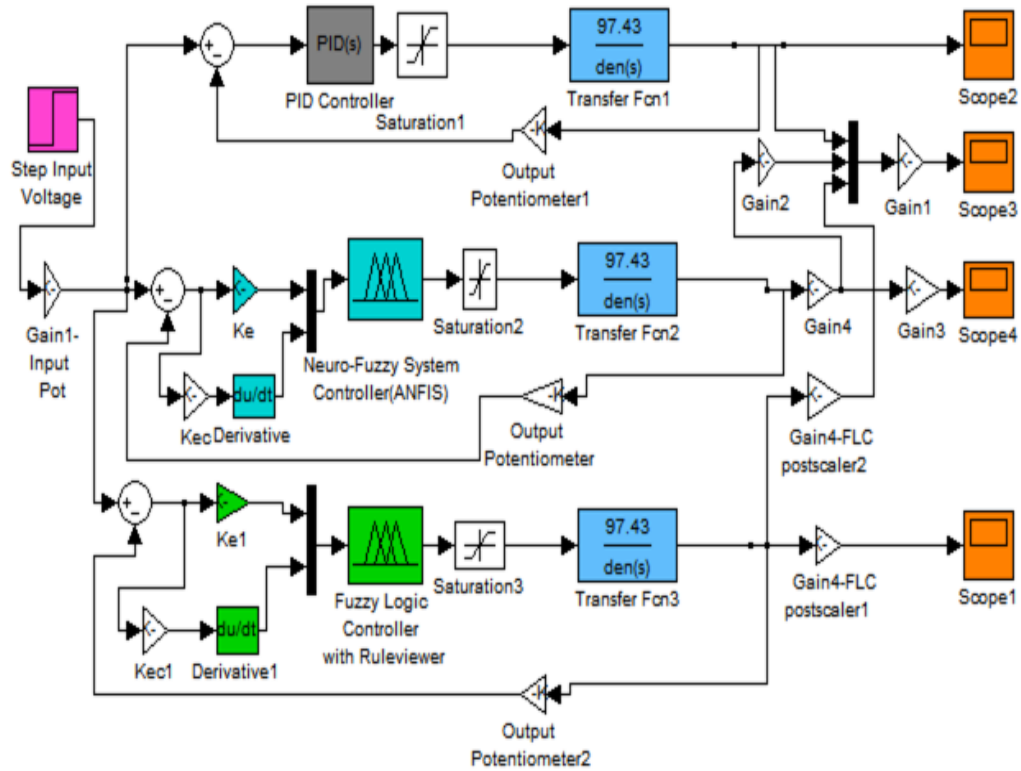
Figure 3.18: PID, FLC and NFSC Prototype SIMULINK Model Layout

However, the results presented used the first approach since it was convenient for the developed model, the available time as well as resources. The SIMULINK model for prototype testing is as shown in Fig. 3.19. The feedback is a signal representing the position.

3.7.3 Prototype Model and Experimental Set up

The first step in prototype system development was the realization of the mechanical assembly required to hold the parabolic antenna and bring it to the desired angular position.
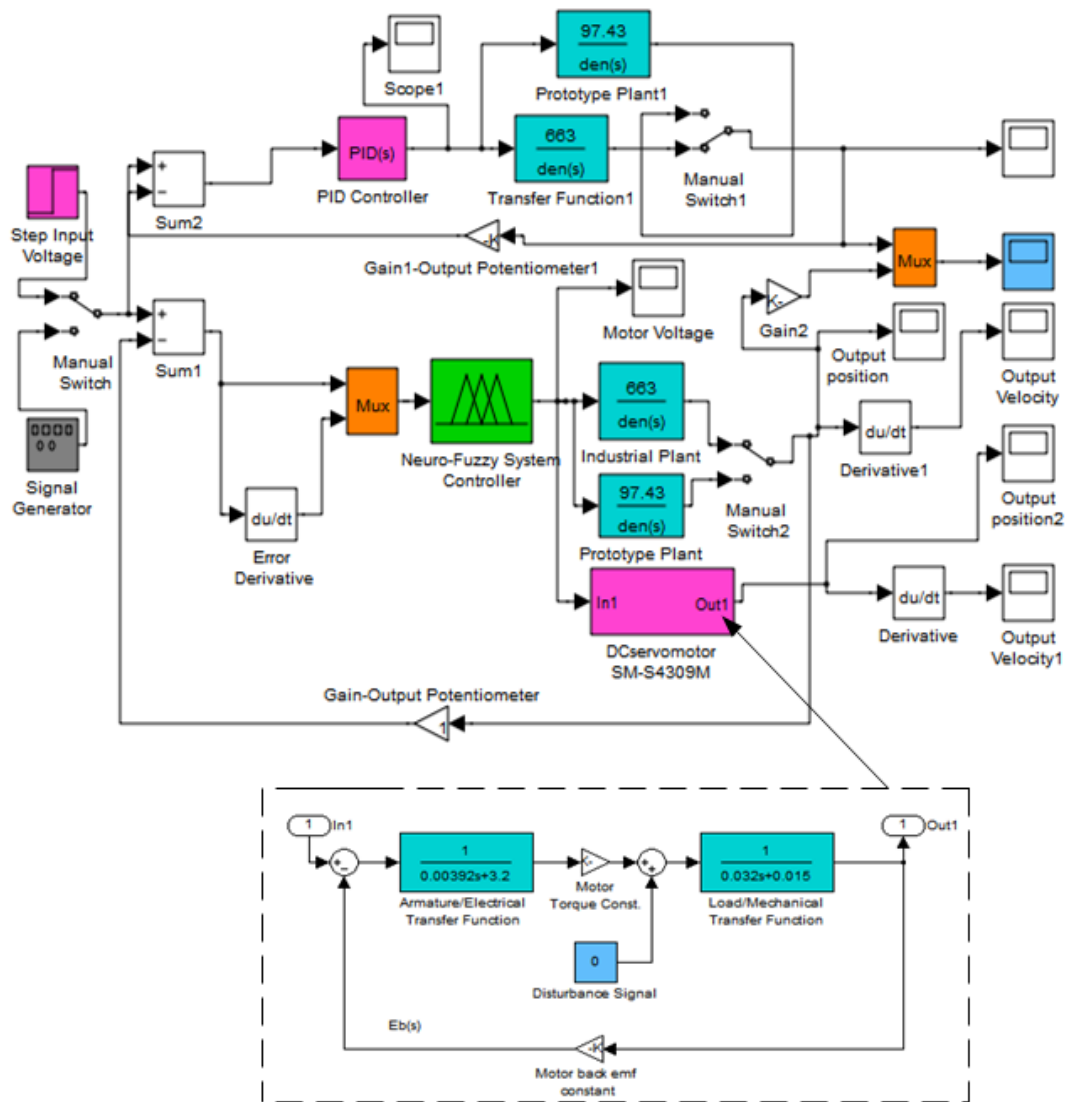
Figure 3.19: SIMULINK Model for antenna position system with PID and ANFIS

By means of the elevation movement system the mechanical design should enable the antenna to move upwards or downwards, depending on the direction of rotation of the elevation motor shaft from the current position through a total angular distance of 70^0. On the other hand, the azimuth tracking system should enable horizontal movement, depending on the direction of rotation of the azimuth motor shaft from the current position through a total angular distance of 180^0. This system was realized by fixing

two DC servomotors-SM-S4309M to an improvised pan-tilt system. A microcontroller (Arduino Mega 2560) preferred for its wide availability and easy manipulation used the NFSC algorithms created using MATLAB/SIMULINK to determine both the direction and amount of the servomotor (antenna) rotation and converted this information into the form of Pulse Width Modulation (PWM) signals sent to the servomotor driver unit. In practice, the alignment should be initiated based on the changing position of the target or only at the instants when the received signal level from the satellite under track (target) falls below the set threshold as monitored by the operator. However, in this case the angular coordinates were first computed off-line with reference to the targeted satellite locations, [43] and [44], and then this information fed to the system through input potentiometers calibrated in terms of volts/degrees rather than using a built-in computation unit. The information obtained regarding the satellites included: the desired Orbit Longitude, Dish Elevation, Azimuth (Magnetic Compass), Motor Drive sideways angle, main angle, downward tilt and polarization. Through calibration and appropriate scaling, these data sets were also converted to convenient forms for use in the training and testing of the ANFIS controller (see Table 4.5 and Table Appendix 2.1). The Neuro-Fuzzy System Controller (NFSC) was realized as two single input and single output closed-loop control systems instead of a two-input and two-output system because movements need to be triggered in only one direction at a time. The prototype circuit diagram constructed within Proteus 8 Professional Simulator environment for software implementation is as shown in Fig.3.20.
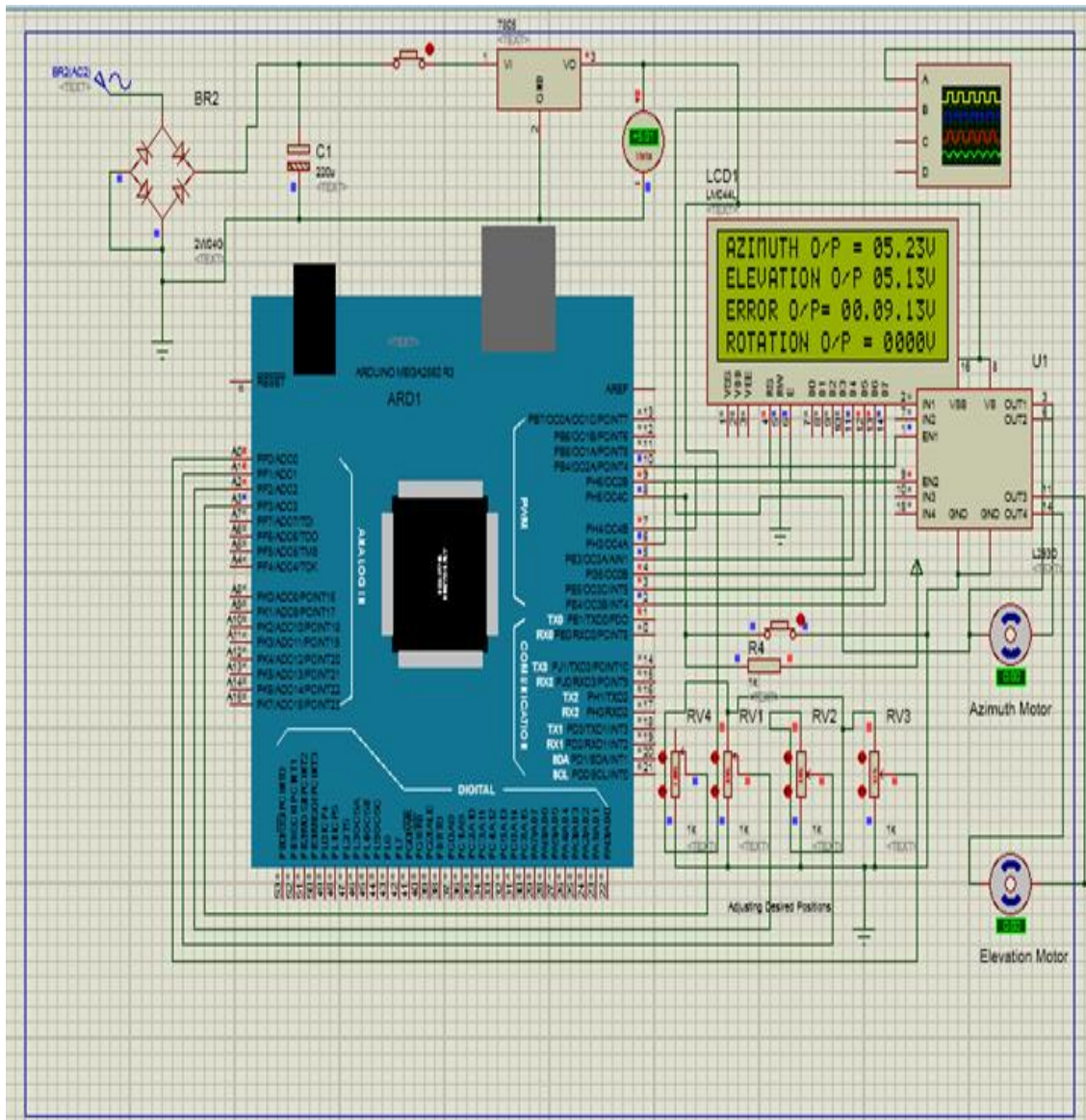
Figure 3.20: Circuit Diagram of Satellite Dish Positioning System Prototype

The experimental set ups for the prototype are as shown in Fig. 3.21 for the DC servomotor SM-S4309M and Fig. 3.22 for the improvised non-loaded pan-tilt platform. The overall hardware setup was centered on the Arduino Mega 2560 board.
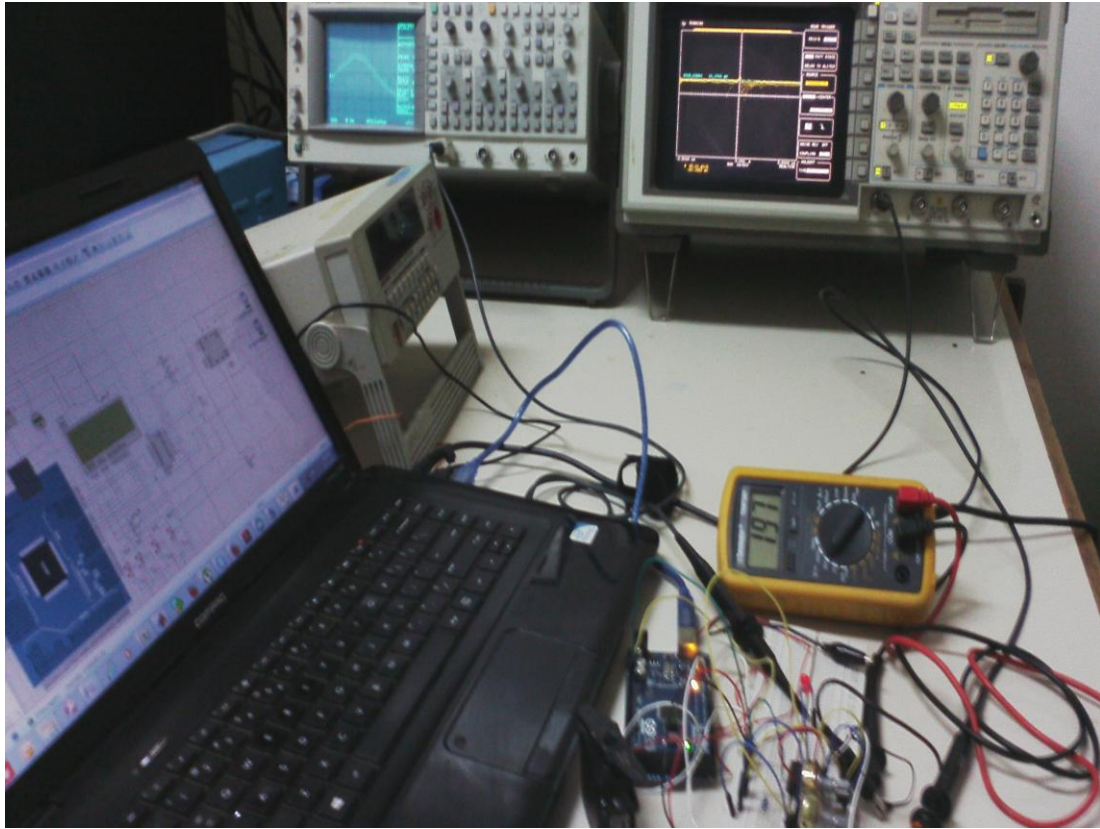
Figure 3.21: Experimental Set up of Prototype with the DC servomotor

The ANFIS code developed in C++ based on information derived from the MATLAB SIMULINK simulated model was converted to Arduino language and downloaded into the kit.

The set up was realized as follows:

1. The input potentiometer was connected to 5V power tapped from the Arduino board and central terminal connected to the A3 pin of the Arduino.

2. The horizontal rotation DC servomotor was connected to 5V power from the Arduino board and its white signal wire connected to PIN 9. Similarly, the vertical rotation DC servomotor was powered and its signal cable connected to PIN 10.
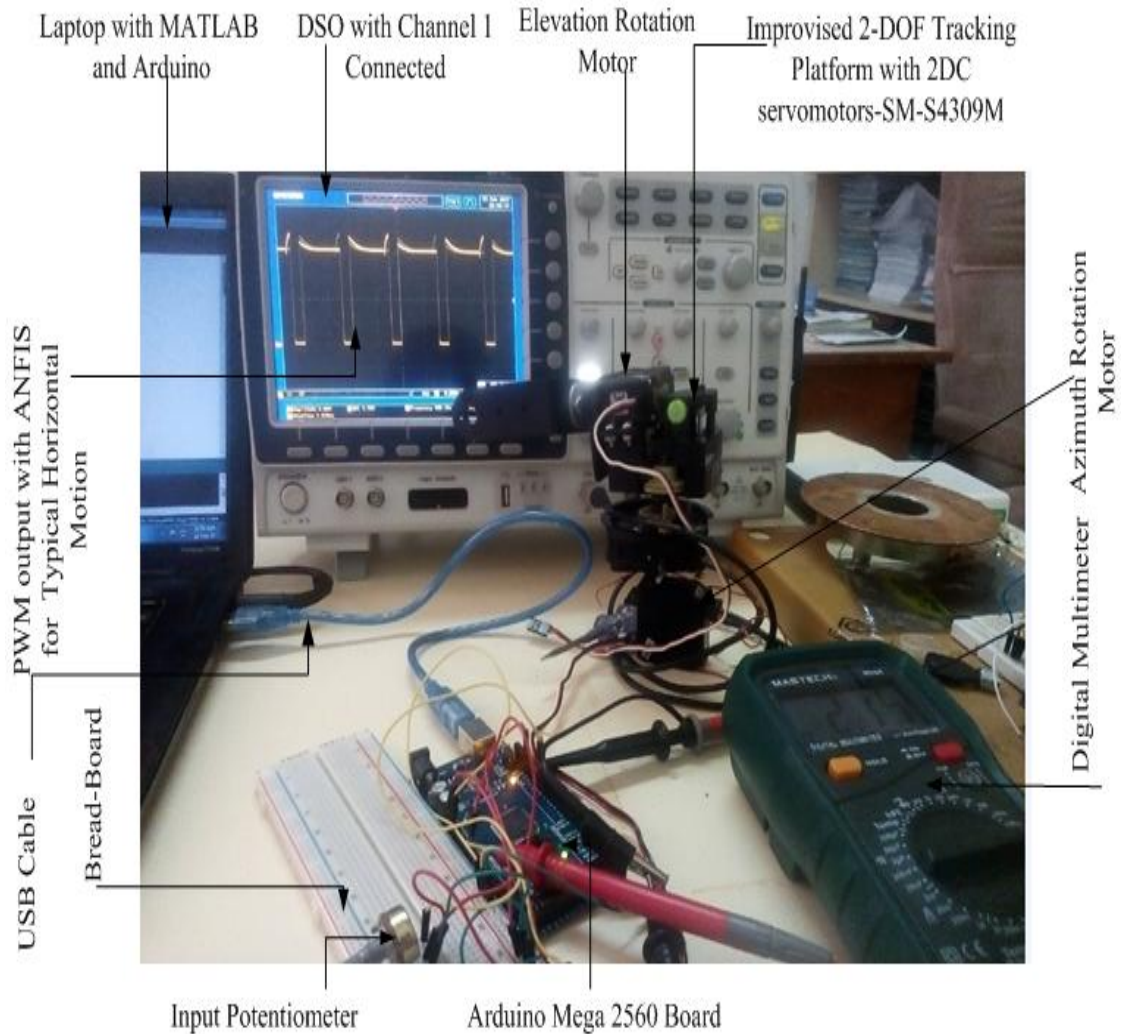
Figure 3.22: Experimental Set up of Prototype with Tracking Platform

3. The PWM outputs were taken from PINs 9 and 10 of the Arduino kit which were connected to the DSO through Channel-1. The DSO was then grounded.

4. The Arduino was connected to a laptop with MATLAB, Proteus and Arduino Development softwares installed through the USB cable and the desired motor drive voltages supplied via the input potentiometers. Finally, the corresponding PWM outputs were checked in the DSO.

73

Angular information about the locations for some satellites accessible from Juja, Kenya (Latitude: -1.1018°, Longitude: 37.0144°-identified based on the laptop's Internet Protocol address), was obtained from online sources [43] and [44].

These were then converted into corresponding voltages via input potentiometers and the output position for the respective servomotor measured via a digital multimeter. Since the system was considered off-line, the positions of the servomotors have been used to represent that of the load or the antenna in a real system. The results are shown in Table 4.4.

CHAPTER FOUR

RESULTS AND DISCUSSION

The goal of this chapter is to present analysis and discussion of the results obtained from the study. The developed Neuro-Fuzzy System Controller (NFSC) for a satellite antenna positioning system, with its algorithm created within the ANFIS framework, has been tested by both simulation and experiments. These were carried out in MATLAB-SIMULINK, Proteus Professional Prototyping Software and micro-controller environments. The NFSC as well as the PID controller was separately applied to both an industrial DC-servomotor satellite tracking plant and an experimental prototype while the FLC was tested on the industrial model only. In all cases, step input signal was selected as the reference signal since it directly represented changes in the position of the motors (load) and provided easy mapping with the potentiometers. The results obtained by using NFSC and FLC were compared with those of the PID in each case. This comparison was made in order to evaluate performance of the FLC and NFSC (in presence of saturation non-linearity) and to validate the accuracy of the design.

4.1 Results on Development of NFSC Algorithm

In the development of the NFSC, two training techniques i.e. back propagation algorithm (which resembles ANN) and the hybrid optimization technique (which is characteristic of ANFIS) were available for deployment. Moreover, there are several types of input membership functions that could be used and also whether the output membership functions took linear or constant forms. Consequently, it was necessary to check the suitability of each optimization technique in minimizing the error between the

desired position and the actual position of the DC servomotor prior to settling on one of them. The results obtained from an investigation of the performance of the two training techniques with different types and number of both input and output membership functions has been summarized in Table 4.1. It was noted that the ANFIS model deploying 7x7 input triangular MFs, 49 linear output MFs and trained by the hybrid algorithm registered the lowest mean squared error of only 1.5×10^{-4} and therefore offered the best dynamic and stabilized performance.

Table 4.1: ANFIS Training and MFs Selection

S/No.	Input Membership Functions (MFs)		Output Membership Functions (MFs)		Training Error Based on Optimization Method	
	Number	Type	Number	Type	Back Propagation	Hybrid
1	5,5	Triangular	25	Constant	0.155	0.165
2	5,5	Triangular	25	Linear	0.020	0.250
3	5,5	Trapezoidal	25	Constant	0.320	0.187
4	5,5	Trapezoidal	25	Linear	0.250	0.032
5	5,5	Gaussian	25	Constant	0.187	0.140
6	5,5	Gaussian	25	Linear	0.250	0.002
7	7,7	Triangular	49	Constant	0.185	0.025
8	7,7	Triangular	49	Linear	0.275	0.00015
9	7,7	Trapezoidal	49	Constant	0.127	0.120
10	7,7	Trapezoidal	49	Linear	0.250	0.00038
11	7,7	Gaussian	49	Constant	0.450	0.100
12	7,7	Gaussian	49	Linear	0.275	0.0006

Surface plots and corresponding contour plots showing relationship between the two inputs parameters i.e. position error (input 2) and change in position error (input 1) and the ANFIS controller output (input signal to motor drive) before training and after training are given in Figure 4.1 and Figure 4.2.
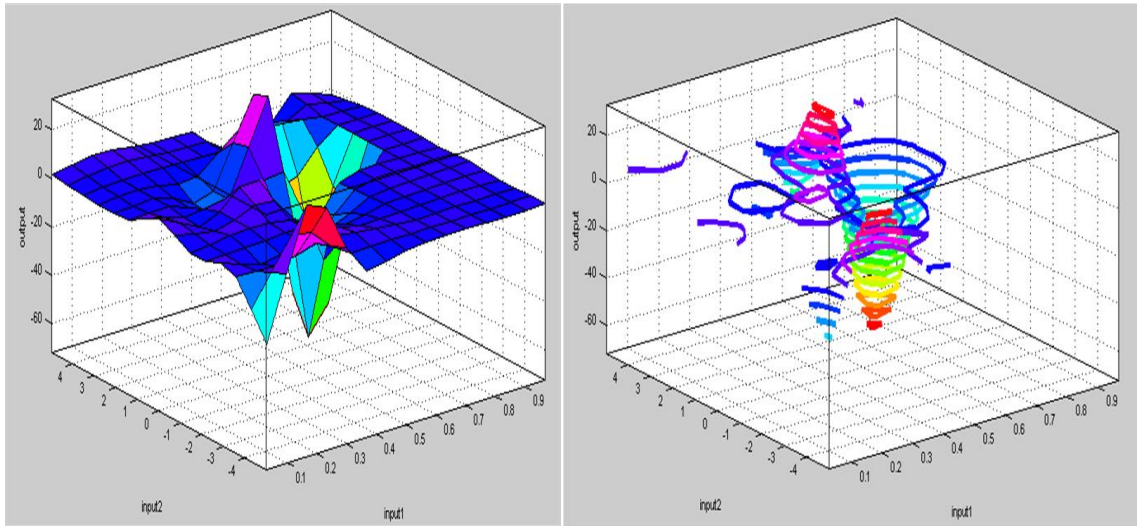
(a) ANFIS Surface Plot Before Training (b) ANFIS Contour Plot Before Training

Figure 4.1: ANFIS Surface and Contour Plots Before Training
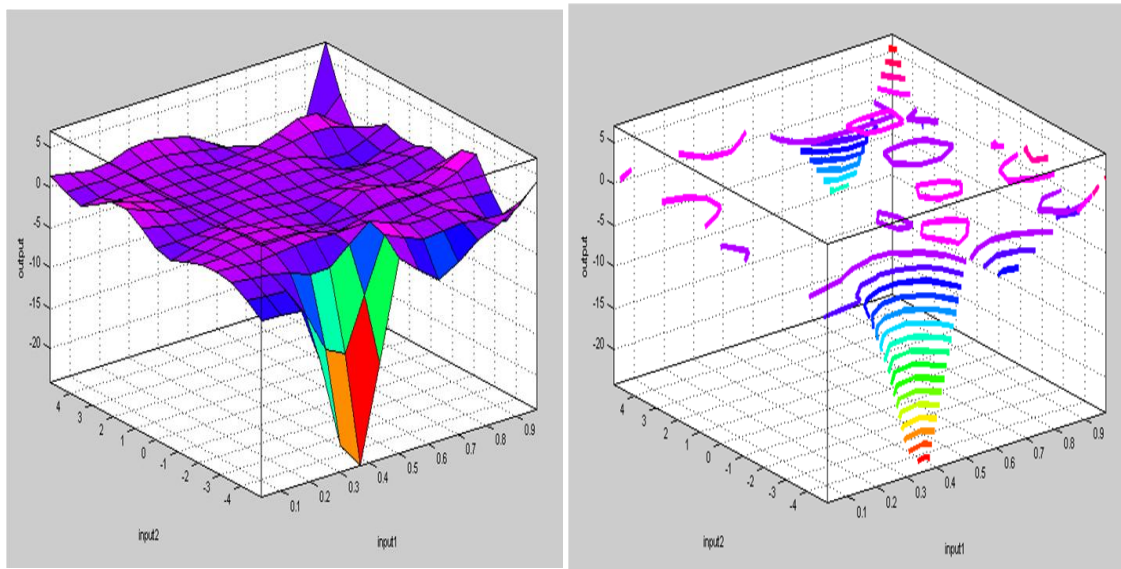
(a) ANFIS Surface Plot After Training (b) ANFIS Contour Plot After Training

Figure 4.2: ANFIS Surface and Contour Plots After Training

From the 3D surface plots and contour plots in Figure 4.1 and Figure 4.2, the blue color
surfaces indicate the low error values i.e. that better output DC servo motor (load)
position can be obtained and also sustained much easily (an almost linearized control

77

surface). The red, yellow and cyan color surfaces indicate the high error values which decrease from the former to the latter. This means that the probability of the ANFIS controller to converge to or predict desired output is low and much difficult to realize (resembling a non-linear control zone). From Figure 4.1, it is observed that before training the ANFIS, the antenna pointing error values are high in the DE range of 0.5 to 0.7 and E range of −1 to 1. However, after training, the error values are high in the DE range of 0.3 to 0.4 and E range of −3 to−4. The error values are low in all other ranges.

4.2 PID, FLC and NFSC Results with Industrial Model

The outputs of the PID and FLC controllers in terms of control signal amplitudes against time are shown in Figure 4.3 and Figure 4.4 respectively. Similarly, the output of the NFSC representing the control signal amplitudes (output of controller) before training and after training are shown Figure 4.5 a) and b) respectively. The comparison between response of Mamdani FLC and Sugeno FLC is presented in Figure 4.6.
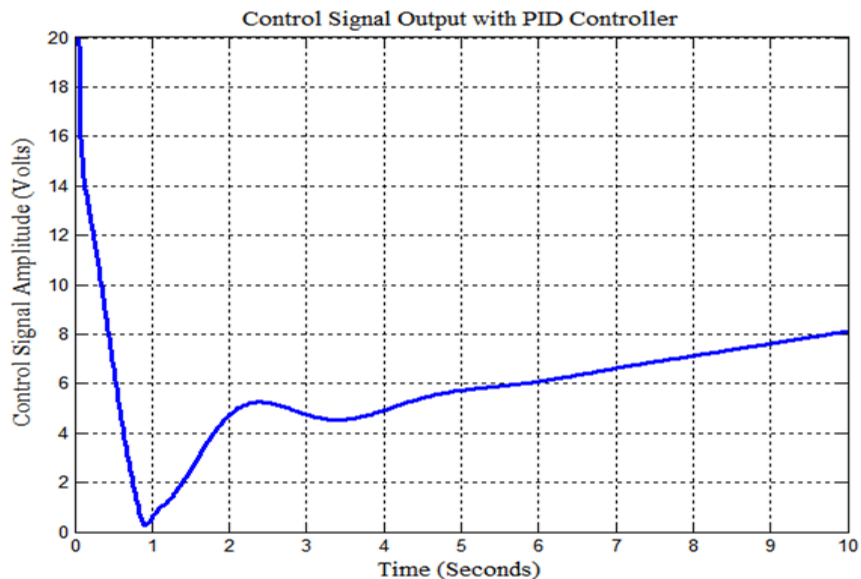
Figure 4.3: PID Controller output

78
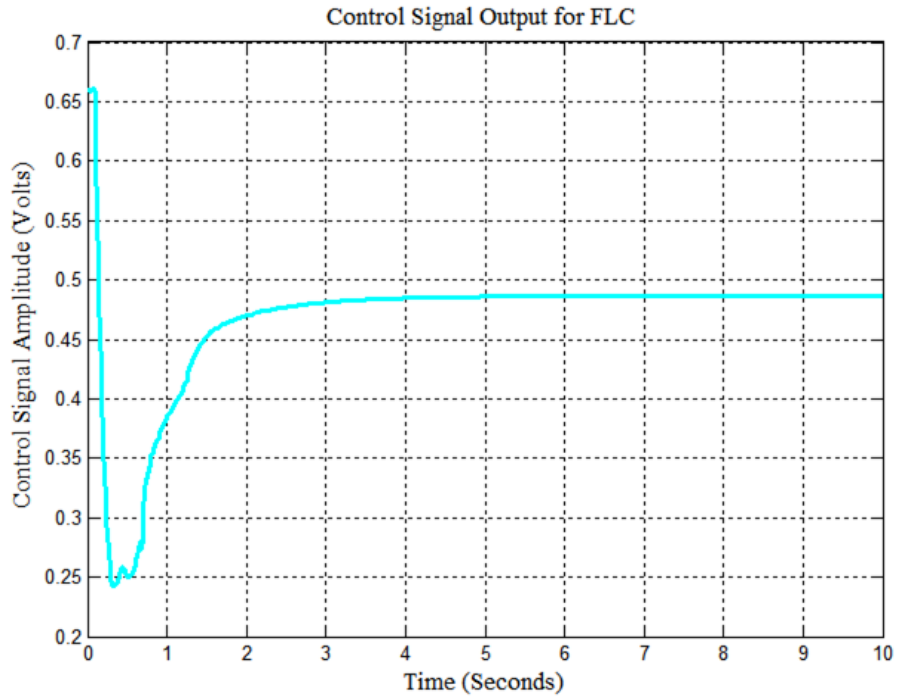
Figure 4.4: FLC Controller output
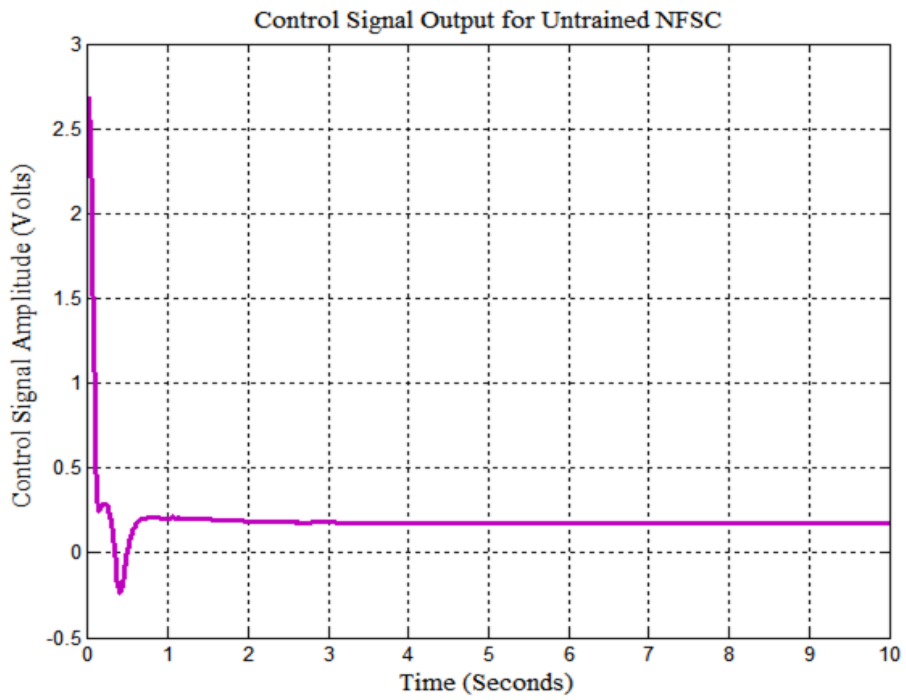
a) Output of NFSC before Training

79

Control Signal Output for NFSC After Training
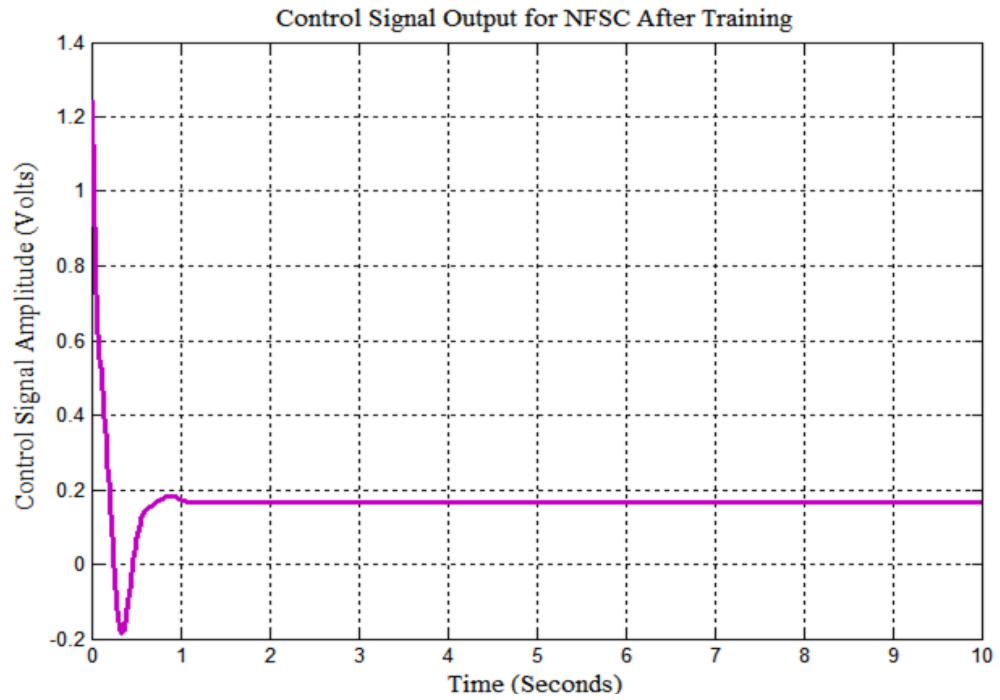
b) Output of NFSC After Training

Figure 4.5: Output of NFSC Before and After Training

Response of Mamdani and Sugeno FLC
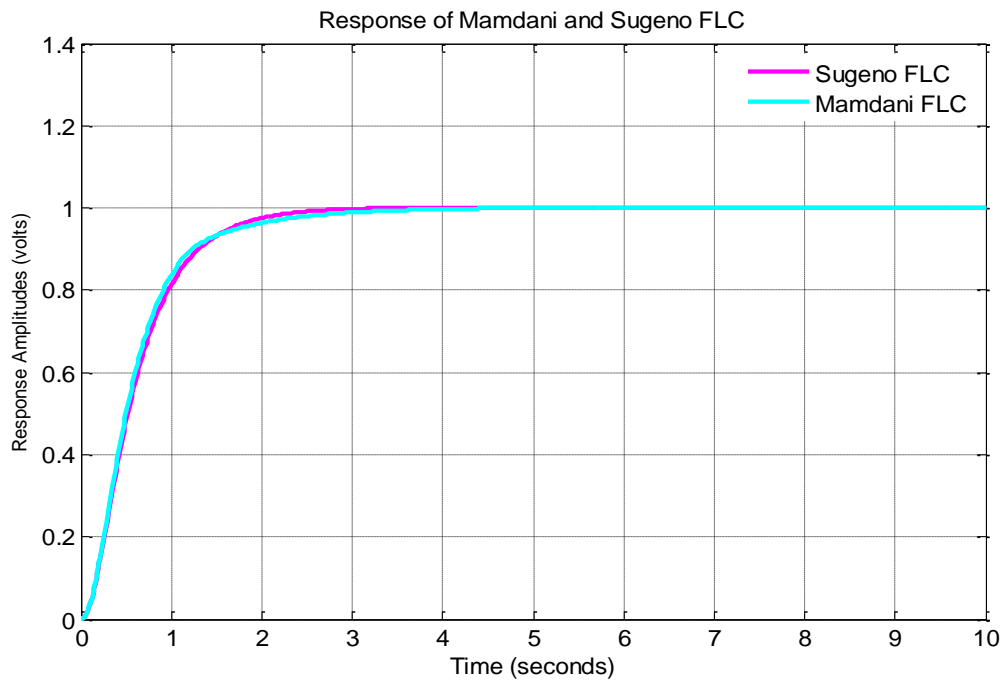
Figure 4.6: Response of Mamdani and Sugeno FLC

Figure 4.7 indicates a comparison between the Untrained NFSC response (plant output) to step input with that of the PID and FLC. With the PID controller acting under step input, it is seen that the response is not good owing to high overshoot and increased settling time. Both the Mamdani type FLC and the Sugeno FLC model responses to step input were investigated and noted to show no overshoot but the rise time is comparatively longer. The performance of the trained NFSC compared with PID and FLC is shown in Figure 4.8.
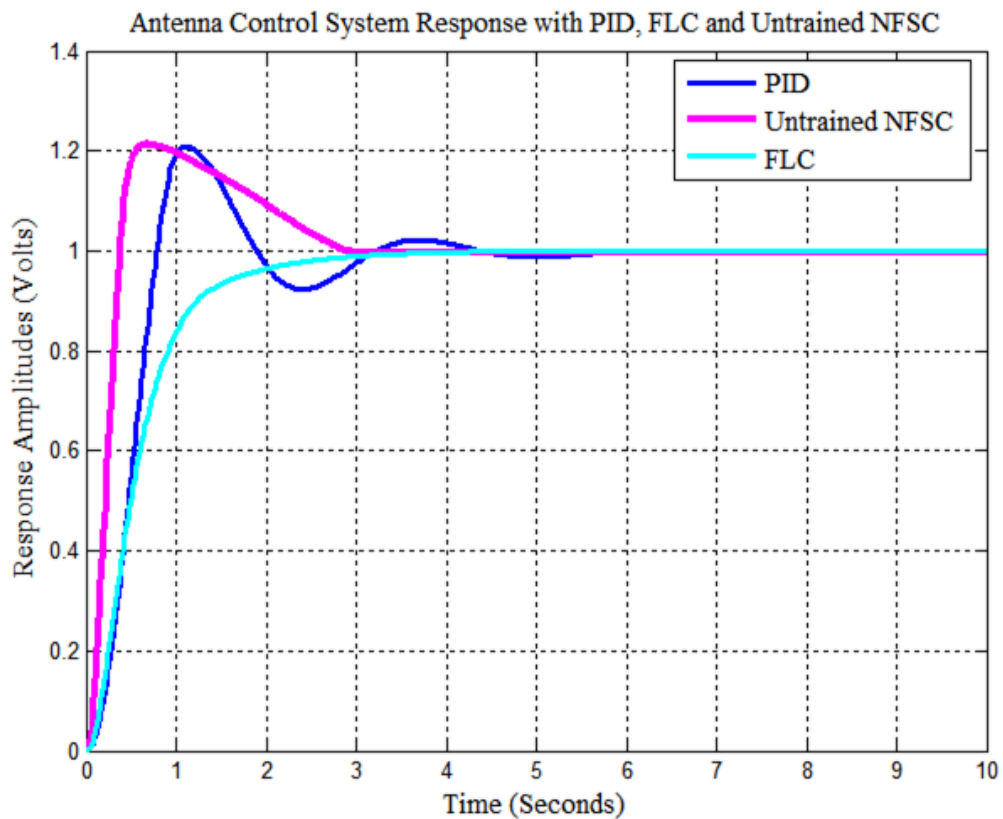
Figure 4.7: Step input response with PID, FLC and Untrained NFSC
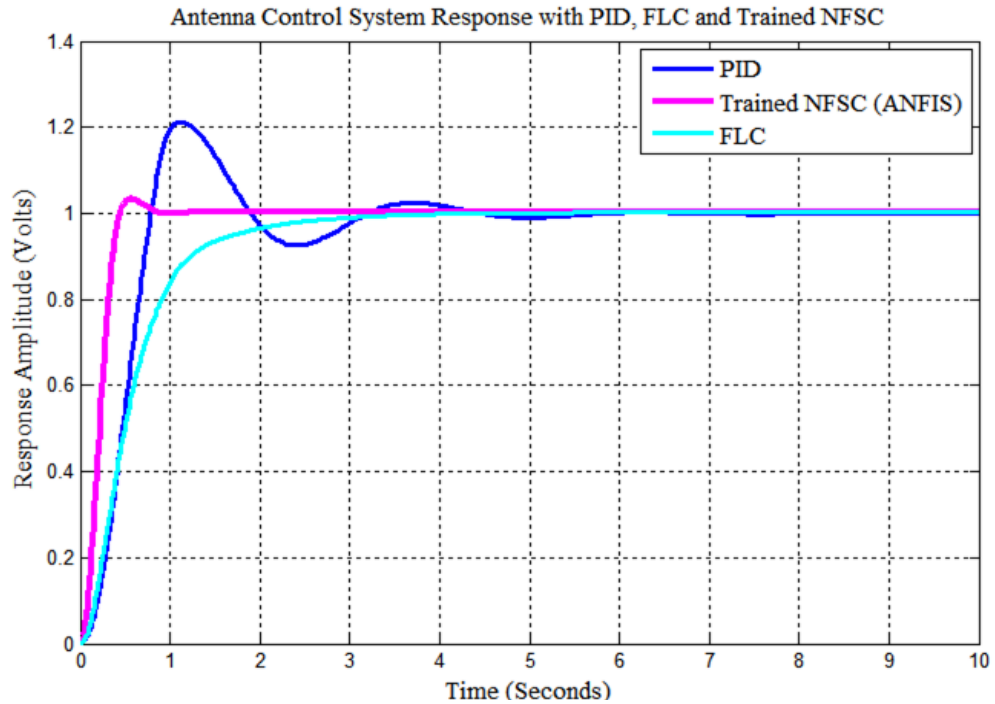
Figure 4.8: PID, FLC and Trained NFSC step input response

Before training, it was observed that the response of NFSC depicted a high overshoot and longer settling time too but with a faster rise time. This is attributed to the fact that the controller had not been acquainted with the input data it was meant to work with and therefore could neither easily predict nor converge to the desired output. Once the NFSC has been trained, it is made aware of the kind of input data it is meant to handle and therefore possesses the ability to predict and promptly converge to the correct output based on the supplied sets of inputs.

In addition, the system response was analyzed using NFSC, FLC and PID Controllers when different values of reference step input signal corresponding to the desired motor (hence load) positions were applied. The corresponding results were studied and the estimated time response characteristics have been summarized in Table 4.2.

Table 4.2: Results With Various Step Inputs

Step Input	PID			FLC-Mamdani			FLC-Sugeno			NFSC		
	t_r	t_s	M_p	t_r	t_s	M_p	t_r	t_s	M_p	t_r	t_s	M_p
(V)	(s)	(s)	(%)	(s)	(s)	(%)	(s)	(s)	(%)	(s)	(s)	(%)
1	0.7	4.0	21.0	1.9	2.5	0.0	1.8	2.1	0.0	0.2	0.8	7.0
2	0.6	4.2	20.0	2.1	2.4	0.0	1.7	2.0	0.0	0.2	0.8	7.0
3	0.7	4.5	21.0	2.2	2.5	0.0	1.8	2.0	0.0	0.3	0.7	8.0
4	0.7	4.4	22.0	2.2	2.4	0.0	1.7	2.0	0.0	0.2	0.8	8.0
5	0.6	4.5	21.0	2.2	2.4	0.0	1.7	2.1	0.0	0.3	0.8	9.0
6	0.7	4.5	22.0	2.0	2.4	0.0	1.8	2.1	0.0	0.2	0.9	9.0
7	0.7	4.2	21.0	2.0	2.3	0.0	1.8	2.1	0.0	0.3	0.9	7.0
Avg	**0.7**	**4.3**	**21.0**	**2.0**	**2.4**	**0.0**	**1.8**	**2.1**	**0.0**	**0.2**	**0.8**	**8.0**

From the results registered with various step inputs, it is seen that NFSC provides response with faster settling times and minimized rise time albeit the presence of saturation nonlinearity. From the average values in Table 4.2, NFSC recorded the best average performance.

The rise time is 2.0 sec. for Mamdani FLC model, 1.8 sec. for Sugeno FLC model, 0.2 sec for the Takagi-Sugeno NFSC model and 0.7 sec for the PID control for response to transit from 10% to 90% of the steady state value.

The maximum overshoot with NFSC is minimized up to 8% while it was 21% with PID though there was no overshoot with the FLC controller.

The settling time is 2.4 sec for Mamdani FLC model, 2.1 sec for Sugeno FLC, 0.8 sec for the NFSC and 4.3 sec for the PID.

It can be understood from this study that while using NFSC the system tends to approach the new set position in the fastest time (0.2 sec) and with acceptable overshoot (8%) as

compared to both PID and FLC controller. The PID controller despite showing unacceptable overshoot does not easily reach a steady state.

Although no overshoot was registered with FLC, it lacks the learning ability offered by the NFSC which has been acquired at the expense of an 8% overshoot introduced in steady state value but which is still within the desired limit of less than 10%. Therefore, the NFSC met all the design specifications.

4.3 Results of PID and NFSC with Prototype Model

In Figure 4.9, a plot is made to compare the step input response between the PID and NFSC before training while Figure 4.10 shows the response after training and optimization the NFSC.
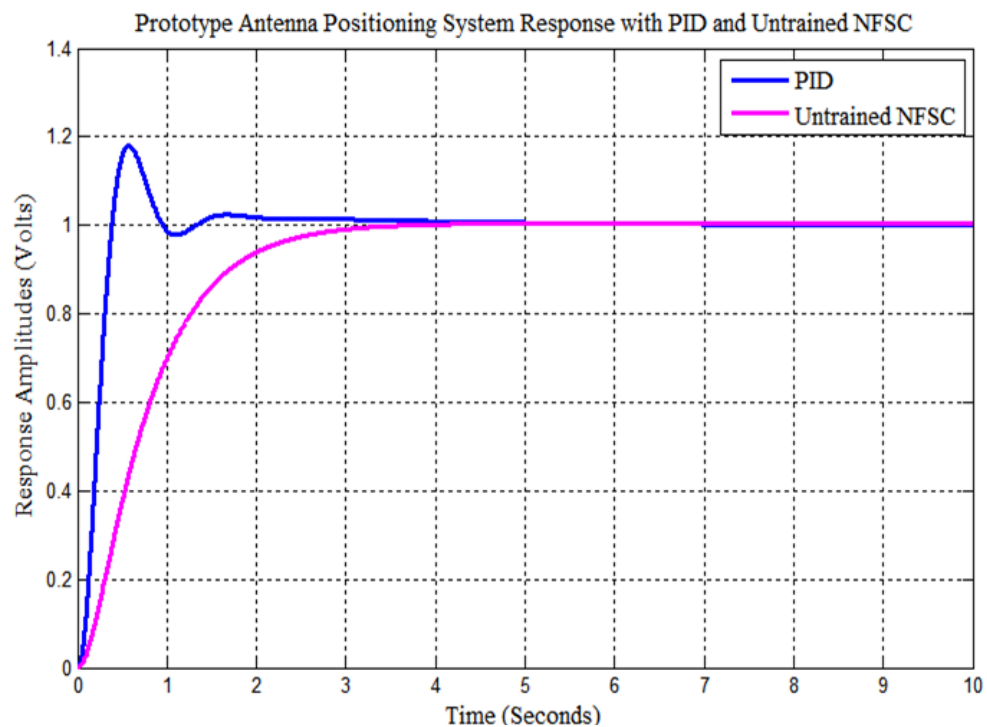
Figure 4.9: Response of PID and Untrained NFSC on Prototype
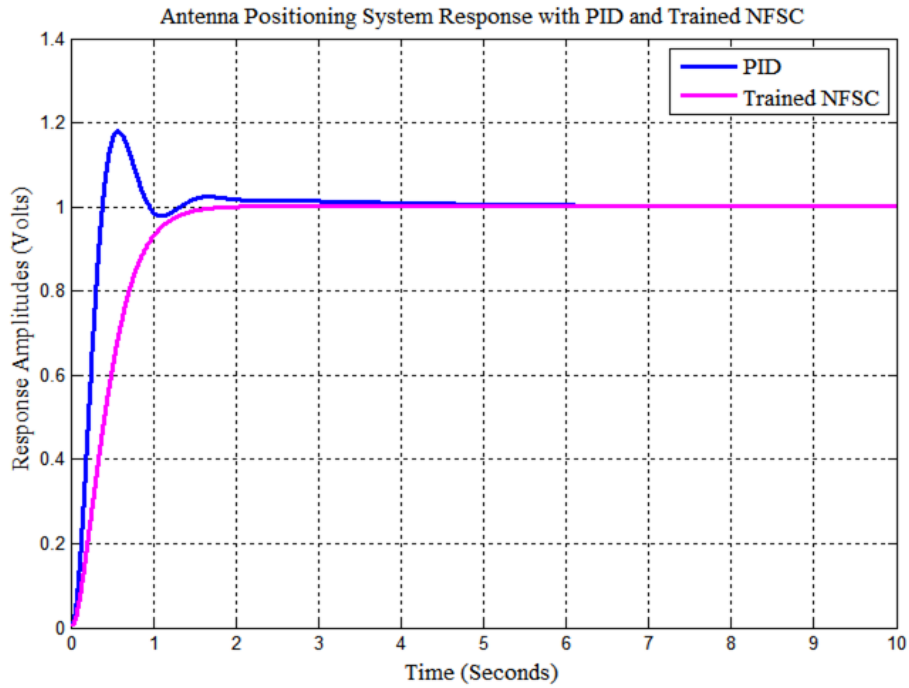
Figure 4.10: Response of PID and Trained NFSC on Prototype

The prototype system response was also tested using the NFSC and PID controllers when different values of reference step input signal commensurate to the desired positions were applied as shown in Table 4.3.

Table 4.3: Prototype Results with Various Step Inputs

Step Input	PID			NFSC Response Before Training			NFSC Response After Training		
	t_r	t_s	M_p	t_r	t_s	M_p	t_r	t_s	M_p
(V)	(s)	(s)	(%)	(s)	(s)	(%)	(s)	(s)	(%)
1	0.4	4.5	18.5	2.2	3.5	0.0	1.5	1.6	0.0
2	0.5	4.2	18.0	2.2	3.7	0.0	1.2	1.7	0.0
3	0.4	4.4	19.0	2.3	3.5	0.0	1.3	1.7	0.0
4	0.5	4.8	18.5	2.2	3.7	0.0	1.2	1.6	0.0
5	0.5	4.9	18.0	2.3	3.6	0.0	1.3	1.5	0.0
Avg	**0.5**	**4.6**	**18.5**	**2.3**	**3.6**	**0.0**	**1.3**	**1.6**	**0.0**

From the average values in Table 4.3, NFSC recorded the best average performance. The rise time is 2.3 sec for the Takagi-Sugeno NFSC model prior to training, 1.3 sec after training and 0.5 sec for the PID controller. The maximum overshoot is 18.5 % with PID and 0.0% with NFSC before and after training the NFSC. The settling time is 3.6 sec and 1.6 sec for the NFSC before and after training respectively due to its learning ability and 4.6 sec for the PID controller.

This can once again be explained by the fact that while using NFSC the system tends to approach and settle at the desired position in the fastest time as compared to PID which apart from its high overshoot takes longer to acquire steady state. The NFSC manifested its learning strength which was achieved at the expense of increased rise time of 1.3 sec introduced in the response. However, this is still well within the desired rise time limit of less than 4 sec and hence highly acceptable.

By comparing the results obtained between the industrial model and the prototype model using the developed control algorithms, it was observed that even with changes in the plant model, there was no significant impact on the control system performance. This is attributed to the training of the NFSC which injected the right level of intelligence to the controller thereby improving its time domain step response characteristics and tolerance to changes in plant dynamics (nonlinearities). This therefore, is a direct pointer towards the ability of the controller to work for the DC servomotor system non-linearities and other dynamic changes in its operating conditions. A typical Pulse Width Modulated (PWM) output from the prototype circuit within the Proteus Professional Software environment is shown in Figure 4.11 at a duty ratio of 25%.
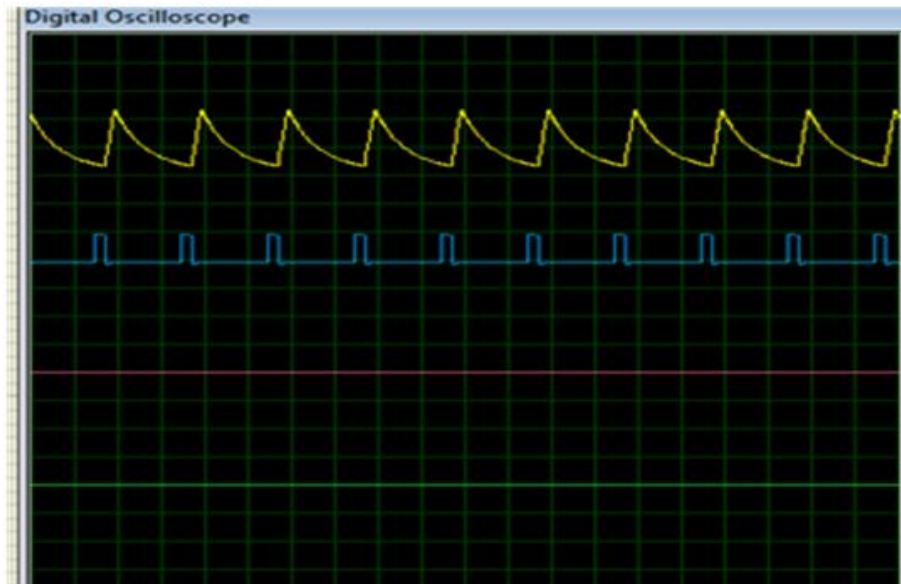
Figure 4.11: DSO PWM signals under ANFIS in Proteus

4.4 Experimental Results

The experimental results, shown in terms of Pulse Width Modulated (PWM) signals, on the performance of the NFSC on the DC servomotor SM-S4309M prototype antenna positioning hardware model with various reference position inputs were observed as shown in Figures 4.12, 4.13, 4.14 and 4.15.
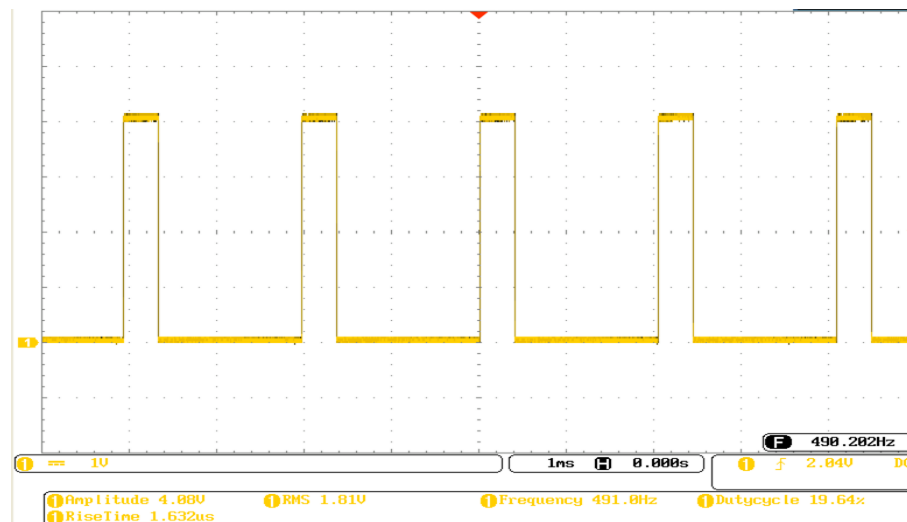
(a) PWM Output for a 0.00V Input
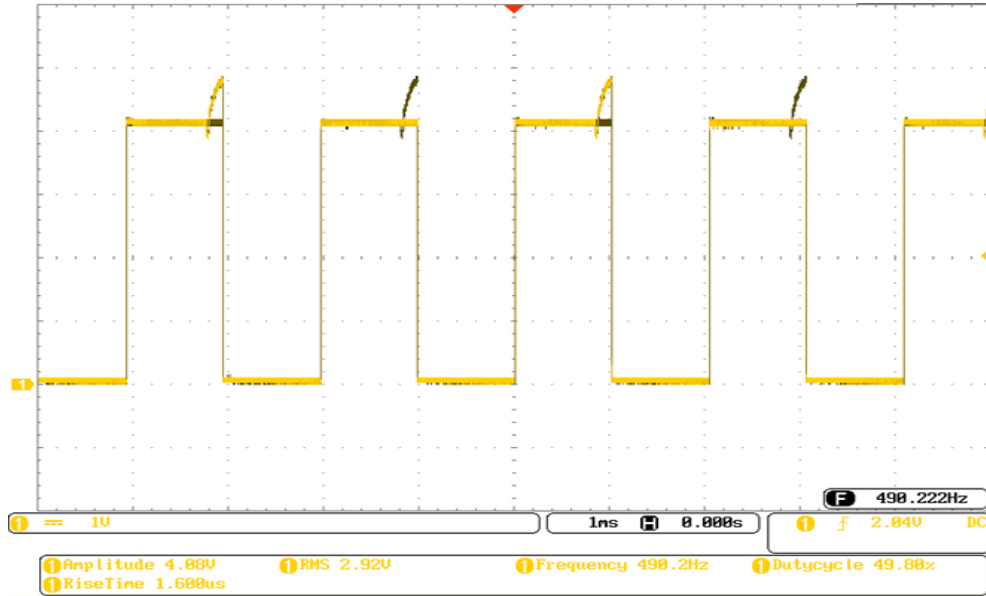
(b) PWM Output for a 1.00V Input

Figure 4.12: PWM Output with NFSC for 0.00V and 1.00V Inputs
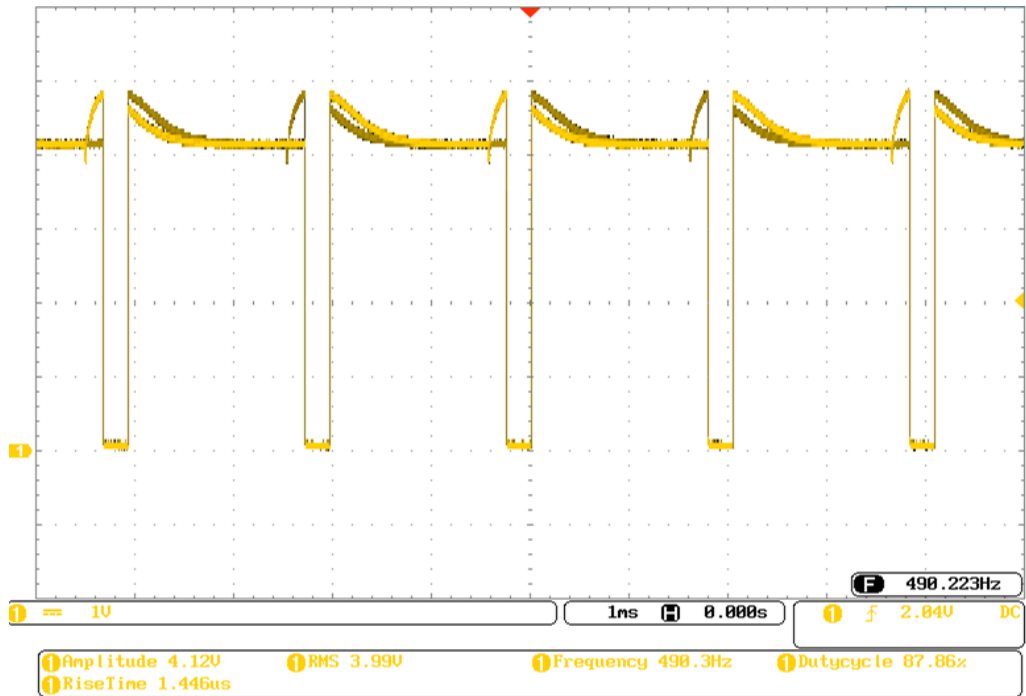
(a) PWM Output for a 1.50V Input
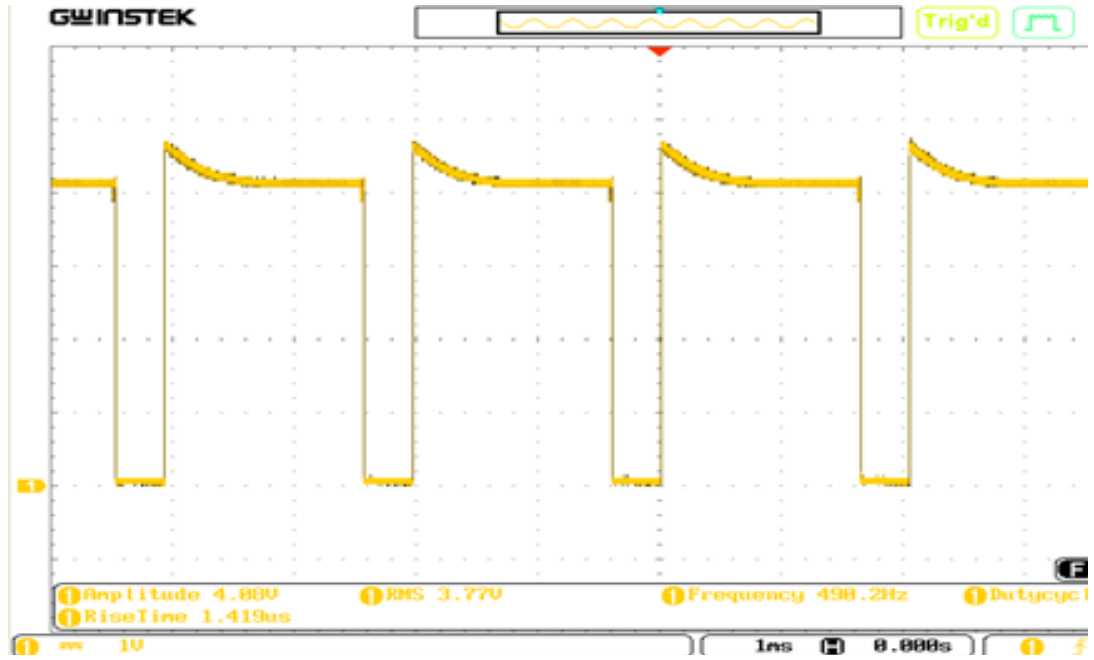
(b) PWM Output for a 2.00V Input

Figure 4.13: PWM Output with NFSC for 1.50V and 2.00V Inputs
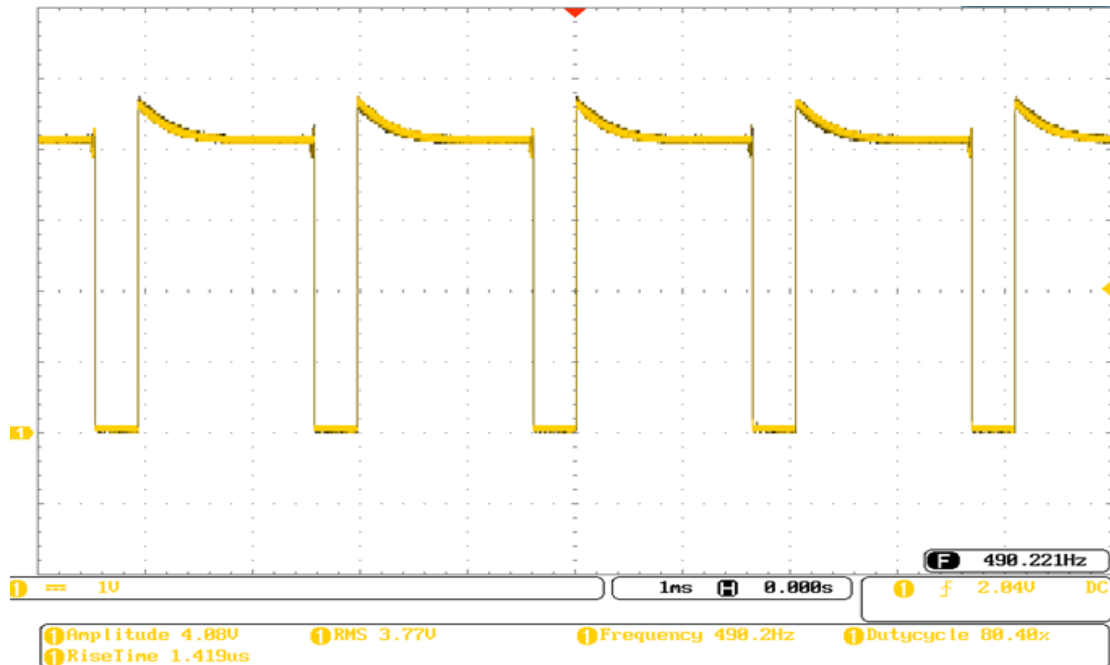
(a) PWM Output for a 2.50V Input
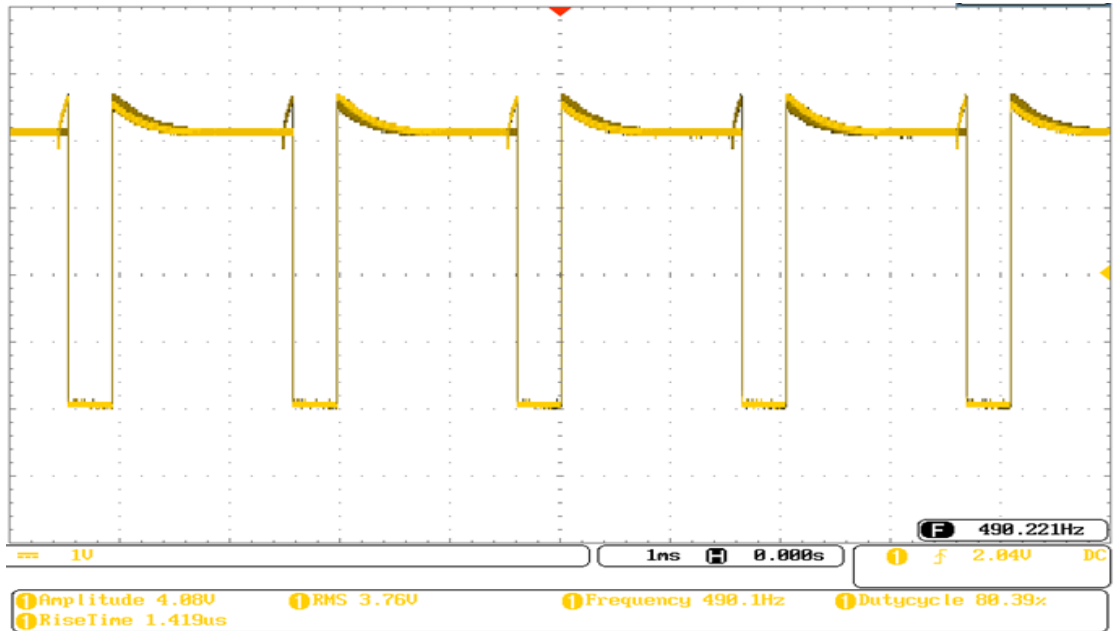
(b) PWM Output for a 3.00V Input

Figure 4.14: PWM Output with NFSC for 2.50V and 3.00V Inputs
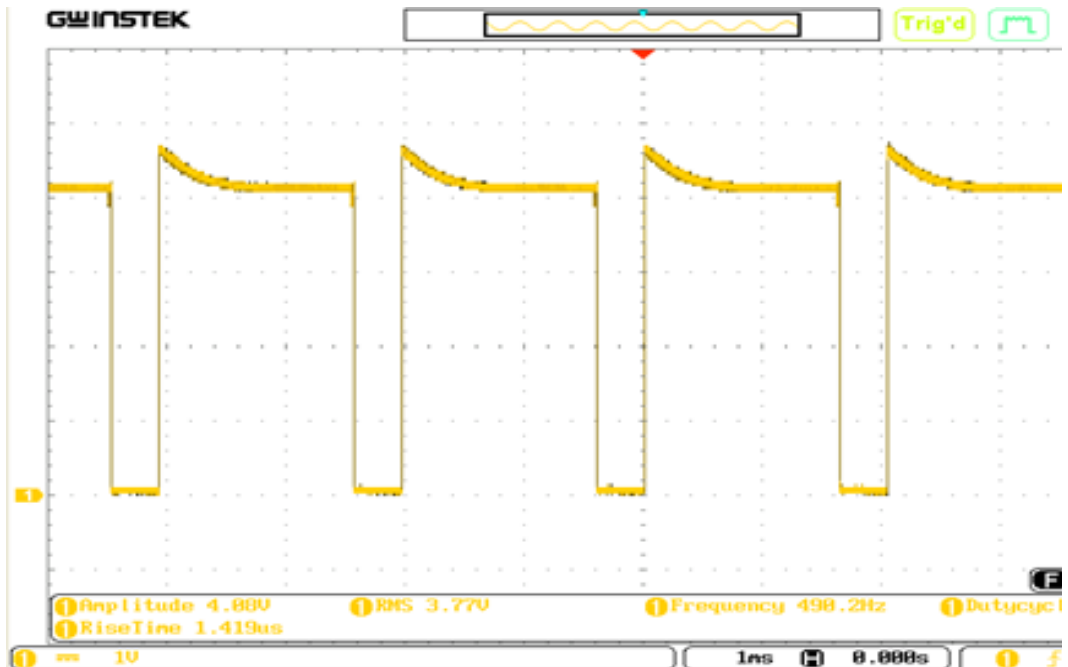
(a) PWM Output for Desired Voltage of 3.50V
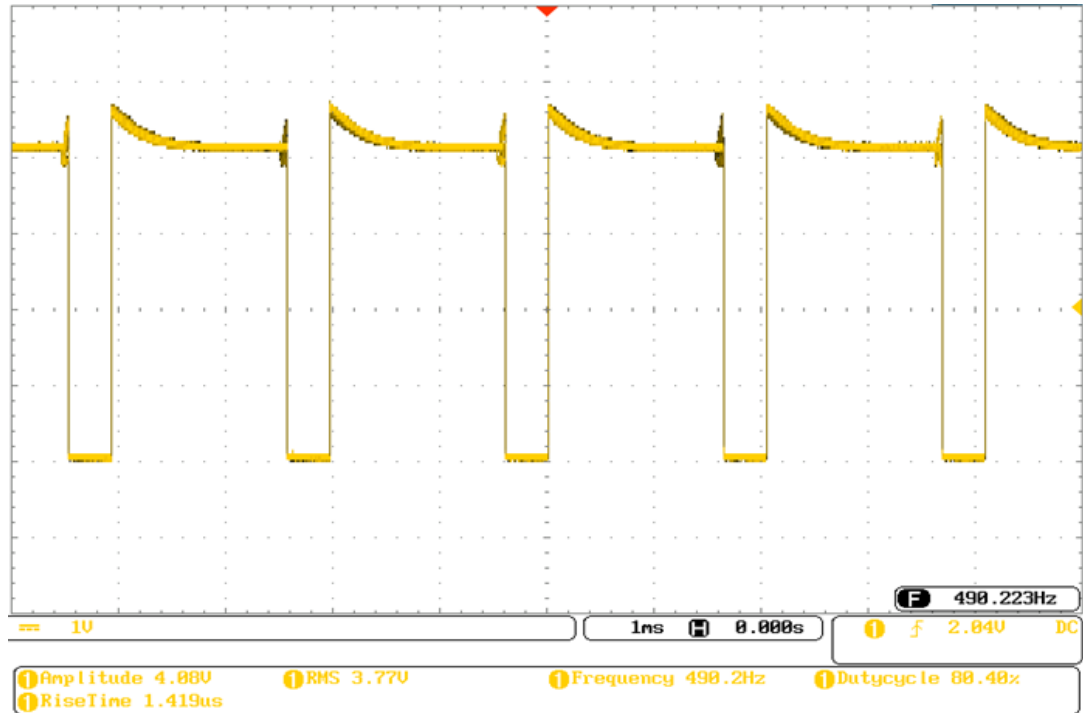
(b) PWM Output for a 4.00V Input

Figure 4.15: PWM Output with NFSC for 3.50V and 4.00V Inputs

The electrical inputs to the DC servo motor were converted to PWM signals using code running on Arduino Mega 2560 microcontroller to provide easy visualization on the Digital Storage Oscilloscope (DSO). The signals also aid in maintaining a particular value of electrical input to the motor for the entire duration of the pulse (based on the duty cycle). Fig. 4.16 assists in extracting the key parameters i.e. duty cycle and the dc voltage, from the PWM waveforms which are summarized in Table 4.4.
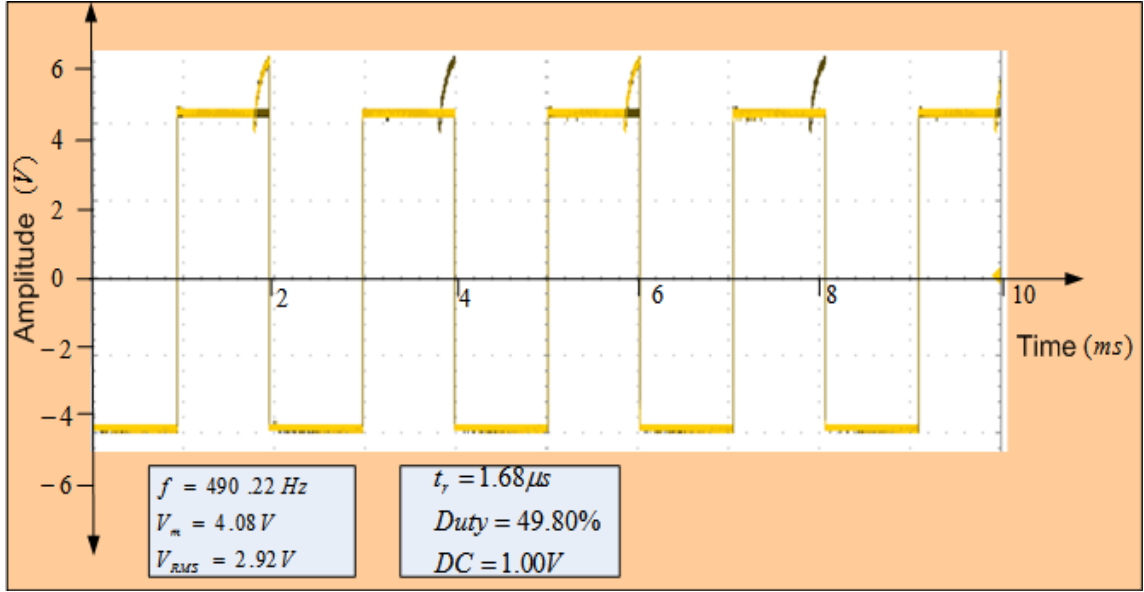
b) **PWM Output with NFSC for 1.00V input**
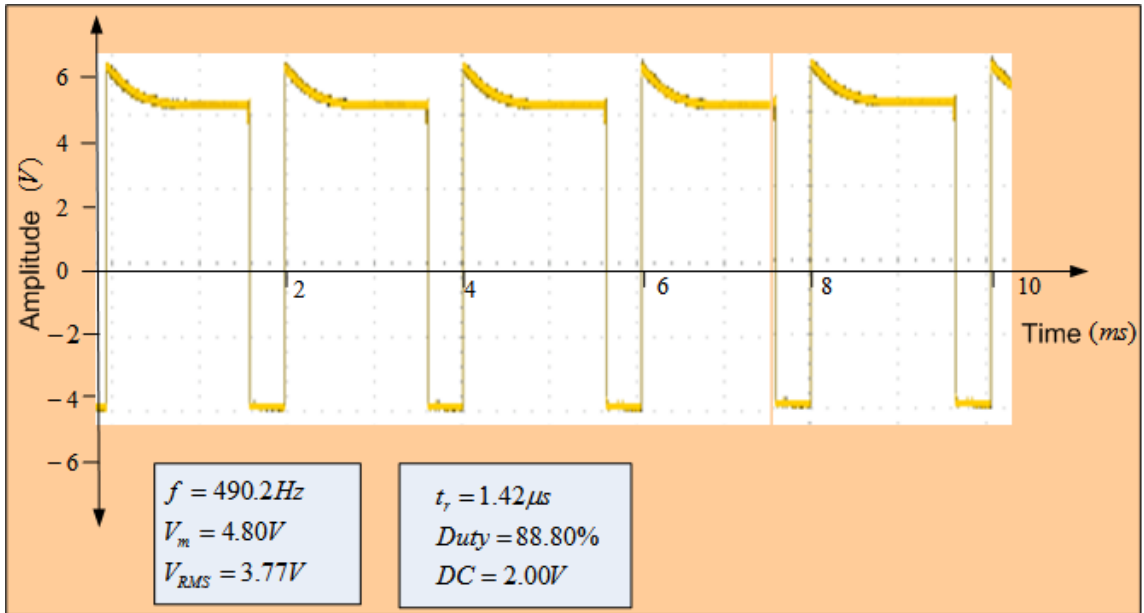
c) **PWM Output with NFSC for 2.00V Input**

Figure 4.16: Interpretation of PWM Outputs with NFSC

The performance of the NFSC in dish antenna positioning was tested with selected satellite locations and the results obtained recorded as shown in Table 4.5. Since the system was considered off-line, the positions of the servomotors have been used to represent those of the load or the antenna in a real system.

Table 4.4: Interpretation of PWM Outputs with NFSC

Figure	Electrical Input to Motor (V)	Amplitude (V)	RMS Value (V)	Rise Time (µs)	Duty Cycle (%)	Frequency (Hz)
4.12(a)	0.00	4.08	1.81	1.632	19.64	490.2
4.12(b)	1.00	4.08	2.92	1.608	49.88	490.2
4.13(a)	1.50	1.50	3.99	1.446	87.86	490.3
4.13(b)	2.00	4.08	3.77	1.419	80.40	490.2
4.14(a)	2.50	4.08	3.77	1.419	80.40	490.2
4.14(b)	3.00	4.08	3.76	1.419	80.39	490.1
4.15(a)	3.50	4.08	3.77	1.419	80.40	490.2
4.15(b)	4.00	4.08	3.77	1.419	80.40	490.2

Table 4.5: Experimental Results with Various Satellite locations

S/No.	Desired Satellite	Desired Motor Drive				Measured Moto Drive With ANFIS			
		Sideways		Vertical		Sideways		Vertical	
		Deg	Volt	Deg	Volt	Deg	Volt	Deg	Volt
1	108E TELKOM 1	79.50	2.21	−34.5	−0.96	78.32	2.04	−35.58	0.99
2	95.2E SKYNET 5A	66.10	1.84	−21.1	−0.59	65.46	1.80	−20.26	−0.57
3	85.1E INTELSAT 15	55.20	1.53	−10.2	−0.28	55.99	1.62	−9.99	−0.27
4	80E COSMOS 2473	49.60	1.38	−4.60	−0.13	50.62	1.28	−4.82	−0.15
5	70.5E EUTELSAT 70B	38.90	1.08	6.00	0.17	37.35	1.00	5.76	0.16
6	66.2E GALAXY 27	34.00	0.94	10.90	0.30	35.64	0.97	10.46	0.29
7	55E GSAT-16	21.10	0.59	23.90	0.66	20.26	0.54	22.94	0.64
8	45E INTELSAT 12	9.40	0.26	35.50	1.00	9.02	0.24	34.08	0.95
9	25.1E SKYNET 5B	−14.0	−0.39	30.90	0.86	−15.0	−0.42	29.66	0.84
10	10E EUTELSAT 10A	−31.5	−0.88	13.40	0.38	−30.2	−0.81	12.86	0.36
11	-5WEUTELSAT-WST A	−48.5	−1.35	−3.50	−0.11	−49.5	−1.41	3.36	−0.14
12	-30W SPAINSAT	−75.4	−2.09	−30.4	−0.84	−74.3	−1.94	−29.18	−0.86

The pointing accuracy was within the stated performance criteria tolerance value of $(\pm 2^0)$ or $\pm 5\%$ of the target angular orientation. For example, for TELKOM 1 at 108^0E, the % error in horizontal position= $((79.5 - 78.32)/79.5) * 100\% = 1.48\%$ and the % error in vertical position= $((-34.50 - -35.58)/(-34.50)) * 100\% = -3.13\%$. Similarly, for SPAINSAT at -30^0W, the % error in horizontal position= $((-75.40 - -74.38)/(-75.40)) * 100\% = -1.35\%$ and the % error in vertical position= $((-30.40 - -29.18)/(-30.40)) * 100\% = -4.01\%$. The discrepancies are due to conversion errors introduced by the potentiometers.

4.5. Summary of Key Features of the Developed NFSC

Compared to what has been done by other researchers and basing on the results obtained, the following aspects are novel to this study:

1. The development of the NFSC, with its algorithms created within the ANFIS framework, for a DC servomotor based satellite antenna positioning and tracking system. The main new features of the developed NFSC include:

a) The training, testing and checking data used are unique to this study and were obtained using a unique MATLAB code customized with information from the selected target satellite locations.

b) The ANFIS model deployed 7x7 triangular input membership functions, 49 linear output membership functions, and trained using hybrid algorithm thereby registering a root mean squared error of only 1.5×10^{-4} which turned out to be the most optimal compared to other possible combinations (See Table 4.1).

c) Presentation and analysis of the developed ANFIS controller performance before training and after training particularly in terms of surface plots and corresponding contour plots. This created a clear picture of the impact of training.

d) The tracking performance parameters obtained with the NFSC for both the industrial and prototype models are unique and better (see Table 4.2 and Table 4.2)

2. The developed prototype was unique in the following sense:

a) The DC servomotor used i.e. SPRINGRC motor SM-S4309M and experimental determination of its parameters.

b) The transfer function developed for the prototype model using this motor.

CHAPTER FIVE

CONCLUSIONS AND RECOMMENDATION

5.1 Conclusions from PID, FLC and NFSC Controllers

The objective of this thesis to design NFSC Controller for D.C. servomotor-based antenna pointing system has been successfully achieved. This was verified through simulated output responses of the system to step input signal which satisfied the design criteria. Also, the experimental results obtained from the prototype showed that the control system developed and its algorithms worked and could be deployed in driving the azimuth and elevation DC servomotors so as to steer a parabolic dish antenna and keep it always within the desired line of sight with a particular satellite.

The FLC by itself increased the settling time to 2.4 seconds but had a rise time of 2.0 seconds and decreased the overshoot to zero (0) %. The Takagi-Sugeno FLC recorded a better rise time of 1.6 seconds and settling time of 2.1 seconds compared to the Mamdani FLC model. The bench-marking PID controller registered a rise time of 0.7 seconds, settling time of 4.3 seconds and an overshoot of 21 %.

The ANFIS approach provided the best performance with a rise time of 0.2 seconds, settling time of 0.8 seconds and an overshoot of 8.0 % thus meeting all the specifications of the tracking system. Therefore, the objectives were achieved in totality for the design, software simulations as well as experiments conducted.

5.2 Recommendation

Some of the feasible advancements and further research work are suggested below:

(a) In this study, the control system was centered on the DC servomotor and the Global Positioning System (GPS) coordinates of the satellites which represented how much rotation was required. Further, the system was considered to be off-line and therefore did not require any signal information being handled by the satellite dish or transceiver system. The controller may be applied in real time to achieve an automatic satellite tracking with parabolic antenna using data derived from the signal strength.

(b) The NFSC can be further optimized using Particle Swarm Optimization (PSO) or Genetic Algorithm (GA) and investigated on whether shorter rise times and settling times may be achieved. This should improve the classification accuracy of the ANFIS system and realization of the optimal number of rules.

(c) The approach can be extended to highly non-linear model such as marine industry to solve the problem of auto-tracking and stabilization of a marine vessel antenna system for offshore Very Small Aperture Terminal (VSAT) communication.

(d) The algorithms may be applied in automated alignment of microwave dishes for Base Transceiver Stations in mobile communication. This process in several occasions is still being done manually where riggers climb the towers and maneuver the dishes manually while measuring signal levels at either ends of the link. This is not only time consuming but is also risky due to the heights involved such as 15m to 50m.

REFERENCES

[1] J.K. Kim, K.R. Cho and C. S. Jang, "Fuzzy control of data link antenna control system for moving vehicles," International Conference on Control, Automation, and Systems (ICCAS), June 2005.

[2] M.M. Kyaw, C.M. Nwe and H.M. Tun, "Satellite dish positioning control by DC Motor using infrared remote control," International Journal of Electronics and Computer Science Engineering, vol. 3, no. 3, pp. 199-207, 2012.

[3] M. N. Soltani, R .Zamanabadi and R. Wisniewski, "Reliable control of ship-mounted satellite tracking antenna," IEEE Transactions on Control Systems Technology, pp. 99, 2010.

[4] T.V. Hoi, N. T. Xuan and B. G. Duong, "Satellite tracking control system using Fuzzy PID controller," VNU Journal of Science: Mathematics and Physics, vol. 31, no. 1, pp. 36-46, 2015.

[5] L. Xuan, J. Estrada and J. DiGiacomandrea, "Antenna azimuth position control system analysis and controller implementation," Design Problem, July 2009.

[6] S. S. Sheth and S. K. Gonsai, "Antenna position control systems, review and new perception," Journal of Information, Knowledge and Research in Electronics and Communication Engineering, vol. 2, no. 2, pp. 627-631, 2013.

[7] C.H. Chang, S.H. Lee, T.Y. Kwon and C. Lee, "Antenna control system using step tracking algorithm with H-infinity controller," International Journal of Control, Automation and Systems, vol. 1, pp. 83-92, March 2003.

[8] M. Ahmed, S.B. Mohd Noor, M. K. Hassan and A.B.Che Soh, "A Review of Strategies for Parabolic Antenna Control," Australian Journal of Basic and Applied Sciences, vol. 8(7), pp. 135-148, May 2014.

[9] A. Mehmet and T. Ismail, "Motion controller design for the speed control of DC servo motor," International Journal of Applied Mathematics and Informatics, vol. 1, no. 4, p. 131, 2007.

[10] A. K. Pandey, "Speed control of DC servo motor by fuzzy controller," International Journal of Scientific and Technology Research, vol. 1, September 2012.

[11] H. C. Lu, "Design and implementation of a digitalized fuzzy logic controller for DC servo drives," Proceedings of the 5th WSEAS Int. Conf. on Artificial Intelligence, Knowledge Engineering and Data Bases, pp. 269-274, February 2006.

[12] T. Agee, "Stabilization of Dish Antennas in Windy Environment," M. S. thesis, Abubakar Tafawa Balewa University, Bauchi, Nigeria, 1992.

[13] W. Gawronski, "An H-Infinity Controller with Wind Disturbance Rejection Properties for the DSS-13 Antenna," TDA Progress Report, pp. 42-127, November 15 1996.

[14] J.E.Slotine and W.Li, "Applied Nonlinear Control," Prentice-Hall, Inc., 1991.

[15] H. S Ahn, D. Chung, K.H. Ko, S. Wang, O. Jung and S. Choi, "Satellite Antenna Control: Design and Performance Validation under given TPF," Proceedings of International Conference on Control, Automation and Systems 2010 in Kintex Gyeonggi-do Korea, pp. 1527-1532, 2010.

[16] J.Jia, L. Xutao and Y. Qin, "Study of Adaptive Variable Structure Attitude Control and its full Physical Simulation of Multi-Body Satellite Antenna Drive Control,"

Proceedings of World Congress on Computer and Information Engineering (WRI), vol. 2, pp. 546-549, 2009.

[17] C. Xin-long, Y.Di, Z.Wen-ya and Z. Li-bin, "Robust Adaptive Control Method for User-Satellite Antenna Acquisition and Tracking," Proceedings of IEEE International Conference on Industrial Technology, pp. 1-6, 2008.

[18] R.S. Burns, "Advanced Control Engineering," Butterworth-Heinemann, 2001.

[19] P.K. Kihato and J.N. Nderu, "Direct neuro-fuzzy approach to motion tuning of servomotors," Kenya Society of Electrical and Electronic Engineers (KSEEE) and Japan Society of Applied Electromagnetic and Mechanics (JSAEM), 2011.

[20] M.Palamar, "Neurocontroller to Tracking Antenna Control of Information Reception from Earth Remote Sensing Satellites," Proceedings of IEEE Workshop on Intelligent Data Acquisition and Advanced Computing Systems (IDAACS): Technology and Applications, Sofia, Bulgaria, pp. 340-344, September 2005.

[21] T. B. Reddy, K. Satyanarayana and T. Himaja, "Modeling and analysis of adaptive neuro fuzzy inference system based BLDC motor under different operating conditions," International Journal of Engineering and Advanced Technology (IJEAT), vol. 3, August 2014.

[22] A.K.Mandal, "Introduction to Control Engineering Modeling, Analysis and Design," New Age Publishers, 2006.

[23] M. C. Rafael, J.B Goncalves and P. P. Leite do Prado, "Development of an Automated System for Maneuvering Parabolic Dish Antennas used in Satellite Communication," ABCM Symposium Series in Mechatronics -Vol. 5, Section II-Control Systems, p. 69, 2012.

[24] A.H. Vardhan, A. S. Bharadwaj, S. S. Raju and N. Archana, "Implementation of Fuzzy PID controller and performance comparison with PID for position control of DC motor," International Journal of Engineering Research and Development, vol. 7, pp. 78-84, July 2013.

[25] H.I.Okumus, E. Sahin and O. Akyazi, "Antenna Azimuth Position Control with Classical PID and Fuzzy Logic Controllers," Proceedings of International Symposium on Innovations in Intelligent Systems and Applications (INISTA), pp. 1-5, 2012.

[26] N.S. Nise, "Control system engineering," John Wiley and Sons, vol. 6th Edition, 2011.

[27] K. Ogata, "Modern control engineering," Prentice-Hall Inc. USA, vol. 4th Edition, 2010.

[28] H.T. Nguyen, N. R. Prasad, C. L. Walker and E. A. Walker, "A First course in fuzzy and neural control," Chapman & Hall/CRC, 2003.

[29] J. Vieira, F. D. Morgado and A. Mota, "Neuro-fuzzy systems: A survey," Department of Electrical Engineering, Castelo Branco, Portugal, 2004.

[30] N. M. Noaman and A. M. Omar, "Design of a neural fuzzy controller for DC motor," AL-Rasheed College of Engineering University of Technology, March 2006.

[31] MathWorks: http://www.mathworks.com/help/simulink/arduino.html, Accessed: 20/8/2016

[32] L. Virgil, "Satellite Communication," Britannica.com, pp. Retrieved 2016-05-25, 2015.

[33] C. S. Rasu, "A Course Material on SATELLITE COMMUNICATION," Department of Electronics and Communication Engineering Sasurie College of Engineering, Vijayamangalam, Dec 2015.

[34] W.L. Pritchard, H. G. Suyderhoud and R. A. Nelson, "Satellite Communication Systems Engineering," Prentice Hall/Pearson, 2007.

[35] G.Maral and M. Bousquet, "Satellite Communication Systems: Systems, Techniques and Technology," John Wiley & Sons Ltd, United Kingdom, vol. 5th Edition, 2009.

[36] A Technical Document TD-1205-a, "Calculation of Azimuth, Elevation and Polarization for non-horizontal aligned Antennas," Technische Universitat Munchen, Lehrstuhl fur Raumfahrttechnik, In cooperation with Eutelsat Communications, vol. Version 2.1, June 2015.

[37] A.R. Chishti, S.F. Bukhari, H.S. Khaliq, M.H. Khan and S.Z. Bukhari, "Radio Telescope Antenna Azimuth Position Control System Design and Analysis in MATLAB/SIMULINK using PID & LQR Controller," The Islamia University of Bahawalpur, Pakistan, 2014.

[38] P.R. Kumar and V.N Babu, "Position Control of Servo Systems using PID Controller Tuning with Soft Computing Optimization Techniques," International Journal of Engineering Research & Technology (IJERT), vol. 3, pp. 976-980, November 2014.

[39] J.S.R.Jang, "ANFIS: Adaptive Network Based Fuzzy Inference System," IEEE, Transactions on system, Man & cybernetics, vol. 23, 1993.

[40] B.A.A. Omar, A.Y.M. Haikal and F.F.G. Areed, "Design adaptive neuro-fuzzy speed controller for an electro-mechanical system," Ain Shams Engineering Journal (ASEJ), vol. 2, pp. 99-107, 2011.

[41] J.P.Lilja, P.M. Kristian and M.H.C Alfonso, "Neuro-fuzzy control," Soft Computing, University of Iceland, 2005.

[42] S.Ghadri, S.Javadi and F.Farokhi, "Decreasing starting current for separate excited dc motor using anfis controller," International Journal of Smart Electrical Engineering, vol. 2, no. 2, 2013.

[43] Satellite Finder/Dish Alignment Calculator with Google Maps: http://www.dishpointer.com/, Accessed: 20/8/2016.

[44] Real Time Satellite Tracking: http://www.n2yo.com/, Accessed: 20/8/2016.

APPENDICES

Appendix 1: Experimental Determination of DC Servomotor Parameters

The parameters of the DC servomotor-SM-S4309M used in the prototype were determined experimentally. The procedures followed and results obtained are presented in this section. All the relevant circuits were connected to a +/- 15V power supply from which a voltage between 0V and 6V (the drive voltage range for the prototype motor) was obtained. The results obtained had been summarized in Table 3.1 in section 3.2, with an offline load of radius $0.20m$ and weight of $5N$.

Appendix 1.1 Determination of Armature Resistance and Inductance

The motor connector was disconnected and the DC resistance across the motor terminals was measured using a digital multimeter. The minimum resistance was found to be 3.2Ω as the shaft was manually rotated while taking different readings since the DC motor resistance is different at different shaft positions. To obtain the armature inductance, a low voltage ac source of 1.2Vpeak-to-peak was applied to the armature winding. The voltage and the current were measured and recorded using two multimeters. Next, the DC motor impedance was calculated using equation (Appendix 1.1):

$$Z = \frac{V}{I} = \frac{1.2}{0.35} = 3.428\Omega \qquad \text{(Appendix 1.1)}$$

where Z is the impedance in ohms, V is the measured ac voltage in volts and I is the measured current in amperes.

The reactance, X in Vars is obtained as 1.231 using equation (Appendix 1.2) with the known values of the other two parameters.

104

$$Z = \sqrt{(X^2 + R_a{}^2)} \qquad \text{(Appendix 1.2)}$$

The armature inductance **L** is then obtained as 0.00393H by using this value of X and frequency, $f = 50\text{Hz}$ in $X = 2\pi fL$. The armature voltage was noted as 4.6V.

Appendix 1.2 Determination of Motor Back e.m.f and Torque Constant

The motor back e.m.f constant was obtained as the ratio of the voltage to the speed in rad/sec by using equation (Appendix 1.3) after measuring the armature voltage and current at a speed of $58rpm$.

$$K_B = \frac{(V_a - I_a R_a)}{\text{Speed [rad/sec]}} = \frac{(4.6 - 0.075\text{x}3.2)}{(58\text{x}2\text{x}\pi)/60} = 0.72 \text{ Vs/rad} \qquad \text{(Appendix 1.3)}$$

When torque constant and voltage constant are given in terms of Nm/Amps andvolts − seconds/radians, then they are numerically equal, hence $K_T = 0.72\text{Nm/A}$.

Appendix 1.3 Motor Inertia and Damping Constants

The motor inertia constant was obtained as $J_a = 0.03\text{kgm}^2$ by using equation (Appendix 1.4) and the motor damping constant taken to be numerically equal to half the inertial constant as $B_a = 0.015\text{Nms/rad}$.

$$J_a = \frac{(1)\, K_B\, K_T}{2\pi f_{45} R_a} = \frac{(1\text{x}0.72\text{x}0.72)}{(2\text{x}\pi)(0.8)(3.2)} = 0.03\text{kgm}^2 \qquad \text{(Appendix 1.4)}$$

Where f_{45} , is the frequency at which the phase lag is about 45^0. This was obtained by recording the tachometer output amplitude at this frequency when a 2V (peak -peak) was applied at frequencies ranging from 0.2 to 1Hz.

Appendix 1.4 Load Inertia and Damping Constants

The load inertia constant was obtained as $J_L = 0.0057 \text{kgm}^2$ by using equation (Appendix 1.5) and the load damping constant taken to be numerically equal to the inertia constant as $B_a = 0.0057 \text{Nms/rad}$.

$$J_L = \frac{(WR^2)}{2g} = \frac{(5 \times (0.15/2)^2)}{(2)(9.8)} = 0.0057 \text{kgm}^2 \qquad \text{(Appendix 1.5)}$$

where

W = Weight (N),

R = Radius (m) and

g = Gravitational constant (N/kg).

Appendix 1.5 Equivalent viscous friction Coefficient and Moment of inertia

The Equivalent viscous friction Coefficient, $B_m = 0.015 \text{Nms/rad}$ and Equivalent Moment of inertia $J_m = 0.03 \text{kgm}^2$ have been obtained using equation (Appendix 1.6) and (Appendix 1.7) where $K_g = \frac{N_1}{N_2}$ is the gear ratio.

$$B_m = B_a + B_L(\frac{N_1}{N_2})^2 = 0.015 + 0.0057(\frac{1}{270})^2 = 0.015 \text{ Nms/rad} \quad \text{(Appendix 1.6)}$$

$$J_m = J_a + J_L(\frac{N_1}{N_2})^2 = 0.03 + 0.0057(\frac{1}{270})^2 = 0.03 \text{kgm}^2 \qquad \text{(Appendix 1.7)}$$

Appendix *2*: Measurements on DC Servo Motor Feedback System

Figure Appendix 2.1 shows the experimental set up while Figure Appendix 2.2 shows the SIMULINK model used in monitoring the DC Servo Motor Feedback System.
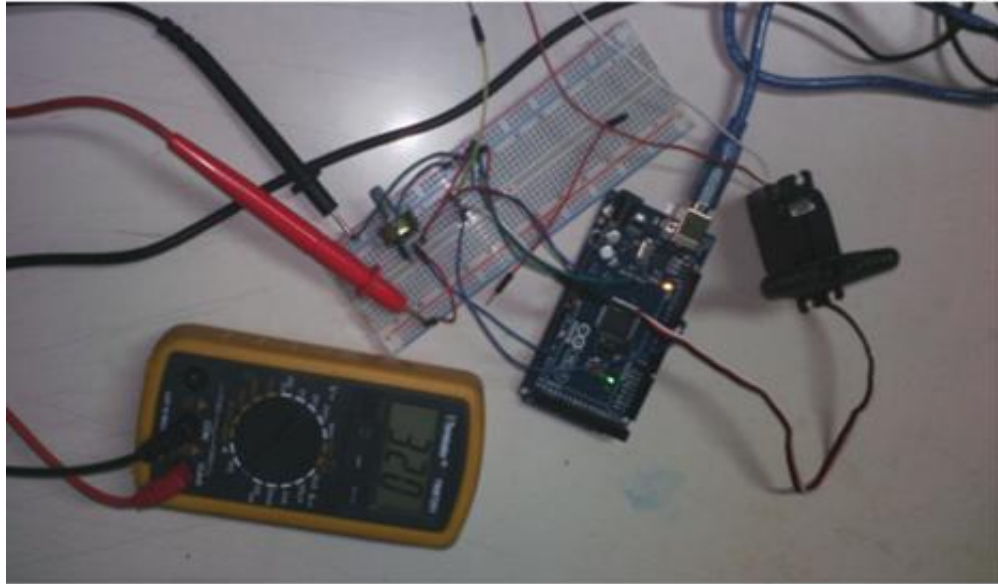
Figure Appendix 2.1: Set up with Arduino board to Measure servo Feedback
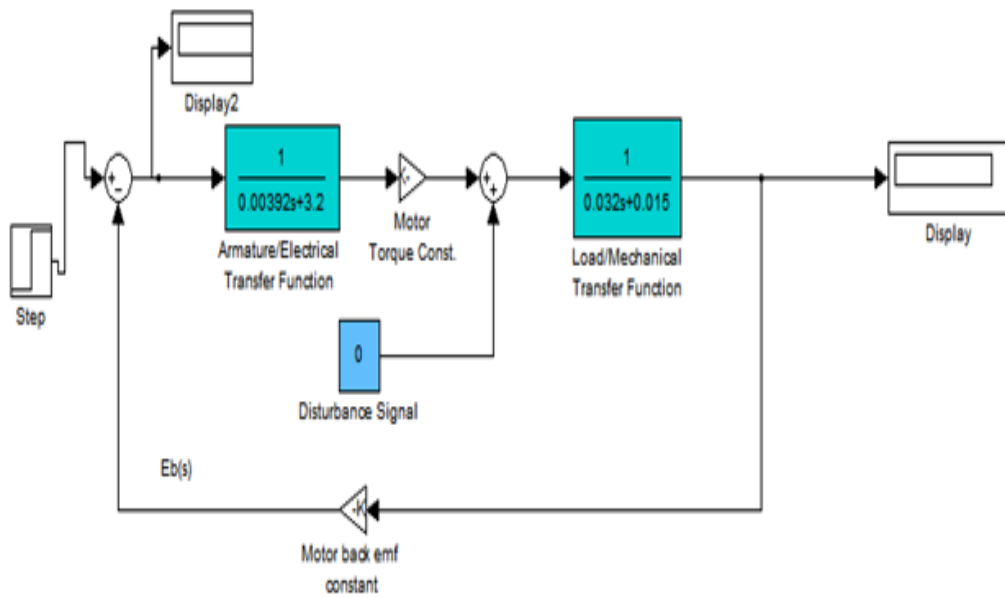
Figure Appendix 2.2: SIMULINK Model for Measuring Servomotor Feedback

The results on the performance of the servo motor feedback system with various reference position inputs were observed and recorded as shown in Table Appendix 2.1. In Table Appendix 2.2, the measurements obtained using SIMULINK model of Figure Appendix 2.2 for the back e.m.f generated is presented. This experiment was important in enabling the testing and verification of the performance of the DC servomotor-SM-S4309M feedback mechanism which influences the ability of the developed NFSC algorithm to control the motor position.

Table Appendix 2.1: Experimental Measurements on DC Servomotor Feedback

S/No.	Reference Voltage (V)	Desired Angle (degrees)	Actual Voltage (V) From Internal Potentiometer	Electrical Input to DC Motor (V)
1	0.00	0.00	0.00	0.00
2	0.40	15.00	0.18	0.22
3	0.80	30.00	0.36	0.44
4	1.21	45.00	0.54	0.66
5	1.61	60.00	0.72	0.88
6	2.01	75.00	0.90	1.10
7	2.41	90.00	1.09	1.32
8	2.81	105.00	1.27	1.55
9	3.21	120.00	1.45	1.77
10	3.62	135.00	1.63	1.99
11	4.02	150.00	1.81	2.21
12	4.42	165.00	1.99	2.43
13	4.82	180.00	2.22	2.60

It was noted that the servomotor would only move in cases where there was a difference between the reference output voltage captured by the internal potentiometer and the external PWM reference voltage supplied externally through the microcontroller.

Table Appendix 2.2: Experimental Measurements on DC Servomotor back e.m.f

S/No.	Reference Step Input Voltage (V)	Output Voltage (V)	Back emf ($K_B = 0.72$)	Electrical Input to DC Motor (V)
1	1.000	1.271	0.915	0.085
2	2.000	2.542	1.831	0.169
3	3.000	3.814	2.746	0.254
4	4.000	5.085	3.661	0.339
5	5.000	6.356	4.576	0.424

Appendix 3: Tuning PID Controller using Ziegler-Nichols Method

The Ziegler-Nichols (ZN) method is a conventional PID tuning method which is widely accepted as standard for design of various controllers. Ziegler-Nichols presented two methods: Step response method and Frequency response method. In this thesis frequency response method was used to tune the PID controller.

The procedure is as follows: First, the derivative time (T_D) is set to zero and integral time T_I set to infinity. This is used to get the initial PID setting of the systems. The critical gain (K_u) and periodic oscillations (P_u) are determined by using Routh-Hurwitz criteria. From the Routh-Hurwitz rows, K_u and P_u are determined by equating the rows containing "s" and "s^2" to zero respectively. Next, the PID gains of K_P , K_I and K_D are obtained using relations presented in Table Appendix 3.1 and the formulas $K_P = 0.6 \times K_u$, $K_I = \frac{K_P}{T_I}$ and $K_D = K_P T_D$ with the critical period, $T_c = \frac{2\pi}{\omega}$. A proportional controller will have the effect of reducing the rise time and will reduce but never eliminate the steady-state error. An integral control will eliminate the steady-state error for a constant or step input, but it may make the transient response slower. A derivative control will

increase the system stability, reducing the overshoot, and improving the transient response.

Table Appendix 3.1: ZN PID Tuning Parameters

Control Type	K_P	T_I	T_D
P	$0.5K_u$	infinity	0
PI	$0.45K_u$	$(0.833T_c)$	0
PID	$0.6K_u$	0	$0.125T_c$

Letting $T_I = \infty$ and $T_D = 0$ in equation 3.25, the azimuth antenna position control system transfer function becomes equation (Appendix 3.1). The value of K_u that makes the system marginally stable so that sustained oscillations occurs is obtained by use of Routh stability criterion.

$$\frac{\theta_o(s)}{\theta_i(s)} = \frac{663\ K_u}{s^3 + 101.71s^2 + 171s + 663 + 663\ K_u} \qquad \text{(Appendix 3.1)}$$

The characteristic equation for the closed loop system is as shown in equation (Appendix 3.2) and the Routh array is as indicated in Table Appendix 3.2.

$$s^3 + 101.71s^2 + 171s + (663 + 663\ K_u) = 0 \qquad \text{(Appendix 3.2)}$$

Table Appendix 3.2: Routh Array for antenna azimuth ZN Critical Gain

Column One	Column Two	Column Three
s^3	1	171
s^2	101.71	$(663 + 663K_u)$
s^1	$(16729.41 - 663K_u)/101.71$	0
s^0	$(663 + 663K_u)$	$-$

The value of the critical gain K_u is evaluated as $K_u < 25.23$ and the roots of the characteristic equation becomes $s_1 = -1.0171$; $s_{2,3} = \pm 0.1308i$ and $0.1308T_c = 2\pi$

or $T_c = 48.043$. The gain parameters for the azimuth PID controller are therefore evaluated as: $K_P = (0.6)(25.23) = 15.138 \approx 15, T_I = (0.5)(48.043) = 24.0215 \approx 24, T_D = (0.125)(48.043) = 6.0054 \approx 6, K_D = K_P T_D \approx 90$ and $K_I = \frac{K_P}{T_I} = \frac{15}{24} = 0.625$. The advantage of this method is that it is easy to conduct the experiment as only the Proportional (P) controller needs to be adjusted. It also gives an indication about the dynamics affecting the behavior of the system since it is an online tuning method. However, the disadvantages of this method are that the experiment can be time consuming and can also upset the process thus venture it into the unstable regions.

Appendix 4: Arduino Mega 2560 and NFSC Design Data

The Arduino Mega 2560 is a microcontroller board based on the ATmega 2560 and is shown in Figure Appendix 4.1. It has 54 digital input/output pins (of which 14 can be used as PWM outputs), 16 analog inputs, 4 UARTs (hardware serial ports), a 16 MHz crystal oscillator, a USB connection, a power jack, an In-Circuit Serial Programming header and a reset button. It contains everything needed to support the microcontroller and can be powered by connecting it to a computer with a USB cable or using an AC-to-DC adapter or battery. The Advantages of using the Arduino Mega are: Arduino simplifies the amount of hardware and software development needed to get the system running, the Arduino hardware platform already has the power and reset circuitry setup, it already has circuitry to program and communicate with the microcontroller over the USB port and it provides a number of libraries to make programming easier.

The technical specifications of the microcontroller are given in Table Appendix 4.1.
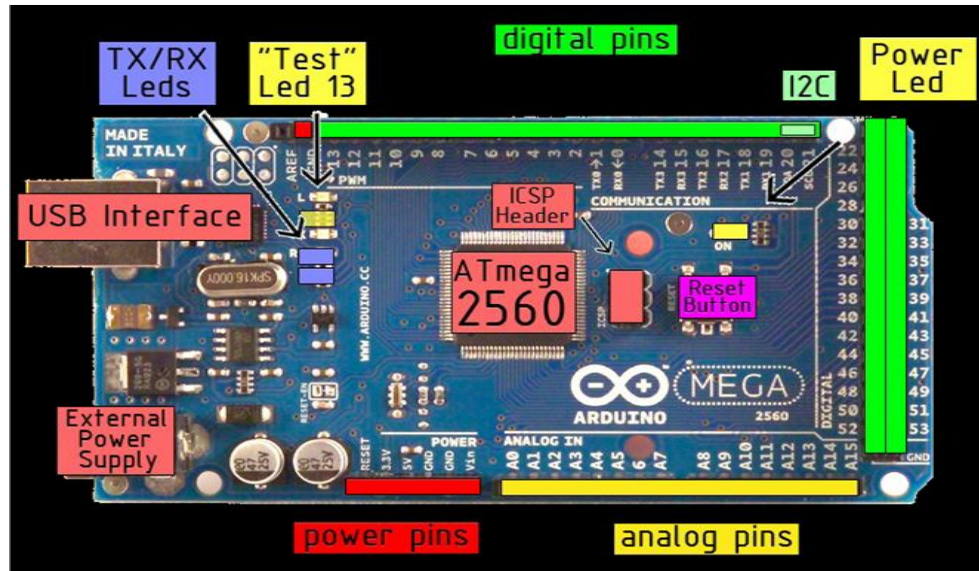
Figure Appendix 4.1: Arduino Mega

Table Appendix 4.1: Arduino Mega 2056 Technical Specifications

Parameter	Specification
Microcontroller	ATmega 2560
Operating Voltage	5V
Input Voltage (recommended)	$7 - 12V$
Input Voltage (limit)	$6 - 20V$
Digital Input/output (I/O) Pins	54 (of which 15 provide PWM output)
Analogue Input Pins	16
DC Current per (I/O) Pin	20mA
DC Current for 3.3V Pin	50mA
Flash Memory	256KB (8KB used by bootloader)
SRAM	8KB
EEPROM	4KB
Clock Speed	16MHz

The control algorithm for positioning the antenna in the satellite tracking system was tested by the established communication link between the Arduino microcontroller and the MATLAB/SIMULINK software models via the USB port.

Table Appendix 4.2: NFSC Training, Checking and Testing Data Sets

	Training Data Set			Checking Data Set-I		
S/No.	Position Error	Change in Error	ANFIS Output	Position Error	Change in Error	ANFIS Output
1	0.814723686	-3.378176918	0.64431813	0.751267059	2.802520683	0.037738866
2	0.905791937	2.942845407	0.378609383	0.255095115	-1.10261163	0.885168008
3	0.126986816	-1.88784958	0.811580458	0.505957052	-2.583087141	0.913286828
4	0.913375856	0.285331355	0.532825589	0.699076723	-0.960878544	0.796183874
5	0.632359246	-3.343512705	0.350727104	0.890903253	-4.035454748	0.098712279
6	0.097540405	1.019819414	0.939001562	0.959291425	-3.680267074	0.261871184
7	0.278498219	-2.370287155	0.875942811	0.54721553	4.420505908	0.33535684
8	0.546881519	1.540790985	0.550156343	0.138624443	4.561345402	0.679727951
9	0.957506835	1.892145031	0.622475086	0.149294006	0.752085951	0.136553137
10	0.964888535	2.481515928	0.587044705	0.257508254	-4.402204571	0.721227499
11	0.157613082	-0.494584015	0.207742293	0.840717256	-2.652200866	0.106761862
12	0.970592782	-4.16178622	0.30124633	0.254282179	-1.468414288	0.653757349
13	0.957166948	-2.710230313	0.470923349	0.814284826	3.211940402	0.494173937
14	0.485375649	4.133373615	0.23048816	0.243524969	-4.845965623	0.779051723
15	0.800280469	-3.47621981	0.844308793	0.929263623	-4.569761983	0.715037078
16	0.141886339	3.258169775	0.19476429	0.349983766	-3.310099705	0.903720561
17	0.421761283	0.383424353	0.225921781	0.19659525	1.49115475	0.890922504
18	0.915735525	4.961347166	0.170708047	0.251083858	2.317223857	0.334163053
19	0.79220733	-4.218244712	0.227664298	0.616044676	1.477459631	0.698745832
20	0.959492426	-0.573217302	0.435698684	0.473288849	-0.490762936	0.197809827
21	0.655740699	-3.933472298	0.311102287			
22	0.035711679	4.618980809	0.923379642	Testing Data Set-I		
23	0.849129306	-4.953657759	0.430207391	0.351659507	0.470088923	0.030540946
24	0.933993248	2.749104647	0.18481632	0.830828628	-2.036791944	0.74407426
25	0.678735155	3.173032207	0.904880969	0.585264091	2.446928071	0.500022436
26	0.757740131	3.686947054	0.979748378	0.549723608	-3.11044985	0.479922141
27	0.743132468	-4.155641545	0.438869973	0.917193664	1.867754334	0.904722238
28	0.39222702	-1.002173509	0.111119223	0.285839019	-3.164888443	0.609866648
29	0.65547789	-2.401295971	0.258064696	0.757200229	-1.315154035	0.61766639
30	0.171186688	3.000684802	0.408719846	0.753729094	1.256185607	0.859442306
31	0.706046088	-0.685861725	0.594896074	0.380445847	2.802274352	0.805489425
32	0.031832846	4.106475944	0.262211748	0.567821641	-4.188742311	0.576721516
33	0.276922985	-3.181529717	0.602843089	0.07585429	4.29385971	0.182922469
34	0.046171391	-2.361970835	0.71121578	0.053950119	2.757126786	0.239932011
35	0.097131781	-3.544610196	0.221746734	0.530797553	-0.132083676	0.886511933
36	0.823457828	-3.639314413	0.117417651	0.77916723	-0.641414114	0.028674152
37	0.694828623	3.692922076	0.296675873	0.934010684	-0.532162506	0.489901389
38	0.31709948	0.797045874	0.318778302	0.129906208	-1.93650528	0.167927146
39	0.950222049	0.498602018	0.42416676	0.568823661	0.085086554	0.97868065
40	0.034446081	-3.550452018	0.507858285	0.469390641	0.107715642	0.712694472
41	0.43874436	3.530311177	0.085515797	0.01190207	3.176277083	0.500471624
42	0.381558457	1.220551315	0.262482235	0.337122644	2.948314169	0.471088375
43	0.765516788	-1.490476191	0.801014623	Checking Data Set-II		
44	0.795199901	0.132495399	0.029220278	0.276025077	-0.827329309	0.963088539
45	0.186872605	-0.981919662	0.928854139	0.679702677	-4.508455697	0.546805719
46	0.489764396	-4.240333083	0.730330863	0.655098004	4.027161099	0.521135831
47	0.445586201	-2.600838464	0.488608974	0.162611735	4.447871897	0.231594387
48	0.64631301	-3.766810652	0.578525061	0.118997682	-0.091359075	0.488897744
49	0.709364831	-3.160922117	0.23728358	Testing Data Set-II		
50	0.754686682	-2.600474743	0.458848828	0.498364052	-0.107473616	0.624060088
51	0.6534234	0.02009876	0.015674246	0.959743959	-1.622805902	0.679135541
52	0.447215535	3.920405908	0.31532432	0.340385727	4.000538464	0.395515216
53	0.557435252	-4.389746311	0.586721516	0.585267751	-1.307532189	0.367436649
54	0.864249807	2.683052471	0.578045705	0.223811939	-3.887972447	0.987982003

Table Appendix 4.2 shows the NFSC Training, Checking and Testing Data sets that were used to achieve the successful design of NFSC Controller within the ANFIS framework.

Appendix 5: Steady State Error

The steady state error (e_{ss}) is a measure of the difference between the desired output and actual output defined using final value theorem as in equation (Appendix 5.1).

$$e_{ss} = \lim_{s \to 0} S. \frac{R(s)}{1 + G(s)H(s)} \qquad \text{(Appendix 5.1)}$$

The steady state error depends on type of input $R(s)$ and the type of system , $G(s)H(s)$. Control systems may depict steady state errors for changes in position, velocity or acceleration. These are analyzed using position error constants (k_P) for step input, velocity error constant (k_V) for ramp input and acceleration error constant (k_a). In this study, since antenna tracking system is a positioning control system relying accurate positioning of the DC servomotors and its load, the step input signal was used as the test signal. The steady state error value regarding position control with the step input signal was zero (0) for both the industrial model and prototype model as given in equations (Appendix 5.2, Appendix 5.3, Appendix 5.4 and Appendix 5.5).

$$k_P = \lim_{s \to 0} G(s)H(s) = \lim_{s \to 0} \frac{20.83}{s[s^2 + 101.71s + 1.71]} * 1 = \infty \qquad \text{(Appendix 5.2)}$$

$$e_{ss} = \frac{1}{1 + k_P} = \frac{1}{1 + \infty} = 0 \qquad \text{(Appendix 5.3)}$$

$$k_P = \lim_{s \to 0} G(s)H(s) = \lim_{s \to 0} \frac{612.24}{s[s^2 + 81.68s + 481.63]} * 1 = \infty \qquad \text{(Appendix 5.4)}$$

$$e_{ss} = \frac{1}{1 + k_P} = \frac{1}{1 + \infty} = 0 \qquad \text{(Appendix 5.5)}$$

Hence, the steady state error was made zero by ensuring that the position control transfer function was a type one system thus resulting to k_P being infinite.

Appendix 6: List of Journal Publications & Conference papers

1. Linus A. Aloo, Peter K. Kihato and Stanley I. Kamau, "DC Servomotor-based Antenna Positioning Control System Design using Hybrid PID-LQR Controller", European International Journal of Science and Technology, Vol. 5, No.2, March, 2016, pp. 17-31.

2. Linus A. Alwal, Peter K. Kihato and Stanley I. Kamau, "Design of Neuro-Fuzzy System Controller for DC Servomotor-Based Satellite Tracking System", IOSR Journal of Electrical and Electronics Engineering (IOSR-JEEE), Volume 11, Issue 4 Ver. III, July-August 2016, pp. 89-102.

3. L.A. Alwal, P.K. Kihato and S.I. Kamau, "Design of Neuro-Fuzzy System Controller for DC Servomotor-Based Antenna Positioning System", Proceedings of the 2nd Dedan Kimathi University of Technology (DeKUT) International Conference on Science, Technology, Innovation and Entrepreneurship, held at the Main Campus, Nyeri, Kenya, 2nd - 4th November, 2016.

4. L.A. Alwal, P.K.Kihato and S.I. Kamau, "DC Servomotor-based Antenna Positioning Control System Design using PID and LQR Controller", Proceedings of 2016 International Annual Conference on Sustainable Research and Innovation, held at Kenya School of Monetary Studies (KSMS), Nairobi, Kenya, 4th-6th May, 2016.